UCLA
UCLA Electronic Theses and Dissertations

Title

Multisensory functional and comparative analysis of object tracking in flying fruit flies

Permalink

https://escholarship.org/uc/item/4h09s391

Author

Rimniceanu, Martha

Publication Date

2024

Peer reviewed|Thesis/dissertation

eScholarship.org Powered by the California Digital Library
University of California

UNIVERSITY OF CALIFORNIA

Los Angeles

Multisensory functional and comparative analysis of object tracking in flying fruit flies

A dissertation submitted in partial satisfaction of the requirements

for the degree Doctor of Philosophy

in Molecular, Cellular and Integrative Physiology

by

Martha Rimniceanu

2024

© Copyright by

Martha Rimniceanu

2024

ABSTRACT OF THE DISSERTATION

Multisensory functional and comparative analysis of object tracking in flying fruit flies

by

Martha Rimniceanu

Doctor of Philosophy in Molecular, Cellular and Integrative Physiology

University of California, Los Angeles, 2024

Professor Mark A. Frye, Chair

The survival and success of animals across phyla is critically dependent on generating appropriate behavioral responses to visual cues that are often complex and ambiguous. Visual objects can represent predators, conspecifics, obstacles and navigational goals, and must be discriminated from moving panoramas whose spatial features can vary greatly across environments. Due to its high-performance demands, insect flight is an excellent system used to study the behavioral algorithms governing the detection and responses to moving objects, and their underlying neural mechanisms. Yet, much of our understanding of the neurobiology of object discrimination comes from highly restrictive preparations that limit or severely compromise the multisensory feedback that modulates visual circuits in freely behaving animals. This dissertation probes how robust and well-characterized object tracking behaviors can be modulated by both multisensory context and visual-ecological adaptations. We demonstrate that the absence of naturalistic body movement cues in classical body-fixed virtual reality paradigms relegates smooth optomotor responses typically reserved for gaze stabilization to object pursuit

tasks. We show that this occurs through a simple gain modulation mechanism and propose the gyroscopic haltere proprioceptive circuit that play a role in actively damping visual circuits. We generate novel genetic reagents in *D. melanogaster* that allow targeted manipulation of haltere feedback and propose experiments to test the integration of proprioceptive and visual feedback *in vivo*. Finally, through comparative studies across *Drosophila* species, we demonstrate that the same object pursuit strategies that we found to be highly dependent on multisensory context are also shaped by the properties of the visual ecology. This series of studies can inform the design and interpretation of neurophysiological assays where parameters are necessarily restricted to probe neural mechanisms. More importantly perhaps, these studies illuminate general principles that expand our understanding of how locomoting animals process visual cues in relevant naturalistic contexts.

The dissertation of Martha Rimniceanu is approved.

Elissa A. Hallem

Alapakkam P. Sampath

Jean-Michel Mongeau

Mark A. Frye, Committee Chair

University of California, Los Angeles

2024

Pentru cei care m-au învățat cum “Să stăm strâmb și să judecăm drept”.

TABLE OF CONTENTS

Abstract of the dissertation……..……ii

Committee……..……..….iv

Dedication……..……..v

Table of Contents……...…….vi

Acknowledgements…….xi

VITA……...xv

Chapter 1: How flying flies track objects…….1-22

Watch out for that tree! The evolution and challenges of visual object tracking……..…..2

Flight control: A balance between gaze stabilization and object tracking……..….3

I just need a little feedback! Multisensory modulation of visual object tracking……....8

Visual object pursuit through the lens of visual ecology…….11

References……16

Chapter 2: Proprioception gates visual object fixation in flying flies……...23-68

Summary……24

Introduction……....24

Results……27

Discussion……..…34

Materials and Methods……41

Figures……..49-64

Figure 2.1: Sensory feedback conditions vary across rigid and magnetic tethering paradigms……49

Figure 2.2: Active bar fixation is body-state dependent……..……51

Figure 2.3: Smooth bar tracking dynamics are body-state dependent……...53

Figure 2.4: Manipulating visual feedback dynamics does not influence smooth object tracking dynamics……55

Figure 2.5: Body fixing increases amplitude and variance of wing and head movements……...57

Figure 2.6: Body fixing increases the wing steering bar response gain…….58

Figure 2.S1: Individual trials, related to Figure 2.2……60

Figure 2.S2: Reduced stimulus velocity does not affect body-state dependence of smooth tracking dynamics, related to Figure 2.3……61

Figure 2.S3: Flies in visual open loop do not smoothly track a motion-defined bar, regardless of initial position, related to Figure 2.4……..62

Figure 2.S4: Head steering responses to compound bar and ground stimuli, related to Figures 2.5 & 2.6……..……..64

References……65

Chapter 3: The role of haltere-mediated proprioceptive feedback in modulating visual object tracking in *D. melanogaster*……..……69-92

Introduction……..….70

Preliminary Results & Methods……..73

Experimental Plan……..……..77

Figures & Tables……..……81-89

Figure 3.1: Preliminary silencing perturbation of haltere descending neuron increases frontal bar fixation……81

Figure 3.2: Strategy for generating novel haltere circuit reagents……..84

Figure 3.3: Future directions comprise behavioral and live functional imaging experiments……..……86

Table 3.1: Anatomical brain region terminology……..…87

Table 3.2: Haltere candidate split Gal4 lines screened and their qualitative characterization**.**……..……88

References……..…90-92

Chapter 4: Cosmopolitan and cactophilic Drosophila species implement divergent visual tracking strategies……..93-137

Summary……..….94

Introduction……...…….94

Results……..….97

Discussion……..……105

Materials & Methods……..……111

Figures…….….119-133

Figure 4.1: Object centering differs across Drosophila species…….....119

Figure 4.2: Smooth bar-tracking responses differ across Drosophila species……...120

Figure 4.3: Desert fly species show stronger smooth & saccadic responses to complex bar motion dynamics.……..….122

Figure 4.4: Steady state bar pursuit dynamics differ across Drosophila species.……..124

Figure 4.5: Object saccade dynamics differ across Drosophila species.…….125

Figure 4.S1: A wide range of bar widths elicit similarly strong tracking responses in desert flies, all larger than in a cosmopolitan fly, related to Figure 4.3…….126

Figure 4.S2: Bar angular velocity predicts saccade probability best in cactophilic flies, related to Figure 4.3……..……128

Figure 4.S3: Optomotor gaze stabilization comprises smooth pursuit and saccades across cosmopolitan and cactophilic desert fly species, related to Figure 4.4 & 4.5.....130

Figure 4.S4: The kinematic variables for clockwise (CW, blue) and counter-clockwise (CCW, red) saccades are similar within species. Related to Figure 4.4……..132

References……134-137

ACKNOWLEDGEMENTS

As a wise mentor likes to point out “science is a social enterprise” and it is this simple fact that has kept me tethered to my scientific path in the easy and in the hard times. Without the following troupe of fun, interesting and encouraging primates, this dissertation may still exist out of sheer stubbornness but the journey here would have been much less enjoyable.

Mark, as the leader of our troupe, you have continuously inspired me to see the positive in a messy situation which, let’s be real, science often is. You have a unique ability to connect with people with vastly different personalities and to play on their individual strengths, making them feel heard, supported and motivated. Many can technically lead, but few people can lead by example as you do on a daily basis. I can only hope to one day become half the mentor you are. You’ve taught me a lot over the years, but perhaps the most important scientific skill is to simply tilt my head and look at the problem from a different perspective. Thank you for always being available, even when you are putting out 20 other fires. It is precisely because of your silly jokes and reminders to just go for a surf sesh over the years that I’m happy to graduate with my love for science intact!

I’d like to acknowledge another special human - Yesenia Rayos, our program SAO, who has a unique and genuine quality of going above and beyond for her students. Yesenia, I’ve seen you mobilize multiple departments at once in record time when an emergency arises and I still don’t understand how you resolve crises in parallel while still keeping a level tone and a smile on your face. I truly believe you are the heart of this program in many ways and I want to thank you for being an inspiration and role model.

To my dedicated committee members: thank you for being supportive and flexible, for questioning the right things and for always being interested to learn about tiny fruit flies and funny control loops.

The list of special humans is long and brevity is not my strong suit, but I will try …

To Mitch McVey, Barry Trimmer and Simon Sponberg – thank you for bamboozling me into a scientific career at various critical points. To Megan Matthews and Anthony Scibelli – thank you for being co-bamboozlers – you showed me first-hand what being a graduate student could look like and by watching you, I learned that 1. This is fun and 2. One needs solid technical skills and even more solid coping skills. To Jean-Michel Mongeau, thank you for warning me about the Frye lab. To Sara Wasserman, thank you for bringing desert flies into my world and helping foster my love for comparative neurobiology. Thank you also for the heart-to-heart conversations and for modeling just the right amount of sass in the work environment.

To members of the Frye troupe over the years: Carola, thank you for teaching me all about fly genetics and about being rigorous and meticulous in my science. Mehmet, thank you for setting the bar super high – trying to fill your shoes for the last 6 years has been excellent motivation. Karen, thank you for being a trail blazer. Rachel, thank you for being my survival buddy in the rough times. Gio, thank you for demonstrating what great scholarship looks like, for challenging me and for always knowing more than me (sometimes). Dave, thank you for fostering my love for neuroethology, for skeptically questioning their “behavioral” assays with me, and for “providing muscle” in key moments. You are no imitation postdoc. Pablo, thank you for always having an idea for an experiment and for always offering a genuine supportive comment when things are tough. Dani, thank you for being down for all the crazy journeys with me and for always being true to yourself despite the external pressures to conform. Lesly, thank you for showing me how to be patient and steadfast and to carry on when things don’t go our way.

To a couple of close friends who I’ve been lucky to coincide on the PhD path with: Ioana Anghel and Tal August, sharing this journey with you throughout the years meant that we were each others’ pillars of psychological support. I feel privileged to have gone through the various

life transitions with you and I can only hope we continue to do so with the chapters that are coming.

To Eric, how lucky am I to have had you as my team-mate over the last decade? I am so grateful to share this and many more adventures to come in this life with you.

Finally, to my parents, if I didn't already know that "Orice şut în fund e un pas înainte", we would not be here today. I also would not be here today without many many difficult decisions you courageously made. Thank you does not even begin to cover it.

Chapter 2 is adapted from Rimniceanu, M., Currea, J.P., Frye, M. A. 2023. *Proprioception Gates Visual Object Fixation in Flying Flies*. Curr. Biol. 33, 1459–1471.e3. https://doi.org/10.1016/j.cub.2023.03.018**.** M.R. contributed to conceptualization, methodology, investigation, software, formal analysis, visualization, writing the original draft, and editing. J.P.C. contributed to methodology, investigation, software, and editing. M.A.F. contributed to conceptualization, funding acquisition, supervision, project administration, writing the original draft, and editing. This work is funded by National Institutes of Health grants R01EY026031 and R01NS120984 to M.A.F. and R01NS120984-02S1 to J.P.C. We thank Sarah Fatkin for assistance with animal care and data collection. We are grateful for helpful discussions and comments on the manuscript from members of the Frye lab. Finally, we thank Dr. Jean-Michel Mongeau and Dr. Ben Cellini for technological resources and insightful collaboration.

Chapter 3 comprises unpublished work that is part of an active grant awarded to Mark Frye and Jean-Michel Mongeau (Grant ID FA9550-23-1-0401) to investigate physiological mechanisms of active damping of visual responses. M.A.F., J.M.M. contributed to conceptualization and methodology. M.R. carried out preliminary investigation and analysis. We would like to

specifically acknowledge the contribution of Frye Lab PhD Candidate Lesly Palacios Castillo for invaluable assistance provided in the generation of split Gal4 reagents described. We would also like to thank Dr. Eugenia Chiappe & Dr. Mert Erginkaya for sharing insights used to select split Gal4 candidate combinations.

Chapter 4 is adapted from a manuscript that is presently in review at Current Biology, authored by Rimniceanu, M., Limbania, D., Wasserman, M.S., Frye, M.A. and entitled *Cosmopolitan and cactophilic Drosophila species implement divergent visual tracking strategies.* M.R. conceptualized the project and contributed to methodology, investigation, software, formal analysis, visualization, writing the original draft, and editing. D.L. contributed to methodology, investigation, and editing. S.M.W. contributed to conceptualization, funding acquisition and editing. M.A.F. conceptualized the project and contributed to methodology, funding acquisition, supervision, project administration, writing the original draft, and editing. This work is funded by National Institutes of Health R01EY026031 and US Air Force Office of Scientific Research FA9550-23-1-0401 to M.A.F. and National Science Foundation IOS-2016188 to S.W. We thank Dr. Jean-Michel Mongeau for insight on frequency domain analysis.

VITA

EDUCATION

2018 – present Univ. California Los Angeles, Los Angeles, CA

Ph.D. Candidate in Molecular, Cellular and Integrative Physiology

2013 – 2017 Tufts University, Medford MA

B.Sc. in Biology and B.Sc. in Psychology, magna cum laude with Highest Thesis Honors for *The Neural Basis of Localized Thermosensation in the tobacco hornworm, Manduca sexta* advised by Dr .Barry Trimmer

PUBLICATIONS

Rimniceanu, M., Limbania, D., Wasserman, M.S., Frye, M.A. (in review, Curr. Biol.). *Cosmopolitan and cactophilic Drosophila species implement divergent visual tracking strategies.*

Rimniceanu, M., Currea, J.P., Frye, M. A. 2023. *Proprioception Gates Visual Object Fixation in Flying Flies*. Curr. Biol. 33, 1459–1471.e3

Caron, D., Rimniceanu, M., Scibelli, A.E., Trimmer, B.A. 2020. *Nociceptive neurons respond to multimodal stimuli in Manduca sexta*. J. Exp. Biol. 223. jeb218859.

Stadele, C., Rimniceanu, M., Frye M.A. 2019. *Drosophila Neuroscience: Should I land or should I jump?*. Curr. Biol. Dispatch. 29. R1089-R1091.

CONFERENCE PRESENTATIONS

Rimniceanu, M., Limbania, D., Wasserman S.M., Frye, M.A. 2023. *Visual ecology shapes object pursuit behaviors across forest and desert-dwelling Drosophilids*. Gordon Research Conference in Neuroethology, Mount Snow, VT.

Rimniceanu, M., Frye, M.A. 2023. *Proprioceptive body-state feedback modulates visual object tracking in D. melanogaster flight*. Bio-Inspired Sensing: Collaborative International Teams Workshop, Washington D.C.

Rimniceanu, M., Frye, M.A. 2022. *Proprioceptive body-state feedback modulates visual object tracking in D. melanogaster flight*. International Congress of Neuroethology, Lisbon, Portugal.

Rimniceanu, M., Frye, M.A. 2021. *I just need a little feedback! The role of body-state signaling on visual object-tracking in D. melanogaster flight*. Illinois State Univ., Neuroscience and Physiology Seminar

Rimniceanu, M., Sponberg, S*.,* 2019. *Moths are distractible fliers – Combining Visual Cues in a Cluttered Sensory Environment.* Society for Integrative Biology Annual Meeting, Tampa, FL.

Rimniceanu, M., Scibelli, A.E., Trimmer, B.A. 2017. *Local Thermosensation in the tobacco hornworm, Manduca sexta*. Society for Integrative Biology Annual Meeting, New Orleans, LA.

AWARDS & FELLOWSHIPS

UCLA Life Science Excellence in Research Award, 2024

UCLA Edith Hyde Fellowship, 2023 - $40,600

UCLA Biosciences Dissertation Year Fellowship, 2023 - $20,000

UCLA Brain Research Institute Travel Award, 2023

Bio-Inspired Sensing: Collaborative International Teams (BISCIT) Travel Award, 2023

UCLA Summer Mentored Research Fellowship (SMRF), 2021 - $6,000

SICB Div. for Neuroethology and Sensory Biology Finalist in Best Student Presentation, 2019

Tufts University Highest Honors Senior Honors Thesis, 2017

SICB Travel Award, 2017, 2019

Tufts University Nelson Summer Scholars Fund, 2016 - $5,500

General Electric (GE) STAR Award, 2013 - $2,500

MENTORSHIP

Sarah M. Fatkin, 2019-2020	UCLA Undergraduate Neuroscience Major, awarded Scheibel Scholarship for Undergraduate Neuroscience Research ($10,500), now Biosciences Graduate Student at UCLA
Gabriella Small, 2018	REU Student, now Biomechanics Graduate Student at UT Austin

TEACHING

Univ. California Los Angeles, Los Angeles, CA
Teaching Assistant - Anatomy & Physiology of Sense Organs, Spring 2020, 2021
Organized and led discussion sections analyzing primary literature related to course content. Adapted course content for online instruction via Zoom in the first COVID-19 remote course iteration. Explored and tailored teaching strategies through participation in pedagogy course.

Tufts University Academic Resource Center, Medford, MA
Tutor & Study Group Leader - Chemistry, Biology, Genetics, Neurobiology, 2014-2017
Instructed first and second year science students in foundational principles of biology in peer groups. Led weekly discussions and facilitated a dynamic conductive to higher-level analysis of course concepts. Developed individualized study and time management strategies based on student needs. Advised students on career options, course selection and personal scientific development.

Chapter 1

How flying flies track objects

Watch out for that tree! The evolution and challenges of visual object-tracking

Each animal's unique version of the physical world it inhabits is constructed from information derived from its sense organs. The continuous stream of sensory information it has access to depends on the properties of the physical environment; the sensory apparatus evolved to detect it and the neural circuits that parse and interpret it. As nature is not static, the ability to actively sense changes in the environment, both locally and globally, is critical to initiate and guide behaviors that sustain survival. Among these, locomotion is one of the most adaptive, subserving navigation, predator avoidance, foraging and reproductive functions. The process by which sensory information results in motor decisions and actions, termed sensorimotor transduction, is a key function of animal brains that is yet to be fully understood, even within the less complex brains in the animal kingdom. This is broadly the topic of this dissertation.

In interacting with the world, animal brains have access to a wealth of information across multiple sensory channels at the same time. At a given time, some channels are more relevant than others, depending on the animal itself, its life stage, internal and external context, and, of course, its ecology. Vision is one of the most fundamental and most elaborated senses, with evolution driving a myriad of designs that exploit various optical principles across phyla. As humans are highly visual creatures, it is intuitive for us to imagine how vision largely defines our sensory world - indeed even the construct of imagining in our brains is in the visual modality. As far as we know, the evolution of the first rudimentary eyes capable of detecting photons took place during the Cambrian explosion, around 0.5 billion years ago [1]. The simplest opsin-based systems capable of detecting light supported basic functions like circadian rhythm regulation and phototaxis. Through sequential evolutionary steps, compound and camera-lens eyes then endowed animals with acute spatial vision that provided detailed information about the environment, enabling planned movement and expanding an animal's sensory volume [2]. As a

long-range sensory modality, it is hypothesized that high quality vision enabled animals to look ahead, both figuratively and literally, giving them a competitive advantage that fueled a predator-prey arms race. In turn, this promoted the diversification of not only more complex visual systems but also brain complexity in general [1,3].

The animal kingdom is rich in specializations for various visual tasks. Among these, identifying and responding to ethologically relevant objects supports complex behaviors, from the commonplace “I am approaching a perch - I ought to engage my landing gear” to the colorful jumping spider mating displays where a female visually centers a male’s frontal legs on her fovea in order to assess the quality of his mating display and make a mate-choice decision. For objects to convey the most information, they must be foveated, or fixated in the visual field of view that has the highest acuity. However, a central challenge to visual systems is that objects are often moving within moving, cluttered panoramas. This is because animals are constantly in motion, therefore relative to them, the visual scene is a complex and dynamic sensory environment. This generates “large-field” patterns of optic flow cues on the retina that must first be stabilized before “small-field” object movement can be discriminated from the background using relative motion and other cues. Stabilization of large-field motion therefore precludes object tracking and the interplay between these two demands to the visual system is an active area of research.

Flight control: A balance between gaze stabilization and object tracking

The survival and success of visual animals is dependent on minimizing image motion blur and generating directed behaviors towards or away from relevant features. Classical modeling efforts define gaze stabilization as an “inner-loop” reflexive process that is always active, generating small corrective optomotor maneuvers to keep the eyes still, maintaining acuity. In primates, smooth movements of the eyes and head comprise the optokinetic reflex

that helps stabilize visual images on the retina when an observer moves relative to the stationary visual scene, either voluntarily or involuntarily. Insect flight control, the timescale of which demands rapid and robust computations, has provided a useful platform to probe the fundamental computations underlying this reflex [4–6]. In the face of an external perturbation, such as a gust of wind, luminance-sensitive visual circuits that comprise theoretical elementary motion detectors (EMDs), detect a “slip” as the world moves relative to the body. In flies, this is implemented in parallel ON and OFF pathways originating in the lamina, the first visual neuropil receiving direct input from the retina, which pool their regional inputs to directionally-selective T4 and T5 cells in the medulla and lobula plate neuropils [7–9]. These columnar neurons supply large-field directionally selective lobula plate tangential cells (LPTCs), namely horizontal system (HS) and vertical system (VS) cells, where optic flow cues about the 6 axes of body rotation and translation are encoded [10–12]. Several classes of LPTCs ultimately relay their signals to populations of descending neurons (DNs) which modulate motoneurons that trim wing and head steering responses to maintain stable flight [13–15].

This well-described motion-sensitive pathway is responsible for continuous course control. Yet, across vertebrates and invertebrates alike, course control does not look like a completely smooth continuous process. Rather, given panoramic rotational motion in the horizontal yaw plane, emergent flight behavior is an alternation of co-directional smooth tracking of the visual panorama, punctuated by counter-directional nystagmus and syn-directional catch-up saccades where gaze is rapidly and ballistically shifted in response to retinal slip error buildup [16,17]. The mathematical model explaining this emergent behavior is therefore a “hybrid system” comprising two control strategies which use both velocity (motion) and positional cues to maintain stable gaze [18,19]. The two components of this hypothesized hybrid controller are classically modeled as “inner-loop” stabilization reflexes that generate smooth pursuit, on top of which “outer-loop” positional responses support whole-body re-orientation maneuvers, either for stabilization purposes or for broader object-related behaviors. Conceptually, only once ground

motion is stabilized, can voluntary outer-loop higher level detection of salient moving cues ensue. Detection of moving targets, the second fundamental motion visual process that is critical to survival, is therefore layered on top of gaze stabilization and constantly interacting with the optomotor reflex. Goal-directed saccadic maneuvers serve to shift gaze towards or away from small-field ecologically relevant features, such as predators, conspecifics, shelters, or perches [19,20]. Despite object tracking being ubiquitous across species, its behavioral control and neural correlates remain much less understood.

As one of the most high-performance object pursuit behaviors observed in nature, insect aerial predation is leveraged in classical studies aiming to understand the complex computations that subserve object-directed behaviors. Predatory insects such as robber flies, hoverflies and dragonflies engage in elaborate high-speed chases where smaller prey flies are fixated in a high-acuity region of the retina and intercepted at a success rate of >95%, largely through the action of small-target motion detectors (STMDs) in the lobula complex [21–23]. The STMD neuron class, akin to mammalian hypercomplex cells [24], comprises cell types responsive to a range of small object sizes and shapes, as well as some classes that are inhibited by widefield motion while others are not [25]. Overall, these feature-detecting neurons are tuned to small, fast moving objects and can detect object motion within moving background clutter, presumably due to both high contrast sensitivity and using relative motion cues [26–28]. One particularly impressive example of this class of neuron is the dragonfly centrifugal STMD 1 neuron (CSTMD1), which selectively “locks" onto a moving target and has the ability to switch targets given multiple competing cues [29,30]. A population vector encoding not only the target’s dynamics but also its future position is then relayed from STMDs to wing motor centers via target-selective descending neurons (TSDNs) to coordinate the interception maneuver [31].

Fixation, or the process of actively centering and tracking moving objects, however, does not occur exclusively in predatory insects. Though its direction and time course differ with the ethological needs, visual object fixation has been described as a robust behavior across model

systems [23,32–37]. For a flying fruit fly, small objects represent predators and therefore elicit avoidance responses, while vertically elongated features, likely representing trees or plant stalks, are readily centered in the field of view and approached [38]. In *Drosophila*, while pathways specialized for object- directed behaviors are not yet fully characterized, several lobula columnar (LC) neuron classes have been described to selectively respond to small objects, or objects that are rapidly expanding on the retina and result in either escape or landing responses [39–44]. Notably, upstream of the lobula, small-field sensitive T3 columnar neurons have been recently associated with the saccadic pursuit of vertical bar objects, presumably through connections with LC populations [45]. This pathway may control bar pursuit through as few as 2 distinct pairs of descending neurons that elicit tracking saccades, though the full circuit remains to be described [46].

Flight trajectories observed in free flight paradigms clearly demonstrate that flies reliably track vertical edges, or bars, producing orientation responses that center the object in the frontal field of view [38,47,48]. In order to probe the computations underlying this robust behavior, animals are typically tethered to a rigid pin and placed in a drum-shaped visual flight simulator. In such an assay, the visual feedback loop can be open and the difference in wing stroke amplitude, the fly's wing steering torque, is quantified. Under open-loop feedback conditions, flies produce powerful smooth steering responses in the direction of a bar [49,50]. Alternatively, the visual feedback loop can be artificially closed such that steering torque is multiplied by a gain factor to control the angular velocity of the bar, allowing the animal to essentially control its position relative to its visual field of view. Presenting a fly tethered in such a paradigm with a dark vertical stripe, reliably results in the fly performing turning maneuvers towards the stripe and fixating it on visual azimuth [33,35,51]. This behavior persists in the face of various optic flow cues, even when the motion of the ground opposes that of the stripe, for bars with complex spatial properties, or motion cues such as flicker, counter-directional motion and higher order cues

[49,50,52–54]. In fact, active bar fixation is so powerful a tethered fly has been shown to steer to fixate a bar on visual midline for up to 36 hours [55].

Conceptually, an object moving relative to an observer generates both a position and a velocity cue. Classical models posit that outer-loop object fixation requires relative motion cues and arises due to a sensitivity to object velocity [52,56]. Contemporary behavioral studies support the hypothesis that velocity can sufficiently drive the strong object responses observed in the aforementioned assays. Using only small-field EMDs sensitive to motion on visual midline, akin to the receptive field properties of “FD” neurons [57], combined with a steering asymmetry where back-to-front stimuli elicit stronger responses than front-to-back motion, one can account for frontal object centering in body-fixed preparations [58,59]. Yet, recent mechanistic studies demonstrated that silencing the small-field motion detectors T4/T5 does not eradicate bar tracking in more naturalistic paradigms [45,60]. Indeed, the readily observed preponderance of body saccades in object pursuit behaviors across species suggests that an alternative motion-independent pathway also modulates how objects are fixated [16,61].

In animals as diverse as insects, arthropods and primates, when the velocity of a target velocity is too high for a smooth velocity-driven system to keep up, a positional error signal will build and eventually trigger a rapid ballistic saccade [23,61]. An object-directed saccade is a predictive maneuver. The future position of the cue is pre-programmed since the visual system is necessarily offline during the saccadic turn - in order to voluntarily redirect gaze towards objects, corrective optomotor movements must be temporarily suppressed [62,63]. Indeed, a recent study in robber flies supports the hypothesis that this predictive maneuver is achieved using both position and velocity cues [64]. Though the interplay between velocity-based smooth pursuit and position-triggered saccadic tracking of moving objects is an active area of research, their relative contribution to object-directed behavior remains unclear. The studies in Chapter 2 challenge the notion that *D. melanogaster* use both smooth and saccadic pursuit for object

tracking, demonstrating that smooth pursuit of objects is an epiphenomenon arising specifically due to the body-fixed nature of classical behavioral paradigms.

I just need a little feedback! Multisensory modulation of visual object pursuit

The computations that govern visual flight control must be robust yet flexible to environmental demands. In a cluttered and dynamic environment, visual processes are highly modular. Both inner-loop stabilization reflexes and outer-loop object pursuit are shaped by multimodal cues and are highly context-dependent. In host-seeking mosquitoes, for example, a CO_2 chemical cue modulates the salience of visual features, helping enhance navigation towards high-contrast small objects [65]. In *D. melanogaster*, an attractive odorant boosts the gain of smooth responses to optic flow cues [66,67] acting at the level of LPTCs likely through the neuromodulatory role of octopamine, the insect analog of noradrenaline [68]. Because large-field integrators themselves are in part sensitive to vertical objects, it is perhaps unsurprising that this gain modulation is accompanied by an increase in bar approach responses [65,69]. This same odor cue can reverse the response to a small object, making this innately aversive cue attractive to *D. melanogaster* [69]. Thus, olfactory feedback signals a context-change and mediates a switch in visuomotor processing, turning a potential predator into a potential food source.

Mechanosensory modulation of flight control has enjoyed a rich research history, in part due to relatively well understood sensor physiology and ease of electrophysiological access in larger non-model insects such as blow flies. The aerodynamic forces typically experienced in flight are detected through a suite of external sense organs, including tactile hairs and campaniform sensilla, in which mechanical force directly gates ion channels on the single sensory neurons that innervate them. The electrical currents produced by forces and deflections can be directly recorded at the receptor itself, as well as at processing bottlenecks such as the

wing hinge where population activity encodes general wing-bending forces [70–73]. Due to sensor dynamics, mechanosensory cues convey locomotor state on fast and reliable timescales. Walking behavior drives extra-visual responses by HS cells that correlate to forward walking velocity with latencies of only a few milliseconds [74,75]. As an animal initiates flight, the gain of large-field optic-flow sensitive VS neurons doubles, presumably to support the transition to high-velocity optic flow [76]. During active flight, proprioceptive feedback is critical to monitor the animal's body position and movement in space, both to coordinate voluntary maneuvers as well as to stabilize the system upon external perturbation. In Diptera, there are numerous mechanosensory organs that encode body dynamics during flight, including the wings, antennae, and most notably the gyroscopic haltere organs [77–81].

Halteres are reduced hindwings, evolved into tiny club-shaped structures behind the front pair of wings. While they serve no aerodynamic purpose, halteres are highly sensitive to inertial forces detected using precisely organized fields of campaniform sensilla strain sensors at their base [82]. They beat back and forth 180° out of phase with the wings to provide stroke-to-stroke feedback on the scale of 2-5 ms to the wing motor system via direct electrotonic connections [83]. Haltere feedback is uniquely suited to adjust the firing phase of wing motor neurons and thus continuously sculpt wing kinematics [84]. Halteres are part of a complex dynamical system integrating multisensory information at many levels of sensory processing. In addition to passively sensing inertial rotational forces, halteres are actuated by steering and power muscles whose activity is gated by descending (efferent) visual input in yaw, pitch and roll [85]. The afferents from their campaniform sensilla fields make local synapses within the ventral nerve cord (VNC), in addition to projecting to sensory bottleneck areas in the central brain such as the gnathal ganglion (GNG) that are densely innervated with pre- and postsynaptic descending neurons [86,87]. Haltere oscillations are even represented in the central complex, a multisensory navigational hub across Diptera, making them strong candidates for

integrating mechanosensory and visual sensory feedback [88]. Their extensive network connections suggest important and multifunctional roles in coordinating visuomotor maneuvers in flight, yet these anatomical projections remain to be functionally characterized.

The proper functioning of haltere feedback circuits is so critical that flies with ablated halteres cannot initiate or maintain stable flight. This likely arises because the halteres are deeply implicated in ground stabilization reflexes through their strong coupling with wing motor centers and neck motor control. Physiological studies in *Calliphora* indicate that information from visual and haltere channels converges in neck motor areas, likely in a nonlinear manner, to control gaze stabilization [89–91]. In *Drosophila* tethered flight preparations, ablating or reducing the mass of halteres increases variability and baseline noise in wing steering torques [92,93]. Further, desynchronizing the haltere and wing motor system produces similar effects [93]. The visual and mechanosensory systems operate on complementary time scales. Visual sensory feedback is low-pass, as metabotropic phototransduction is a relatively slow multi-synapse process. By contrast, mechanosensors relay rapid feedback via ionotropic signaling and electrical synapses. Sensory fusion across these two feedback channels helps tune flight visuomotor flight control across a larger frequency band of angular velocities relevant to behavior [94]. While the precise populations of neurons performing this computation remain unknown, a model integrating visual and mechanosensory feedback during gaze stabilization suggests that the sensory channels are differentially weighted such that the presence of even a small amount of mechanosensory feedback decreases the gain of visual responses [81]. But what adaptive advantage does mechanosensory gain modulation impart to flight control?

The studies described in this dissertation, alongside several lines of evidence, suggest that fast latency mechanosensory feedback actively damps high-gain visual responses, which is critical to maintaining stable flight. Conceptually, active damping serves to impart stability and robustness to inherently unstable biological systems in which small changes in gain and timing

phase can push the system into an unstable regime [61]. In a dynamically scaled robotic fruit fly model, mechanosensory feedback delays on the time scale of a single wing stroke can destabilize yaw velocity control. Thus, this feedback channel is proposed to actively damp yaw rate, thereby imparting the high gain visuomotor control system with robustness and stability [95]. In a well-tuned feedback system, perturbing compensatory active damping, as would occur by body-fixing a fly and/or compromising proprioceptive signaling, would be expected to extend the duration of yaw dynamics beyond those seen under free flight conditions [95]. The studies in Chapter 3 aim to mechanistically test the hypothesis that the haltere proprioceptive feedback channel actively damps velocity-driven smooth responses to objects in *D. melanogaster* - in its absence, the smooth responses to object motion observed in body-fixed paradigms may arise.

Visual object pursuit through the lens of visual ecology

As demonstrated in Chapters 2 and 3 of this dissertation, both at the level of neural computations and at the level of emergent behavior, the manner in which navigational objects and ground motion cues are interpreted by the nervous system is not hard-wired. Rather, object responses are flexibly modulated by multisensory context, with naturalistic proprioceptive feedback playing a crucial role. The multisensory modulation of visual processing pathways we describe is adaptive, as the neural control can truly be split across inner and outer loop tasks. However, a split hybrid control architecture is highly sensitive to the spatial properties of both panoramic ground and the object to be pursued. While it is tempting to think of large-field ground motion and small-field objects as inherently distinct cues in a moving visual scene, objects are defined by the environment they are in and this distinction between the two is often ambiguous and context-dependent. Elementary motion detectors are optimally tuned to dark edges moving across the retina [9,96,97]. If the wide field panorama does not sufficiently drive the smooth gaze stabilization motion pathway or conversely if the objects' spatial properties drive

the motion pathway very strongly, the contribution of smooth tracking and saccadic pursuit to object responses may be leaky. Width of a feature, for example, is a defining characteristic that modulates whether the object is processed as a figure or a ground cue. Increasing the width of a motion-defined bar progressively switches the tracking strategy from predominantly saccadic "bar" pursuit to predominant smooth "optomotor" pursuit [16].

To explore how the spatial features of the environment shape visual processing, chapter 4 will consider whether and how the visual ecology of an animal affects object pursuit strategies. Much of our understanding of figure-ground discrimination during active flight comes from studies carried out in the widely used model system *D. melanogaster*. This fly species originated in sub-Saharan Africa and radiated outward starting 10,000 years ago to colonize essentially all niches where climate conditions are favorable [96,97]. *D. melanogaster* is an ecological generalist that is part of the "cosmopolitan guild" of the *Sophophora* subgenus of *Drosophila*, feeding and breeding on varied decomposing fruit matter, which contributes to their success in diverse environments [98,99]. As a human commensal, *D. melanogaster* is adapted to cluttered visual environments such as forests and, more recently, city landscapes. Such ecologies present a complex figure-ground discrimination challenge as they are largely composed of diverse vertical elongated features that both define the panoramic ground but can also represent potentially relevant objects within the panorama. In a naturalistic body state context, *D. melanogaster* solves this challenge by adapting their control mechanism to neurally and computationally separate pathways to stabilize gaze and track objects. In a flying animal, this results in alternation between engaging the ground using smooth dynamics and engaging the object of interest using ballistic saccades.

Visual clutter is not a defining feature of all visual landscapes, however. By contrast to cosmopolitan *D. melanogaster*, *Drosophila mojavensis* is a Drosophilid whose natural history resulted in specialization to visually sparse desert climates. Separated from *D. melanogaster* by approximately 30 million years, these members of the repleta species subgroup first radiated in

South America and specialized on fermenting cacti [100,101]. Today, four geographically separated subspecies comprise the *D. mojavensis* species. Within these, *D. moj. baja* and *D. moj. moj* are hypothesized to have diverged approximately 250,000 years ago and specialize on agria cacti (*Stenocereus gummosus*) and barrel cacti (*Ferocactus cylindraceus*), respectively [100,102,103]. The host cacti of both subspecies are native to bright, barren desert environments where there are relatively fewer vertical features available. These sparse features comprise both optic flow cues and salient landscape cues representing navigational landmarks such as feeding and breeding sites. Thus, Chapter 4 tests the hypothesis that adaptation to such ecologies shifts the demands on widefield motion-sensitive pathways and feature-detecting pathways, resulting in categorically distinct object tracking strategies across cosmopolitan and desert-adapted *Drosophila* species.

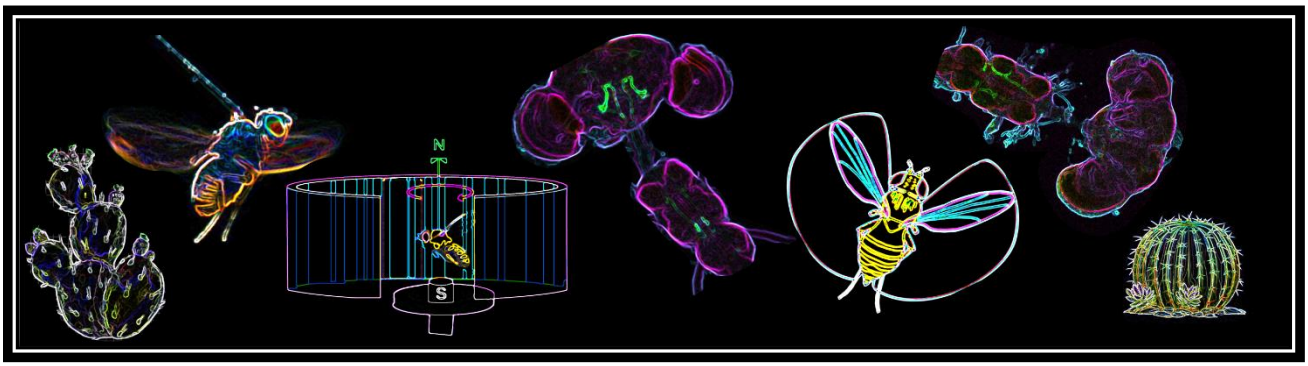

This dissertation uses the genetic model system *D. melanogaster*, along with closely related species, to investigate the roles of smooth continuous and saccadic discontinuous pursuit in bar-tracking behavior. The insect model system enjoys a rich history in the field of visual flight control. Fortunately, the toolkit available to test hypotheses, both at the level of ecologically relevant behavior and that of neurophysiology, has rapidly advanced in *D. melanogaster* over the last decade. Rather than describing behavioral algorithms in highly restrictive body-fixed paradigms, the development of a “yaw-free” magnetic tethering paradigm

now allows movement and naturalistic body cues in one plane of motion. Recent work in this adapted apparatus showed that flies surprisingly react very little to object motion across visual midline, contrary to predictions from body-fixed paradigms over the last 60 years [16,104].

Chapter 2 of this dissertation follows up on this study and addresses whether and how smooth control is used in *D.melanogaster* for object tracking. Here, I will present evidence that challenges the notion that freely flying flies in naturalistic settings superpose both motion-sensitive and position-sensitive subsystems to track objects [56,59], a control architecture that is supported by data from body-fixed flies [59]. I demonstrate that yaw-free flies do not frontally fixate a motion-defined bar and that this arises because robust motion-driven smooth steering responses to bars are eradicated in flies experiencing body dynamics present in true flight. A primary goal of Chapter 2 is to highlight that carrying out experiments in more naturalistic contexts is critical to understanding behavior and its underlying mechanisms [105].

Chapter 3 sets up studies that aim to describe how the phenomenon discovered in Chapter 2 arises at the level of neural circuits and mechanisms. From the history of studies that implicate them in yaw rate control and visuomotor integration, one can speculate that haltere afferent pathways are sensitive to changes in body-state and may play an active damping role in stabilizing visual responses. Chapter 3 posits that feedback in the proprioceptive modality modulates the contribution of motion and position pathways to object pursuit behavior. In this model, the removal of real body-state feedback cues biases the object-pursuit control strategy towards the motion sensitive smooth pursuit controller. Conversely, the mere presence of naturalistic body-state feedback, irrespective of visual feedback, offloads object pursuit to the position-sensitive saccadic controller. In this case, proprioceptive feedback may essentially act as a switch to gate visual processing pathways that drive object responses. Here, I present preliminary evidence from circuit-breaking studies that supports this hypothesis, describe the

generation of novel genetic reagents and propose physiological studies to test the proposed role of haltere-mediated active damping in modulating object pursuit behaviors.

Finally, Chapter 4 explores how the visual ecology an animal operates in is highly relevant to the visuomotor flight control mechanism, particularly in the case of adaptive object fixation behaviors. It would appear that cosmopolitan *D. melanogaster* is best suited to flying through a visually cluttered panorama with broadband small field objects, such as a high tree canopy, and therefore necessarily separates smooth gaze stabilization and saccadic object pursuit mechanisms. The ground is stabilized using smooth dynamics and objects are tracked using spatiotemporal integration cues that trigger saccades. This object tracking strategy is odd in that it heavily favors saccades at the expense of smooth pursuit, while most other seeing systems among humans and arthropods alike combine the two strategies to track objects. This provokes the question: is the "spatiotemporal integration" rule describing saccadic object tracking in *D. melanogaster* the norm among dipterans? In this chapter, I present evidence supporting the hypothesis that, much like our own visual target pursuit strategy, desert-adapted Mojavensis subspecies that negotiate visually sparse environments appear to fuse the smooth pursuit and saccadic controllers, resulting in high gain smooth responses to object motion that work in tandem with saccadic pursuit.

Overall, this dissertation expands on our current understanding of how visual object pursuit is accomplished in visual pathways that are highly modular and critically sensitive to multisensory and adaptive environmental demands. By integrating techniques from comparative behavior and modeling to circuit analysis and neurophysiology, I aim to underline the importance of internal and external context in shaping a complex and robust flight behavior that supports critical adaptive behaviors yet remains poorly understood across phyla.

References

1. Land, M.F., and Nilsson, D.E. (2002). Animal Eyes (Oxford University Press).

2. Nilsson, D.E. (2009). The evolution of eyes and visually guided behaviour. Philos. Trans. R. Soc. Lond. B Biol. Sci. *364*, 2833–2847.

3. Zhao, F., Bottjer, D.J., Hu, S., Yin, Z., and Zhu, M. (2013). Complexity and diversity of eyes in early Cambrian ecosystems. Sci. Rep. *3*, 2751.

4. Hassenstein B, R.W. (1956). Systemtheoretische Analyse der Zeit-, Reihenfolgen- und Vorzeichenauswertung bei der Bewegungsperzeption des Rüsselkäfers Chlorophanus. Zeitschrift fu r Naturforsch B.

5. Borst, A., and Haag, J. (2002). Neural networks in the cockpit of the fly. J. Comp. Physiol. A Neuroethol. Sens. Neural Behav. Physiol. *188*, 419–437.

6. Mauss, A.S., and Borst, A. (2020). Optic flow-based course control in insects. Curr. Opin. Neurobiol. *60*, 21–27.

7. Joesch, M., Schnell, B., Raghu, S.V., Reiff, D.F., and Borst, A. (2010). ON and OFF pathways in Drosophila motion vision. Nature *468*, 300–304.

8. Strother, J.A., Wu, S.-T., Wong, A.M., Nern, A., Rogers, E.M., Le, J.Q., Rubin, G.M., and Reiser, M.B. (2017). The Emergence of Directional Selectivity in the Visual Motion Pathway of Drosophila. Neuron *94*, 168–182.e10.

9. Maisak, M.S., Haag, J., Ammer, G., Serbe, E., Meier, M., Leonhardt, A., Schilling, T., Bahl, A., Rubin, G.M., Nern, A., et al. (2013). A directional tuning map of Drosophila elementary motion detectors. Nature *500*, 212–216.

10. Schnell, B., Joesch, M., Forstner, F., Raghu, S.V., Otsuna, H., Ito, K., Borst, A., and Reiff, D.F. (2010). Processing of Horizontal Optic Flow in Three Visual Interneurons of the Drosophila Brain. J. Neurophysiol. *103*, 1646–1657.

11. Blondeau, J., and Heisenberg, M. (1982). The three-dimensional optomotor torque system ofDrosophila melanogaster. J. Comp. Physiol. *145*, 321–329.

12. Krapp, H.G., and Hengstenberg, R. (1996). Estimation of self-motion by optic flow processing in single visual interneurons. Nature *384*, 463–466.

13. Palmer, E.H., Omoto, J.J., and Dickinson, M.H. (2022). The role of a population of descending neurons in the optomotor response in flying Drosophila. bioRxiv, 2022.12.05.519224. 10.1101/2022.12.05.519224.

14. Zhao, A., Nern, A., Koskela, S., Dreher, M., Erginkaya, M., Laughland, C.W., Ludwigh, H., Thomson, A., Hoeller, J., Parekh, R., et al. (2023). A comprehensive neuroanatomical survey of the Drosophila Lobula Plate Tangential Neurons with predictions for their optic flow sensitivity. bioRxiv. 10.1101/2023.10.16.562634.

15. Wei, H., Kyung, H.Y., Kim, P.J., and Desplan, C. (2020). The diversity of lobula plate tangential cells (LPTCs) in the Drosophila motion vision system. J. Comp. Physiol. A. *206*, 139–148.

16. Mongeau, J.-M., and Frye, M.A. (2017). Drosophila Spatiotemporally Integrates Visual Signals to Control Saccades. Curr. Biol. *27*, 2901–2914.e2.

17. Cellini, B., and Mongeau, J.-M. (2020). Active vision shapes and coordinates flight motor responses in flies. Proc. Natl. Acad. Sci. U. S. A. *117*, 23085–23095.

18. Bausenwein, B., Wolf, R., and Heisenberg, M. (1986). Genetic dissection of optomotor behavior in Drosophila melanogaster. Studies on wild-type and the mutant optomotor-blindH31. J. Neurogenet. *3*, 87–109.

19. Cellini, B., and Mongeau, J.M. (2020). Hybrid visual control in fly flight: insights into gaze shift via saccades. Preprint at Elsevier Inc., 10.1016/j.cois.2020.08.009 10.1016/j.cois.2020.08.009.

20. Hardcastle, B.J., and Krapp, H.G. (2016). Evolution of Biological Image Stabilization. Curr. Biol. *26*, R1010–R1021.

21. Olberg, R.M. (2012). Visual control of prey-capture flight in dragonflies. Curr. Opin. Neurobiol. *22*, 267–271.

22. Collett, T.S., and Land, M.F. (1975). Visual control of flight behaviour in the hoverfly Syritta pipiens L. Journal of Comparative Physiology A *99*, 1–66.

23. Land, M.F., and Collett, T.S. (1974). Chasing behaviour of houseflies (Fannia canicularis). J. Comp. Physiol. *89*, 331–357.

24. Hubel, D.H., and Wiesel, T.N. (1962). Receptive fields, binocular interaction and functional architecture in the cat's visual cortex. J. Physiol. *160*, 106–154.

25. Nordström, K., and O'Carroll, D.C. (2006). Small object detection neurons in female hoverflies. Proc. Biol. Sci. *273*, 1211–1216.

26. Nordström, K., Barnett, P.D., and O'Carroll, D.C. (2006). Insect detection of small targets moving in visual clutter. PLoS Biol. *4*, e54.

27. Nordström, K. (2012). Neural specializations for small target detection in insects. Preprint, 10.1016/j.conb.2011.12.013 10.1016/j.conb.2011.12.013.

28. O'Carroll, D. (1993). Feature-detecting neurons in dragonflies. Nature *362*, 541–543.

29. Wiederman, S.D., and O'Carroll, D.C. (2013). Selective attention in an insect visual neuron. Curr. Biol. *23*, 156–161.

30. Geurten, B.R.H., Nordström, K., Sprayberry, J.D.H., Bolzon, D.M., and O'Carroll, D.C. (2007). Neural mechanisms underlying target detection in a dragonfly centrifugal neuron. J. Exp. Biol. *210*, 3277–3284.

31. Gonzalez-Bellido, P.T., Peng, H., Yang, J., Georgopoulos, A.P., and Olberg, R.M. (2012). Eight pairs of descending visual neurons in the dragonfly give wing motor centers accurate population vector of prey direction. Proc. Natl. Acad. Sci. U. S. A. 10.1073/pnas.1210489109.

32. Kennedy, J.S. (1940). The visual responses of flying mosquitoes. Proc. Zool. Soc. Lond. *A109*, 221–242.

33. Reichardt, W., and Wenking, H. (1969). Optical detection and fixation of objects by fixed flying flies. Naturwissenschaften, 424.

34. Land, B.Y.M.F. (1971). Orientation by Jumping Spiders in the Absence of Visual Feedback. Journal of Experimental Biology, 119–139.

35. Virsik, R.P., and Reichardt, W. (1976). Detection and Tracking of Moving Objects by the Fly Musca domestica. Biol. Cybern. *23*, 83–98.

36. Baker, P.S. (1979). Flying locust visual responses in a radial wind tunnel. J. Comp. Physiol. *131*, 39–47.

37. Lönnendonker, U. (1991). Dynamic Properties of Orientation to a Visually Fixated Target by Walking Colorado Beetles.

38. Maimon, G., Straw, A.D., and Dickinson, M.H. (2008). A simple vision-based algorithm for decision making in flying Drosophila. Curr. Biol. *18*, 464–470.

39. Ribeiro, I.M.A., Drews, M., Bahl, A., Machacek, C., Borst, A., and Dickson, B.J. (2018). Visual Projection Neurons Mediating Directed Courtship in Drosophila. Cell *174*, 607–621.e18.

40. Keleş, M.F., and Frye, M.A. (2017). Object-Detecting Neurons in Drosophila. Curr. Biol. *27*, 680–687.

41. Klapoetke, N.C., Nern, A., Rogers, E.M., Rubin, G.M., Reiser, M.B., and Card, G.M. (2022). A functionally ordered visual feature map in the Drosophila brain. Neuron *110*, 1700–1711.e6.

42. Städele, C., Rimniceanu, M., and Frye, M.A. (2019). Drosophila Neuroscience: Should I Land or Should I Jump? Curr. Biol. *29*, R1089–R1091.

43. Ache, J.M., Namiki, S., Lee, A., Branson, K., and Card, G.M. (2019). State-dependent decoupling of sensory and motor circuits underlies behavioral flexibility in Drosophila. NAtuRe NeuRoSCieNCe | *22*, 1132–1139.

44. Ache, J.M., Polsky, J., Alghailani, S., Parekh, R., Breads, P., Peek, M.Y., Bock, D.D., Von Reyn, C.R., and Card, G.M. (2019). Neural Basis for Looming Size and Velocity Encoding in the Drosophila Giant Fiber Escape Pathway In Brief. Curr. Biol. *29*. 10.1016/j.cub.2019.01.079.

45. Frighetto, G., and Frye, M.A. (2023). Columnar neurons support saccadic bar tracking in Drosophila. Elife *12*. 10.7554/eLife.83656.

46. Ros, I.G., Omoto, J.J., and Dickinson, M.H. (2024). Descending control and regulation of spontaneous flight turns in Drosophila. Curr. Biol. *34*, 531–540.e5.

47. Frye, M.A., Tarsitano, M., and Dickinson, M.H. (2003). Odor localization requires visual feedback during free flight in Drosophila melanogaster. J. Exp. Biol. *206*, 843–855.

48. van Breugel, F., and Dickinson, M.H. (2012). The visual control of landing and obstacle avoidance in the fruit fly Drosophila melanogaster. J. Exp. Biol. *215*, 1783–1798.

49. Theobald, J.C., Shoemaker, P.A., Ringach, D.L., and Frye, M.A. (2010). Theta motion processing in fruit flies. Front. Behav. Neurosci. *4*, 35.

50. Fox, J.L., Aptekar, J.W., Zolotova, N.M., Shoemaker, P.A., and Frye, M.A. (2014). Figure-ground discrimination behavior in Drosophila. I. Spatial organization of wing-steering responses. J. Exp. Biol. *217*, 558–569.

51. Poggio, T., and Reichardt, W. (1973). A theory of the pattern induced flight orientation of the fly Musca domestica. Kybernetik, 185–203.

52. Reichardt, W., Poggio, T., and Hausen, K. (1983). Figure-ground discrimination by relative movement in the visual system of the fly. Biol. Cybern. *46*, 1–30.

53. Reiser, M.B., and Dickinson, M.H. (2010). Drosophila fly straight by fixating objects in the face of expanding optic flow. J. Exp. Biol. *213*, 1771–1781.

54. Theobald, J.C., Duistermars, B.J., Ringach, D.L., and Frye, M.A. (2008). Flies see second-order motion. Curr. Biol. *18*, R464–R465.

55. Götz, K.G. (1987). Course-Control, Metabolism and Wing Interference During Ultralong Tethered Flight in Drosophila Melanogaster. J. Exp. Biol. *128*, 35–46.

56. Reichardt, W., and Poggio, T. (1976). Visual control of orientation behaviour in the fly: Part I. A quantitative analysis. Q. Rev. Biophys. *9*, 311–375.

57. Egelhaaf, M. (1985). On the neuronal basis of figure-ground discrimination by relative motion in the visual system of the fly. Biol. Cybern. *52*, 195–209.

58. Fenk, L.M., Poehlmann, A., and Straw, A.D. (2014). Asymmetric processing of visual motion for simultaneous object and background responses. Curr. Biol. *24*, 2913–2919.

59. Aptekar, J.W., Shoemaker, P.A., and Frye, M.A. (2012). Figure tracking by flies is supported by parallel visual streams. Curr. Biol. *22*, 482–487.

60. Bahl, A., Ammer, G., Schilling, T., and Borst, A. (2013). Object tracking in motion-blind flies. Nat. Neurosci. *16*, 730–738.

61. Land, M.F. (1992). Visual tracking and pursuit: Humans and arthropods compared. J. Insect Physiol. *38*, 939–951.

62. Burr, D.C., Morrone, M.C., and Ross, J. (1994). Selective suppression of the magnocellular visual pathway during saccadic eye movements. Nature *371*, 511–513.

63. Fenk, L.M., Kim, A.J., and Maimon, G. (2021). Suppression of motion vision during course-changing, but not course-stabilizing, navigational turns. Curr. Biol. *31*, 4608–4619.e3.

64. Talley, J., Pusdekar, S., Feltenberger, A., Ketner, N., Evers, J., Liu, M., Gosh, A., Palmer, S.E., Wardill, T.J., and Gonzalez-Bellido, P.T. (2023). Predictive saccades and decision making in the beetle-predating saffron robber fly. Curr. Biol. *33*, 2912–2924.e5.

65. van Breugel, F., Riffell, J., Fairhall, A., and Dickinson, M.H. (2015). Mosquitoes Use Vision to Associate Odor Plumes with Thermal Targets. Curr. Biol. *25*, 2123–2129.

66. Chow, D., and Frye, M. (2008). Context-dependent olfactory enhancement of optomotor flight control in D.melanogaster. J. Exp. Biol. 10.1242/jeb.018879.

67. Chow, D.M., Theobald, J.C., and Frye, M.A. (2011). An olfactory circuit increases the fidelity of visual behavior. J. Neurosci. *31*, 15035–15047.

68. Wasserman, S.M., Aptekar, J.W., Larsen, C., and Correspondence, M.A.F. (2015). Olfactory Neuromodulation of Motion Vision Circuitry in Drosophila. Curr. Biol. *25*, 467–472.

69. Cheng, K.Y., Colbath, R.A., and Frye, M.A. (2019). Olfactory and Neuromodulatory Signals Reverse Visual Object Avoidance to Approach in Drosophila. Curr. Biol. *29*, 2058–2065.e2.

70. Elson, R.C. (1987). Interneuronal processing of inputs from the campaniform sensilla of the locust hindwing. Journal of Comparative Physiology A *161*, 761–776.

71. Dickinson, M.H. (1990). Comparison of encoding properties of campaniform sensilla on the fly wing. J. Exp. Biol. *151*, 245–261.

72. Tuthill, J.C., and Wilson, R.I. (2016). Mechanosensation and Adaptive Motor Control in Insects. Preprint at Cell Press, 10.1016/j.cub.2016.06.070 10.1016/j.cub.2016.06.070.

73. Pratt, B., Deora, T., Mohren, T., and Daniel, T. (2017). Neural evidence supports a dual sensory-motor role for insect wings. Proc. Biol. Sci. *284*. 10.1098/rspb.2017.0969.

74. Fujiwara, T., Cruz, T.L., Bohnslav, J.P., and Chiappe, M.E. (2017). A faithful internal representation of walking movements in the Drosophila visual system. Nat. Neurosci. *20*, 72–81.

75. Fujiwara, T., Brotas, M., and Chiappe, M.E. (2022). Walking strides direct rapid and flexible recruitment of visual circuits for course control in Drosophila. Neuron *110*, 2124–2138.e8.

76. Maimon, G., Straw, A.D., and Dickinson, M.H. (2010). Active flight increases the gain of visual motion processing in Drosophila. Nat. Neurosci. *13*, 393–399.

77. Straw, A.D., Tómasson, E., and Dickinson, M.H. (2011). Active and passive antennal movements during visually guided steering in flying Drosophila. Journal of.

78. Cellini, B., and Mongeau, J.-M. (2020). Hybrid visual control in fly flight: insights into gaze shift via saccades. Curr Opin Insect Sci *42*, 23–31.

79. Taylor, G.K., and Krapp, H.G. (2007). Sensory Systems and Flight Stability: What do Insects Measure and Why? In Advances in Insect Physiology, J. Casas and S. J. Simpson, eds. (Academic Press), pp. 231–316.

80. Sane, S.P., Dieudonné, A., Willis, M.A., and Daniel, T.L. (2007). Antennal mechanosensors mediate flight control in moths. Science *315*, 863–866.

81. Sherman, A., and Dickinson, M.H. (2004). Summation of visual and mechanosensory feedback in Drosophila flight control. J. Exp. Biol. *207*, 133–142.

82. Cole, E.S., and Palka, J. (1982). The pattern of campaniform sensilla on the wing and haltere of Drosophila melanogaster and several of its homeotic mutants. Development *71*, 41–61.

83. Pringle, J.W.S. (1948). The gyroscopic mechanism of the halteres of Diptera. Philos. Trans. R. Soc. Lond. B Biol. Sci. *233*, 347–384.

84. Fayyazuddin, A., and Dickinson, M.H. (1996). Haltere afferents provide direct, electrotonic input to a steering motor neuron in the blowfly, Calliphora. Journal of Neuroscience *16*, 5225–5232.

85. Dickerson, B.H., De Souza, A.M., Huda, A., and Dickinson Correspondence, M.H. (2019). Flies Regulate Wing Motion via Active Control of a Dual-Function Gyroscope. Curr. Biol. *29*, 3517–3524.e3.

86. Namiki, S., Dickinson, M.H., Wong, A.M., Korff, W., and Card, G.M. (2018). The functional organization of descending sensory-motor pathways in Drosophila. Elife *7*. 10.7554/eLife.34272.

87. Tsubouchi, A., Yano, T., Yokoyama, T.K., Murtin, C., Otsuna, H., and Ito, K. (2017). Topological and modality-specific representation of somatosensory information in the fly brain. Science *358*, 615–623.

88. Kathman, N.D., and Fox, J.L. (2019). Representation of Haltere Oscillations and Integration with Visual Inputs in the Fly Central Complex. Journal of Neuroscience *39*, 4100–4112.

89. Strausfeld, N.J., and Seyan, H.S. (1985). Convergence of visual, haltere, and prosternal inputs at neck motor neurons of Calliphora erythrocephala. Cell Tissue Res. *240*, 601–615.

90. Huston, S.J., and Krapp, H.G. (2009). Nonlinear integration of visual and haltere inputs in fly neck motor neurons. J. Neurosci. *29*, 13097–13105.

91. Rauscher, M.J., and Fox, J.L. (2021). Haltere and visual inputs sum linearly to predict wing (but not gaze) motor output in tethered flying Drosophila. Proc Biol Sci *288*. 10.1098/rspb.2020.2374.

92. Mureli, S., and Fox, J.L. (2015). Haltere mechanosensory influence on tethered flight behavior in Drosophila. J. Exp. Biol. *218*, 2528–2537.

93. Rauscher, M.J., and Fox, J.L. (2022). Asynchronous haltere input impairs wing and gaze control in Drosophila. bioRxiv, 2022.09.29.509061. 10.1101/2022.09.29.509061.

94. Sherman, A., and Dickinson, M.H. (2003). A comparison of visual and haltere-mediated equilibrium reflexes in the fruit fly Drosophila melanogaster. J. Exp. Biol. *206*, 295–302.

95. Elzinga, M.J., Dickson, W.B., and Dickinson, M.H. (2012). The influence of sensory delay on the yaw dynamics of a flapping insect. J. R. Soc. Interface *9*, 1685–1696.

96. Lachaise, D., Cariou, M.-L., David, J.R., Lemeunier, F., Tsacas, L., and Ashburner, M. (1988). Historical Biogeography of the Drosophila melanogaster Species Subgroup. In Evolutionary Biology, M. K. Hecht, B. Wallace, and G. T. Prance, eds. (Springer US), pp. 159–225.

97. David, J.R., and Capy, P. (1988). Genetic variation of Drosophila melanogaster natural populations. Trends Genet. *4*, 106–111.

98. Atkinson, W., and Shorrocks, B. (1977). Breeding site specificity in the domestic species of Drosophila. Oecologia *29*, 223–232.

99. Markow, T.A. (2015). The secret lives of Drosophila flies. Elife *4*. 10.7554/eLife.06793.

100. Smith, G., Lohse, K., Etges, W.J., and Ritchie, M.G. (2012). Model-based comparisons of phylogeographic scenarios resolve the intraspecific divergence of cactophilic Drosophila mojavensis. Mol. Ecol. *21*, 3293–3307.

101. Throckmorton, L.H. (1975). The Phylogeny, Ecology & Geography of Drosophila. In Handbook of Genetics, R. C. King, ed., pp. 421–469.

102. Date, P., Crowley-Gall, A., Diefendorf, A.F., and Rollmann, S.M. (2017). Population differences in host plant preference and the importance of yeast and plant substrate to volatile composition. Ecol. Evol. *7*, 3815–3825.

103. Heed, W.B. (1982). Ecological genetics and evolution: The cactus-yeast-drosophila model system. (New York, NY: Academic Press).

104. Keleş, M.F., Mongeau, J.-M., and Frye, M.A. (2019). Object features and T4/T5 motion detectors modulate the dynamics of bar tracking by Drosophila. J. Exp. Biol. *222*. 10.1242/jeb.190017.

105. Ding, S.S., Fox, J.L., Gordus, A., Joshi, A., Liao, J.C., and Scholz, M. (2024). Fantastic beasts and how to study them: rethinking experimental animal behavior. J. Exp. Biol. *227*. 10.1242/jeb.247003.

Chapter 2

Proprioception gates visual object fixation in flying flies

SUMMARY

Visual object tracking in animals as diverse as felines, frogs, and fish supports behaviors including predation, predator avoidance, and landscape navigation. Decades of experimental results show that a body-fixed rigidly tethered fly within a visual “virtual reality” flight simulator steers to faithfully follow the motion of a vertical bar, thereby “fixating” it on visual midline. This powerful behavior likely reflects a desire to seek natural features such as plant stalks, and has inspired algorithms for visual object tracking predicated on behavioral responses to bar velocity, particularly near visual midline. Using a modified flight simulator equipped with a magnetic pivot to allow frictionless turns about the yaw axis, we have discovered that bar fixation, as well smooth steering responses to bar velocity, are attenuated or eliminated in yaw-free conditions. Body-fixed *Drosophila melanogaster* respond to bar oscillation on a stationary ground with frequency-matched wing kinematics, and fixate the bar on midline. Yaw-free flies respond to the same visual stimulus by ignoring the oscillating bar and maintaining their original heading. This difference in behavioral output is driven by the open state of the proprioceptive channel, rather than the visual channel, as artificially “clamping” a bar in the visual periphery of a yaw-free fly has no effect on fixation behavior. When presented with a bar and ground oscillating at different frequencies, a yaw-free fly follows the frequency of the ground while a body-fixed fly robustly steers at the frequencies of both the bar and ground. Overall, our findings support a model in which proprioceptive feedback generated by body movements promotes active damping of high gain optomotor responses to object motion.

INTRODUCTION

The survival and success of animals is dependent on approaching or avoiding relevant features in their environment. Vertically elongated edges form conspicuous visual navigational landmarks indicating ethologically important objects such as plant stalks. A clever experimental manipulation developed in the 1960's - in which the steering torque generated by a tethered fly controlled a servo motor that rotated a cylinder around the fly - revealed active centering or "fixation" of a vertical bar on the animal's visual midline [1,2]. Frontal bar fixation persists with luminance-defined moving bars (dark or bright on uniform background), with motion-defined bars (sometimes called "fourier bars", randomly textured to match the ground), and even when the bar is presented against a ground moving in the opposite direction, independently from the moving bar [3–5]. In fact, this object orientation response is so powerful that a single fly, with sufficient in-flight refueling, will actively center a vertical bar continuously for up to 36 hours [6].

The robustness and experimental tractability of bar fixation behavior inspired a classical theoretical model of object orientation driven by two variables: the static azimuthal position of the bar, and its motion, or image velocity [2,7,8]. Whereas tracking can be elicited with bars containing no net motion energy, or bars that present surface motion oriented opposite bar motion, responses to velocity-independent cues such as these are always smaller in magnitude and delayed by comparison to velocity-dependent responses [9]. Motion-elicited tracking responses are strongest near the fly's visual midline [3,10,11], and flies with genetically silenced motion detecting neurons show diminished fixation capability in flight, supporting the role of image velocity for active bar fixation [12].

Under normal flight conditions, the central nervous system integrates motion cues from visual and proprioceptive sources as the fly maneuvers (Fig. 1A). Bar fixation is typically studied with a fly rigidly fixed to a stiff wire [13]. An optical readout of wing kinematics by the body-fixed fly is used to control an electronic visual display to revolve at a velocity proportional to the steering effort (Fig. 1B), while the body remains stationary. A newer innovation for more naturalistic flight control has a fly tethered to a magnetic pin suspended within a magnetic field on a nearly

frictionless pivot [14]. In contrast to “body-fixed” flies, we refer to flies in this paradigm as “yaw-free” because the body can rotate freely in the horizontal plane, thereby providing real closed loop feedback conditions in yaw for both vision and proprioception feedback channels (Fig. 1C) [15,16]. Two recent studies indicate that as a bar crosses visual midline in the yaw-free paradigm the fly’s heading does not seem to follow bar motion [17,18]. Rather interestingly, flies seem to ignore bar velocity within the very visual field that generates the strongest responses by body-fixed flies. To probe this paradox, we asked whether the fly’s proprioceptive state, body-fixed vs yaw-free, directly influences velocity dependent control of bar fixation. Given the importance of image velocity for models of object detection, such a finding would change our understanding of the mechanisms underlying visual object tracking behavior.

Recent work used a systems identification approach to show how the control of head movements, which stabilize gaze upon the visual ground, are modulated by the yaw-free state [19]. Here, we expand this framework to examine how body state influences active object orientation. We make comparisons of well-known and robust large-field compensatory optomotor responses and small-field bar orientation behaviors across proprioceptive body state. We selectively open and close yaw feedback channels (Fig. 1A) to show for the first time that yaw-free flies show weak or no velocity-driven smooth tracking responses to bar motion along the visual azimuth. We show that the influence of the fly’s body state on bar tracking is due to proprioceptive signals rather than visual feedback. Although the precise source of the relevant body movement signals remains speculative, our results support a model that has emerged several times in the literature in which intact proprioceptive signaling is necessary to actively damp optomotor control [19–21]. We build upon this model by empirically demonstrating that when yaw proprioceptive feedback is compromised, classical “frontal fixation” behavior emerges from saturating optomotor responses. However, under more naturalistic body movement conditions, bar tracking is achieved by means other than frontal fixation.

RESULTS

Yaw-free flies do not frontally fixate vertical bars

We developed an experiment to test the influence of body state on canonical active bar fixation. We first confirmed prior findings by evoking classical frontal bar fixation with the rigid tether paradigm in which the visual feedback loop was closed artificially (Fig. 1B). We used a motion-defined bar stimulus in which randomly distributed ON-OFF pixels matched the ground thus making it distinguishable from the visual panorama only by relative motion, not brightness or any other parameter (see Methods). The bar was programmed to oscillate +/- 30° at constant velocity on a triangle waveform, and was presented to the fly at the start of each trial at one of three azimuthal positions: 0° (midline), +60°and -60°. We chose a relatively small oscillation amplitude, and short duration trials in order to examine smooth steering responses while evoking minimal saccades, which motion-defined bars readily evoke over long trajectories in yaw-free flies [22,23].

In the body-fixed paradigm, the fly's wing steering kinematics controlled the oscillating bar embedded within the ground. If the fly flew straight, the ground was stationary and the bar oscillated about a fixed azimuthal position. If the fly attempted to turn right, then the coupling electronics shifted the oscillating bar and ground pattern together to the fly's left. Visually, the flies were in an artificial closed loop while the proprioceptive feedback channel was open. By contrast, in the yaw-free paradigm, if the fly turned right, its body rotated, thereby shifting the oscillating bar and ground together to the left (Fig. 1C). In the yaw-free paradigm, both the visual and proprioceptive feedback channels were closed about the yaw axis. As our study aimed to investigate small-field bar-directed responses, we did not restrain the head because prior work demonstrated that head movements do not follow small-field bar stimuli [24]. Since the

head was free to move, we report the position of the bar relative to the major body axis rather than its retinal position.

Given virtual control over the angular position of the oscillating bar, body-fixed flies produced steering effort towards it, as expected. A space-time plot and sample response trajectories of the visual stimulus relative to the fly's body axis demonstrate typical "jittery" movement of the bar and the ground as the fly produces continuously variable steering responses to both (Fig. 2A *right,* C,E,G *left*). Body-fixed flies generally steer towards the bar, thereby bringing it to visual midline even within the brief 4-second trail (Fig. 2C,E,G *middle*). Population histograms show that regardless of where the bar initially appeared (orange histograms), the bar position was most frequently positioned at 0° by the end of the trial (blue histograms Fig. 2C,E,G *right*). In stark contrast, a space-time plot and individual sample traces demonstrate that yaw-free flies do not track the bar oscillation (Fig. 2B *right*, D,F,H *right*). Nor do yaw-free flies produce steering jitter, but rather fly straight between saccades. Remarkably, yaw-free flies do not orient towards the oscillating bar (Fig. 2D,F,H *middle*). We quantified fixation behavior by summing the probability of bar position within 60-degree bins at the start and end of the trials, we found significant differences only for body-fixed flies, indicating that the bar was centered on midline by the end of the trial regardless of its starting location (Fig. 2C,E,G dot plots). By contrast, we found no significant differences between the start and end of the trial for yaw-free flies (Fig. 2D,F,H dot plots). Our results demonstrate that whereas body-fixed flies actively fixate a bar oscillating on a stationary ground, yaw-free flies do not.

Yaw-free flies do not smoothly track bar dynamics

A central tenet of frontal fixation is asymmetric smooth steering responses to bar motion about visual midline, which therefore visually centers the object [12]. In order to test for body-state effects on bar steering dynamics, we reproduced prior results in which body-fixed flies produce robust directional wing steering responses to a motion-defined bar [5,11]. We presented open-loop

constant-velocity bar oscillations across a stationary ground (triangle wave stimuli). Wing steering traces were filtered to remove any slow steering effort toward the bar's position, as well as saccades, in order to quantify responses to 2 Hz bar oscillation. In addition to trials with the bar positioned at -60°, 0°, and 60°, a 360° large-field ground oscillation condition was added to normalize each fly's bar response to their maximum optomotor response (Fig. 3A). Note that the visual ground is a large-field stimulus because it subtends a large portion of the visual field, whereas the bar is a small-field stimulus. As expected, bar motion elicited robust smooth steering responses in body-fixed flies, with the largest amplitude at midline (Fig. 3B) [11]. We observed bilateral asymmetry in the average response trajectory for the bar at +/- 60°. We have observed similar asymmetries before, which are not an artifact of the electronics but rather invert under some visual conditions; as yet we do not understand their basis.

As the steering responses were roughly sinusoidal to the constant velocity stimuli, we used a frequency domain analysis to quantify response strength. For each fly, we determined the magnitude of the Fast Fourier Transform (FFT) peak for bar movement at 120°/s (2 Hz). In body-fixed flies, the bar stimulus elicited steering responses approximately half as large as those elicited by the ground stimulus (Fig. 3B, D, yellow). In contrast, we show that the same bar stimulus evoked essentially zero smooth body dynamics in yaw-free flies, despite an intact ground optomotor response (Fig. 3C, E). Comparisons between bar responses normalized to the ground response revealed that body fixing results in a significant increase in bar smooth tracking for bar placement at any of the three azimuthal positions (Fig. 3F, Wilcoxon Rank-sum test, $p<0.01$). This difference in smooth steering responses persisted for slower 30°/s (0.5 Hz) trials, suggesting that this phenomenon is independent of bar velocity (Fig. S2). Body-fixed flies smoothly track bar motion; yaw-free flies do not.

In this experiment, body-fixed flies were in both visual and proprioceptive open loop conditions, which precludes isolation of the sensory modality that might govern body state effects on visual object tracking. We therefore designed a complementary experiment in which

flies experienced the proprioceptive signals associated with yaw-free flight, but we used a tracking camera and high resolution digital projector to immobilize the visual scene under artificial open-loop. Prior work using a similar approach showed that artificially triggering large-field visual rotation during yaw-free body saccade has no influence over the trajectory of the saccade, thereby highlighting the role of proprioceptive rather than visual control in terminating a saccade [15]. Our advance was to dynamically "clamp" the visual image to all body axis movements (smooth and saccadic) at a 60 Hz update rate. This corresponds to a delay of 17 ms in coupling body movement to visual stimulus update, well below the 44 ms onset delay to a large-field velocity impulse [11] (Fig. 4A, see STAR Methods).

We validated this new paradigm by showing that under normal visual closed-loop conditions, robust ground optomotor body responses were elicited by constant velocity image oscillations (Fig. 4B *middle*). We verified that upon the onset of open-loop ground motion, the amplitude of 2 Hz body yaw oscillation increased significantly (Fig. 4B *right*). By contrast, yaw-free flies showed no obvious smooth steering responses to bar oscillation regardless of whether they were under normal closed-loop (Fig. 4C *middle*) or artificial open loop visual conditions (Fig. 4D *middle*). In both the presence and absence of visual feedback, and independent of the azimuthal position of the bar, flies did not steer back-and-forth with bar motion (Fig. 4C,D *right*, Fig. S3B). Comparisons across conditions revealed that the effect of ground motion was stronger than that of bar motion in either feedback condition; furthermore, the effects of bar motion were not different between artificial open and closed visual feedback conditions (Fig 4E). Similar to previous experiments, bar responses in visual open loop were still mostly composed of periods of straight flight interspersed with saccades (Fig. S3A) [22]. Together, these results show that the bar-elicited smooth steering behavior that results in frontal fixation in body-fixed flies is due not to compromised visual feedback, but rather to compromised proprioceptive feedback.

Body-fixing introduces variability to head and wing control

Comparisons across tethering paradigms are inherently problematic, in part due to the different control variables and measurement units for steering typically used in the two setups. More critically, it is not feasible to assess the behavior of the same animal across the two setups, precluding powerful within-subjects analysis on behaviorally relevant timescales. To facilitate body-state comparisons within subjects and directly assess the effect of compromising proprioceptive feedback, we designed a pneumatic gripper apparatus that allows switching between body states in a magnetically tethered fly (Fig. 5A). Mounted above the magnetic tether arena, two arms clasp the rotating magnetic pin, locking the fly in place at a desired angular orientation relative to the visual display. A fly in the yaw-free state can therefore quickly become body-fixed and *vice versa*.

In this setup, we first quantified the angular dynamics of the body, head, and wings, across body state within the same fly. We switched from the constant velocity stimuli of our previous experiments to constant frequency stimuli from here forward to facilitate frequency domain analysis. We found that a 2° difference between the left and right wing beat amplitude drives body movements roughly 3 times larger (Fig. 5B data trace insets). In line with previous work, we confirmed that the body, wings and head of a yaw-free flies smoothly track large-field optic flow and minimize integrated error using syn-directional saccades generated by both head and wing motor systems (Fig. 5B top row) [17,25]. We observed that the smooth dynamics and precise coordination of wing and head movements seen in the open gripper yaw-free state were severely impaired upon body-fixing by closing the gripper (Fig. 5B bottom row). The mean amplitude and variance for both wing and head steering dynamics increased upon body-fixing (Student's unpaired samples t-test $p<0.01$) (Fig. 5C,D), a result that would appear as jitter in the visual panorama had these kinematics been artificially coupled to visual motion (Fig. 2A).

Body-fixing increases gain of smooth tracking responses to vertical bars

The increased amplitude and variability of head and wing steering responses to image slip has been suggested to result from saturating gain of the large-field optomotor response in the body-fixed state [19]. We hypothesized that impairing proprioceptive feedback by body fixing would similarly increase the gain of optomotor responses to small-field bars. To test this, we presented flies with a compound motion stimulus consisting of an oscillating ground and an oscillating vertical bar, each moving on separate single frequency sinusoid trajectories (Fig. 6A). To remain within the dynamic range of all behaviors, we chose stimulus frequencies for which both body and head movements contribute to gaze stabilization and visual responses to large-field and small-field stimuli are comparable [26,27]. We placed the bar stimulus on midline and measured the amplitude of the ground and bar responses at the relevant stimulus frequencies. Conceptually, we presented two independent inputs to the fly and computed the output gain for each to assess how strongly each stimulus is tracked across body states (Fig. 6B). We performed this experiment using motion defined bars, and solid dark bars, switched the frequencies of the bar and ground, and measured body angle, wing steering, and head smooth steering responses.

Based on the responses to bar and ground motion individually, we reasoned that given a compound stimulus, yaw-free flies smoothly track ground motion over that of the bar. We computed the FFT of the body response and confirmed that the fly responded to the ground stimulus, with a significantly weaker response to bar motion (Wilcoxon Rank-sum test, $p<0.001$) (Fig. 6C). Regarding wing and head responses to the compound stimulus, previous work has demonstrated that the head optomotor responses track ground motion and are unresponsive to a moving bar [24]. We thus focused on the steering responses of the wings to test whether object

responses are affected by body state. We found that the yaw-free wing steering response matched the oscillation dynamics of the ground (Fig 6D, left). Correspondingly, the gain of the ground response was higher than that of the bar in the yaw-free state (Fig 6E). Upon opening the yaw proprioceptive feedback loop by closing the gripper, the wings showed increased response gain to the bar, while the ground response remained unchanged (Fig 6E). The increase in the smooth tracking gain of the bar upon body-fixing persisted when we swapped the frequencies to oscillate the ground faster than the bar (Fig 6F,G).

A motion-defined bar stimulus tests motion dependent tracking behavior because it does not provide positional cues such as static luminance; rather it is defined only by its movement relative to the background. In this sense, the stimulus is challenging for the visual system to detect. Physiologically, vertical bars with high spatial frequency content have been shown to reduce the efficacy of T4/T5 motion detecting neurons that supply the optomotor system [18]. By contrast, a low spatial frequency solid dark bar more strongly stimulates T4/T5 motion detectors [18]. Thus, we reasoned that if body-fixing increases the gain of the smooth steering response to a motion-defined bar, then this gain effect may be even more apparent for a dark bar that better drives the optomotor pathway. The dark bar did elicit more coherent steering and higher peaks at the bar FFTs for both head and wing responses (Fig. 6H,J, Fig. S4E,G), and response gain was similarly dependent on body state for the dark bar (Fig. 6I,K). The effect of body-fixing was again independent of the relative frequencies of the bar and ground, persisting when oscillation frequencies were swapped (Fig. 6J,K).

How head responses to large-field motion are modulated by body state has been described elsewhere [19]. Our results confirm that body-fixing induces an overall gain increase in the amplitude of head responses, and thereby help to validate our gripper apparatus. We show that the head primarily tracks the dynamics of the ground rather than the bar, particularly for motion-defined bars, and notably show for the first time that large-field selectivity for the head optomotor response persists across body states (Fig. S4 A,C,E,G). Finally, we also show that

fixing the body in place causes an increase in amplitude of head movements regardless of the visual stimulus conditions (Fig. S4 B,D,F,G).

DISCUSSION

We discovered that flies that are free to steer in the yaw plane do not fixate a motion-defined bar on visual midline the way they do in body-fixed experimental paradigms. While high gain smooth tracking responses to bar motion are characteristic of body-fixed flies and result in the bar being fixated on midline, yaw-free flies do not show smooth optomotor responses to the same bar stimuli. Switching from a yaw-free to a body-fixed state immediately induces exaggerated head and wing movements, as well as high gain wing steering responses to bar movement. Our results support a model proposing that proprioceptive signals engage active damping of optomotor steering control [19–21]. In this manner, object tracking and frontal fixation are enhanced by reduced proprioceptive feedback in body-fixed flight; the corollary is that intact proprioception reduces object optomotor responses and fixation. Our results extend this concept to the limit of no object fixation by yaw-free flies. Object tracking models that use a velocity dependent term resulting in midline bar fixation shall have to be updated in light of active modulation by mechanical body-state dependent mechanisms.

Body state modulates inner-loop optomotor responses for bar fixation

Discriminating relevant visual features of the environment requires maintaining stable gaze during locomotion. Stable gaze facilitates feature detection, after which a goal directed orientation maneuver may ensue. From an engineering perspective, these tasks can be described as low-level “inner-loop” stabilization responses and higher-level “outer-loop” goal-directed orientation [28] that interact in order to generate flexible yet stable flight control [25]. Inner-loop flight control involves first detecting slip of the visual panorama on the retina arising from self motion or an external perturbation, and then generating a corrective optomotor maneuver to

stay on course [8]. In flies, retinal slip is detected by small-field T4 and T5 neurons, which in turn supply retinotopic, directionally selective signals to spatially integrating large-field neurons housed in the lobula plate. Lobula plate large-field neurons project to pre-motor descending pathways [29,30] to control wing optomotor control [31]. Smooth optomotor responses may be evoked both by large-field (panoramic) stimuli, and small-field stimuli (single vertical stripe or bar). Large-field responses operate over a lower frequency range than small-field stimuli and are therefore thought to be mediated by separate lobula plate neurons [26,32], but both pathways presumably draw from T4/T5 directional motion detectors. Here, we show that the transition from yaw-free to body-fixed state within individual flies evokes a concomitant transition to high gain, high variance kinematics of both the head and wings (Figs. 5, 6, S4 and see [19]). Based on these results, we conclude that rigidly fixing the body acts to increase inner-loop optomotor gain to modulate both large-field and small-field responses.

Several robust features of frontal bar fixation by body-fixed flies have implicated optomotor control, which is traditionally considered an inner-loop variable, in outer-loop visual orientation behavior. First, smooth steering responses to imposed bar motion are the strongest near visual midline, thereby centering the object on approach [10]. Steering responses to long stimulus paths are stronger when a bar recedes from midline than when it approaches midline, an asymmetry that tends to “sink” the bar on midline [33]. Such findings have inspired object tracking models that rely heavily on bar velocity term [7,10,12].

If velocity-dependent bar responses and frontal fixation are a manifestation of the inner-loop optomotor system then several predictions would follow. First, blocking the activity of T4/T5 motion detectors ought to compromise frontal bar fixation. Indeed, for body-fixed flight under virtual closed loop feedback, blocking synaptic transmitter release by T4/T5 neurons was found to significantly attenuate frontal bar fixation, particularly for fast movements [12]. However, body-fixed flies walking on a spherical treadmill under virtual closed loop conditions persisted in orienting toward a bar even with blocked motion detection neurons [30]. This discrepancy may

result from known differences in neuromodulatory state between walking and flight or the fact that body-fixed walking flies do receive stride-coupled proprioceptive signals from leg mechanosensors [34]. A second prediction would be that bar stimuli composed of the spatial properties that best drive T4/T5 motion detectors would evoke correspondingly stronger smooth bar responses. Indeed we found that compared to a higher spatial frequency motion-defined bar, a solid black bar evokes stronger directional wing steering responses (Fig. 6), and stronger T4/T5 calcium responses [18]. Similarly, we found that in transitioning from a yaw-free to a body-fixed state, the resultant increase in bar evoked steering was more pronounced for the solid dark bar than for the motion-defined bar (Fig. 6 and Fig. S4). Furthermore, the body-state effect is accentuated at lower bar oscillation frequency (compare bar frequency in Fig. 6D vs F and 6H vs J), consistent with the notion that bar responses are driven by the low-pass optomotor system [35].

Proprioceptive signaling actively damps high gain visual responses

As we have discussed, but it is worth repeating, body movements attenuate inner-loop ground stabilization responses [19]. However, optomotor gain could in principle be mediated by visual mechanisms alone, accentuated by the coupling algorithm that governs virtual closed loop visual conditions. Simply varying the coupling gain changes the sharpness of a bar fixation histogram during body-fixed flight [36,37]. However, our visual open-loop experiment showed that clamping the position of the oscillating bar relative to the fly's body axis had no influence over bar steering behavior in a yaw-free fly (Fig. 4).This suggests a non-visual mechanism of body state modulation of object tracking.

Our results are the first to demonstrate that body movement signals influence the gain of small-field (bar) responses and active visual fixation. By what mechanism does this occur? Proprioception is broadly defined as the sense of body position and movement, encoded by mechanosensory organs. A study that mechanically oscillated a body-fixed flying fly showed

that even a small amount of body rotation decreases the gain of optomotor responses in *Drosophila* [38]. Our results show that naturalistic yaw proprioception essentially eliminates optomotor responses to bar motion across a range of conditions (Figs. 2,3,5). In a control theoretic framework, robotics studies have posited that short latency proprioceptive feedback could be used to actively damp yaw rate, thereby imparting robustness and stability to a high gain visuomotor control system [20]. Physiological evidence for proprioceptive damping of optomotor responses has not yet emerged, but the hypothesis is broadly consistent with the behavioral observations we have made here.

In principle, any appendage equipped with a mechanosensory organ could serve a proprioceptive role. In flies, numerous mechanosensory organs encode body dynamics during flight, including the wings, antennae, and most notably, in Diptera, the multimodal haltere organs [38–42]. The haltere sensorimotor system acts both as a metronome to temporally pattern wing kinematics, and as a gyroscope to correct for rotational displacements of the body during flight.

As metronomes, halteres provide wingstroke-coupled feedback[43] on the timescale of 2-5 ms to wing motorneurons[44], which is combined with other afferents to modulate wing steering muscle activity [45]. Halteres are not passive sensors, but rather are actuated by their own set of muscles that are gated by descending visual signals [46]. Metronomic haltere control of wing kinematics operates continuously in body-fixed flies, and surgical ablation causes decreased open-loop optomotor gain and enhanced closed-loop bar fixation [21,37]. By contrast, we find that transitioning from the yaw-free to the body-fixed state, which presumably constrains proprioceptive feedback signals, causes increased small-field optomotor gain (Figs. 3,4,5,6) and, in line with the studies above, stronger frontal bar fixation (Fig. 2). One possible explanation for this mismatch is that the proprioceptive modulation of small-field object tracking is mediated not by the metronome, but rather by the gyroscope function of the haltere system.

Feedback from this system is presumably either attenuated or drastically altered in the body-fixed state.

There are at least two plausible models of haltere gyroscope function that could underlie our results. When a fly experiences an involuntary perturbation like a gust of wind, gyroscopic haltere-elicited reflexes act to stabilize the body [38]. However, descending visual signals directly activate the haltere steering muscles, which in turn modulate wing steering responses [47]. Thus, in order to initiate a voluntary turn, an external visual command could activate the haltere muscles and trigger a fictive compensatory steering maneuver. In this model, the haltere sensory pathways of a body-fixed fly are overstimulated because the body cannot complete the turn that resets the gyroscope. Overstimulated haltere sensory signals would evoke exaggerated optomotor responses that act on small-field objects. An alternative model is that, in the yaw-free state, continuous small body movements activate gyroscopic signals that actively damp high gain optomotor signals to a more optimal dynamic range. In this scenario, body-fixing results in under-stimulated gyroscopic haltere signals and high gain optomotor control that operates on small-field objects to drive stripe fixation as well as exaggerated head and wing movements. Discerning between these two hypotheses will be experimentally challenging. But tackling the first-order question - whether the haltere system is involved at all - is feasible; any neurogenetic manipulation that re-engages frontal bar fixation in a yaw-free state and/or disengages frontal bar fixation in a body-fixed state would be promising.

For neurophysiology, a broken feedback loop is a feature not a bug

Our results show that yaw-free flies do not frontally fixate a motion-defined bar (Fig. 2). And yet, both in free flight and free walking arenas, *Drosophila melanogaster* readily orient towards vertical stripes or posts [48–51]. Yaw-free and freely flying flies intersperse periods of straight flight with rapid body saccades for outer-loop object orientation either toward or away

from visually discrete objects [17,23,50], reserving smooth, proportional steering movements for inner-loop gaze stabilization via the wings and head [27]. Body-fixed flies simply show an additional control variable - the small-field optomotor response. Does this imply that body-fixed flight preparations are compromised by experimental artifacts? On the contrary, we know of no other sensory manipulation that imparts the same degree of robustness to a visual behavior. If one wishes to study the neurophysiology of inner-loop optomotor control topology, then the body-fixed bat tracking paradigm is the exemplary experimental model. Breaking feedback loops has provided us with the insight that object tracking does not require a continuous velocity component, and that frontal fixation does not represent the natural setpoint for object navigation in *Drosophila melanogaster*.

From a visual ecological perspective*, Drosophila melanogaster* is a generalist, occupying myriad habitats containing diverse visual background clutter that generates large-field self motion cues superposed with optically distinguishable foreground features. Other *Drosophila* species have specialized visually sparse habitats, and thereby have different control strategies for object pursuit. For example, *D. melanogaster* approaches high contrast elongated vertical objects, and avoids small objects that presumably reflect a threat [49]. By contrast, the desert dwelling *Drosophila mojavensis* approaches either of these object classes equally well, presumably reflecting its own visual ecological context [52]. Even within body-fixed *D. melanogaster*, bar fixation is not “hard wired”, but rather can be modulated by food odor cues [53]. This suggests that ecologically adaptive visual-proprioceptive circuit interactions can be achieved with small changes to the low-level inner-loop optomotor responses that are ubiquitous across taxa.

To build a comprehensive understanding of how neural mechanisms govern behavior, we must be able to examine the isolated and combined effects of feedback across multiple sensory modalities. Well-tuned feedback is indispensable for control and stability of locomotion behaviors, and is compromised to some extent by tethering animals in place [54]. Yet, the

approach of selectively opening and closing feedback loops is essential for probing how information flows through a dynamical sensory system [55,56]. In *Drosophila melanogaster,* body-fixed experimental paradigms have revealed much about visual information processing and continue to be necessary for functional imaging of circuits and individual neurons. Here, we provide an experimental framework to formalize control models and gain a deeper mechanistic understanding of the underlying circuit effects of manipulating the damping of inner-loop control. Our work highlights the importance of accounting for and experimentally exploiting proprioceptive feedback in body-fixed preparations.

MATERIALS AND METHODS

Key Resources Table

REAGENT or RESOURCE	SOURCE	IDENTIFIER
Electronic equipment		
LED panel visual display system	IO Rodeo	[13]
Neutral density filters	Rosco	Cat# 59
Wingbeat Analyser	JFI Electronics	N/A
BlackFly USB camera	FLIR	BFS-U3-04S2M-CS
Experimental models: Organisms/strains		
Drosophila melanogaster	Wild	Population Cage Flies (PCF)
Mechanical equipment		
Pneumatic gripper	McMaster-Carr	Cat# 6220K51

REAGENT or RESOURCE	SOURCE	IDENTIFIER
Electronic equipment		
LED panel visual display system	IO Rodeo	[13]
Neutral density filters	Rosco	Cat# 59
Wingbeat Analyser	JFI Electronics	N/A
BlackFly USB camera	FLIR	BFS-U3-04S2M-CS
Experimental models: Organisms/strains		
Drosophila melanogaster	Wild	Population Cage Flies (PCF)
Mechanical equipment		
Software and algorithms		
MATLAB	MathWorks	http://www.mathworks.com/
CrazyFly wing and head tracker	Jean Michel Mongeau	https://github.com/boc5244/CrazyFly

Experimental Model and Subject Details

A wild-type *Drosophila melanogaster* strain was maintained at 25°C under a 12 hr:12 hr light:dark cycle with access to food and water *ad libitum*. All experiments were performed with 3- to 6- day-old female flies within 4 hours of lights on and 4 hours of lights off.

Method details

Animal Preparation

We prepared the animals for each experiment according to a protocol that has been previously described [17]. Briefly, we cold-anesthetized the flies by cooling them on a Peltier stage maintained at approximately 4°C. For magnetic tether paradigms, we glued stainless steel minutien pins (Fine Science Tools, SKU 26002-10) onto the thorax by applying UV-activated glue (Esslinger, SKU 12.201). The pin's length was approximately 1 cm to minimize the moment arm about which the fly can generate cross-field torques in pitch and roll. The pins were less than 1 percent of the fly's moment of inertia about the yaw axis. For rigid tether paradigms, we used thicker tungsten pins (diameter: 0.1mm). In both cases, the pin was placed on the thorax projecting forward at an angle of approximately 30°, in order to closely mimic the fly body's angle of attack during free flight. Before running experiments, flies were allowed at least half an hour to recover upside-down in a custom-designed holder, inside a covered acrylic container where humidity and temperature could be controlled in order to avoid rapid dehydration (~ 24°C, 50% humidity). After recovering from anesthesia, flies were given small pieces of Kimwipe to cling to and prevent flight and energy expenditure.

Rigid tether experimental protocol

As previously described [49], the rigid tether arena is a cylindrical display that consists of an array of 96 × 32 blue light emitting diodes (470 nm emission peak). The arena is modified by removing two columns of 8-pixel panels behind the animal for access into the center of the arena. Additionally, in order to maintain consistency with the magnetic tether paradigm, the top

and bottom 8-pixel rows of LEDs were kept off. Thus, the visual panorama in this setup wrapped around the fly, subtending 300° horizontally and 60° vertically (Figure 1B). Each singular LED subtended 3.75° on the flies' retina. Flies were illuminated from the top with an infrared diode (880 nm emission peak) which cast a shadow of the beating wings onto an optical sensor. An associated "wing-beat analyzer" (JFI Electronics Laboratory, University of Chicago) converted the optical signal into an instantaneous voltage measuring right and left wing beat amplitude (WBA) and frequency (WBF). The difference in the left and right WBA (ΔWBA), which is highly correlated with the fly's steering effort in the yaw axis [57], connected to the panel display controller to close a feedback loop with the rotational velocity of the visual display for the artificial closed loop feedback experiment in Figure 2. For open-loop experiments, signals from the wing-beat analyzer as well as from the panel display controller encoding the visual display position, were recorded on a DAQ (National Instruments USB 6259) at 1 kHz. The data acquisition was triggered through a voltage step sent by a second DAQ (USB-1208LS, Measurement Computing) interfaced with MATLAB that in turn controlled the pattern presentations. At the beginning of each experiment, we presented a dark bar on a uniform ground in closed-loop to calibrate the fly's position within the arena. Flies which did not stabilize the bar on midline or displayed incorrect hutches, which is indicative of poor tethering, were discarded from the experiment. Only flies that flew continuously for at least 75% of the trials were included in the analysis. If flies stopped flying during a trial or wing beat frequency dropped below 150 Hz, the trial was discarded.

Magnetic tether and gripper experimental protocol

As previously described [14,16], the magnetic-tether arena is comprised of a cylindrical display that consists of an array of 96 × 16 blue light emitting diodes (470 nm emission peak) that wrap around the fly, subtending 360° horizontally and 60° vertically (Figure 1C). Each singular LED subtended 3.75° on the flies' retina. Flies were suspended between two magnets,

allowing free rotation along the vertical (yaw) axis. We illuminated the fly from above with an array of six infrared LEDs (940 nm emission peak). Both the wings and body of the flies could clearly be visualized from below using an infrared-sensitive camera (BlackFly BFS-U3-04S2M-CS) fitted with a zoom lens (InfiniStix 1.0x/94mm, Edmund Optics) and an 850 nm longpass filter (FGL850M, ThorLabs) to block light from the LED panels. We recorded the angular position of the fly within the arena at 100 frames/s. At the beginning of each experiment, we characterized flies average optomotor behavior by presenting a large-field panorama rotating at 120°/s for 20s in the CW and the CCW directions. Flies who did not complete this trial or displayed excessive wobble were discarded from the experiment.

A pick-and-place pneumatic gripper (McMaster Carr Cat# 6220K51) was mounted above the arena, on a rail traversing its diameter. The gripper was fitted with custom designed 3D printed black PVA fingers that closed smoothly around the magnetic pin, locking it in place. The gripper was actuated manually by opening and closing a pneumatic switch connected to house air at 20 psi. When not actuated, the gripper was lifted out of the arena above the fly's field of view. The order of body-fixed and yaw-free trial blocks were randomized across individual animals.

Visual clamp paradigm projector display

To open the visual feedback loop on a behaviorally relevant timescale, we built a custom virtual reality flight simulator combining the magnetic tether paradigm with the high resolution projector display and graphics library of [58]. Instead of the LED display described above, this setup used a digital projector and well-placed first-surface mirrors to wrap the projection around the 4 vertical sides of a 4"x4"x4" perspex cube lined with gray rear projection material along the cube's inner surface. The projector (TI DLP LightCrafter 4500 EVM) produced frames 1280 x 800 pixels in size resulting in ~.4°/pixel at 120 Hz. The magnetic tether was set up as described above, positioning the fly at the center of the cube. From this position, the display subtends the

fly's visual field by 360° horizontally and 70–90° vertically, decreasing from the center of each panel to the corners. This discrepancy is accounted for by programmatically restricting the vertical subtended angle to 70° all around and correcting for perspective. Using the same infrared-sensitive camera described above, this system detected the heading of the fly and optionally subtracted its generated motion by the next frame at 60 Hz. This results in a 17 ms delay between a change in the fly's heading and a change in the visual display, which is less than half of the 44 ms onset delay in measured responses to ground perturbations along the yaw axis [11]. Additionally, this generates temporal frequencies up to 30 Hz, which is above the flies' behaviorally measured temporal resolution of 20 Hz [59]. In half of the trials, the fly was placed in virtual open-loop control, clamping the center of the bar's oscillation to the initial position relative to their heading. In the other half, the fly remained in closed-loop, allowing them to turn towards or away from the bar. Though the stimuli projected are RGB, only the blue channel was used in order to mimic parameters of the LED display. Finally, all visual stimulus resolutions were matched to those of the 96 pixel LED arena.

Visual Stimuli Across Paradigms

Experiments for figures 2,3,4 were designed to test responses to constant velocity stimuli, thus containing power across frequencies. Trials lasted 4 s with 2-4 s rests between trials. Trials were explicitly kept short to assess immediate responses to bar motion and mitigate any learning effects of stimulus predictability [60]. Bar trials used either a 30° wide motion-defined bar on a randomized panorama or a 30° wide dark bar on a uniform grayscale panorama. Motion defined bars were used to elicit responses to object movement and eliminate luminance contrast cues that might provoke static positional responses. We repeated one experiment using a solid dark bar because this low spatial frequency stimulus better stimulates the columnar directional motion detecting neurons and their downstream pathways that control optomotor responses. As expected, the dark bar highlighted the key phenomenon that body-

fixing increases bar tracking responses. In all cases, we presented a spatially randomized background scene to produce behaviorally relevant visual conditions.

In each bar trial, bars were presented in one of 12 pseudorandomized evenly distributed azimuthal positions relative to the fly's heading. Bars were oscillated on a velocity triangle waves with 60° peak-to-peak amplitude moving at either 30°/s (0.5 Hz) or at 120°/s (2 Hz). Ground trials where the whole panorama oscillated were interleaved with bar trials as a positive control measurement of large-field optomotor performance. These trials were either a broadband randomized ground or a 30° wavelength grating. Flies that did not show significant optomotor responses were discarded from the dataset.

Experiments for figures 5 and 6 were designed to test responses to constant frequency stimuli, thus containing power across velocities. For experiments using the gripper apparatus, visual stimuli consisted of a bar and ground oscillating concurrently, on different sinusoidal motion trajectories at either 2.3 Hz or 2.7 Hz with 30° peak-to-peak amplitude. The frequencies of oscillation were selected to be 1) prime numbers with non-overlapping harmonics, 2) within a dynamical range where both heads and bodies are involved in ground stabilization [27] and 3) within a dynamical range where flies have been shown to track both large and small-field stimuli robustly [26]. Ideally, the amplitudes of the oscillations ought to be scaled such that both stimuli would generate equal power in velocity - however, because the frequencies we chose are very close together, the amplitude difference is below the 3.75° resolution of our LED displays, and thus the amplitudes were kept equal at 15°. In these experiments, each trial was 10 s long. The angular position of the fly was extracted live at the start of each trial and the stimulus position was such that the bar, either dark or Fourier, was initially placed on the fly's azimuth.

Quantification and statistical analysis

All steering responses, heading angle extraction and statistical analyses were performed using MATLAB (MathWorks, Natick, MA, USA). For rigidly tethered flight experiments, wing beat amplitudes (open-loop experiments) and bar angular positions (closed-loop experiments) were directly extracted from the data acquisition device. For magnetic tether experiments, the angular heading of the fly, the head angular position and the wing steering amplitudes were all extracted from video data recorded at 100 fps using a suite of custom machine vision tools provided by the Bio-Motion Systems lab at Penn State University (https://github.com/BenCellini/CrazyFly). Raw data was band-pass filtered and for all angular data extraction, clockwise (CW) was defined as the positive direction of motion. Head and body saccades were then identified from thresholded angular velocity [22]. Flies' angular heading relative to the moving bars was back-calculated from the position of the bar and that of the fly within the 360° arena and data was wrapped to 180°. If flies were yaw-free and free to reorient within the arena, we isolated inter-saccadic flight bouts of at least 1 s duration where the bar was on the fly's visual midline and averaged all such bouts within an individual fly to obtain a mean fly response. If the flies were body-fixed, no such segmentation of the data was necessary and saccades were eliminated from the time-domain traces by virtue of the filters applied and trial averaging. Fly means were averaged across the population for each dataset. Fast Fourier Transforms (FFTs) were performed for each individual fly and the amplitude of bar responses for each fly was normalized to that fly's optomotor ground response. The magnitude ratios at the relevant peaks were compared across yaw-free and body-fixed datasets using unpaired samples Student's t-test. For analyses comparing variance and amplitude of wing and head responses across body states, all individual trials were plotted and unpaired Student's t-tests were performed. For all experiments where bars and ground stimuli were presented concurrently, input-to-output gains were calculated for the bar and ground sinusoidal stimuli and the gains were compared using a nonparametric Wilcoxon Rank-sum Test. Unless otherwise specified, each dot in a scatter plot represents an individual fly's mean response.

FIGURES

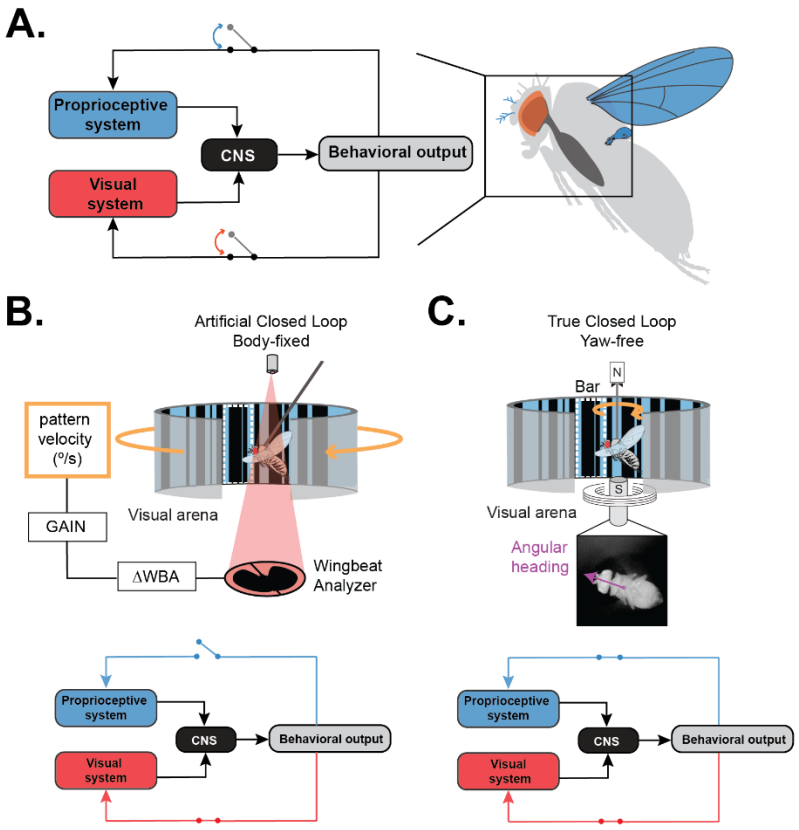

Figure 1. Sensory feedback conditions vary across rigid and magnetic tethering paradigms. A. (left) Conceptual block diagram of signal flow in the visual and proprioceptive modalities. Flight behavior generates feedback within sensory pathways. These channels can be opened or closed in different experimental paradigms. (right) Visual sensory feedback is primarily relayed through the eyes while proprioceptive feedback is relayed through multiple sensory structures covering the entire body, such as wings, halteres and aristae of the antennae. **B**. In a rigid tether arena, the fly's body is fixed to a stationary pin, the fly is

illuminated with infrared light from above and wing steering kinematics are measured using a photodiode below. The difference in wing beat amplitude across the two wings (ΔWBA) is representative of steering torque and can be coupled with variable gain to control the velocity of visual patterns such as a textured “motion-defined” bar on the LED display (outlined in dotted white line). In this condition the visual feedback channel is artificially closed but the proprioceptive feedback channel remains open since the fly’s body is stationary. **C**. In a magnetic tether arena (top), the fly’s body is glued to a magnetic pin suspended between magnetic north and south poles. The fly’s body is free to rotate in the yaw plane and orient toward visual cues. In this condition, the proprioceptive and visual feedback channels are both closed in the yaw plane of motion (bottom). The fly’s instantaneous angular heading in the 360º arena is recorded with a high-speed camera from below the animal.

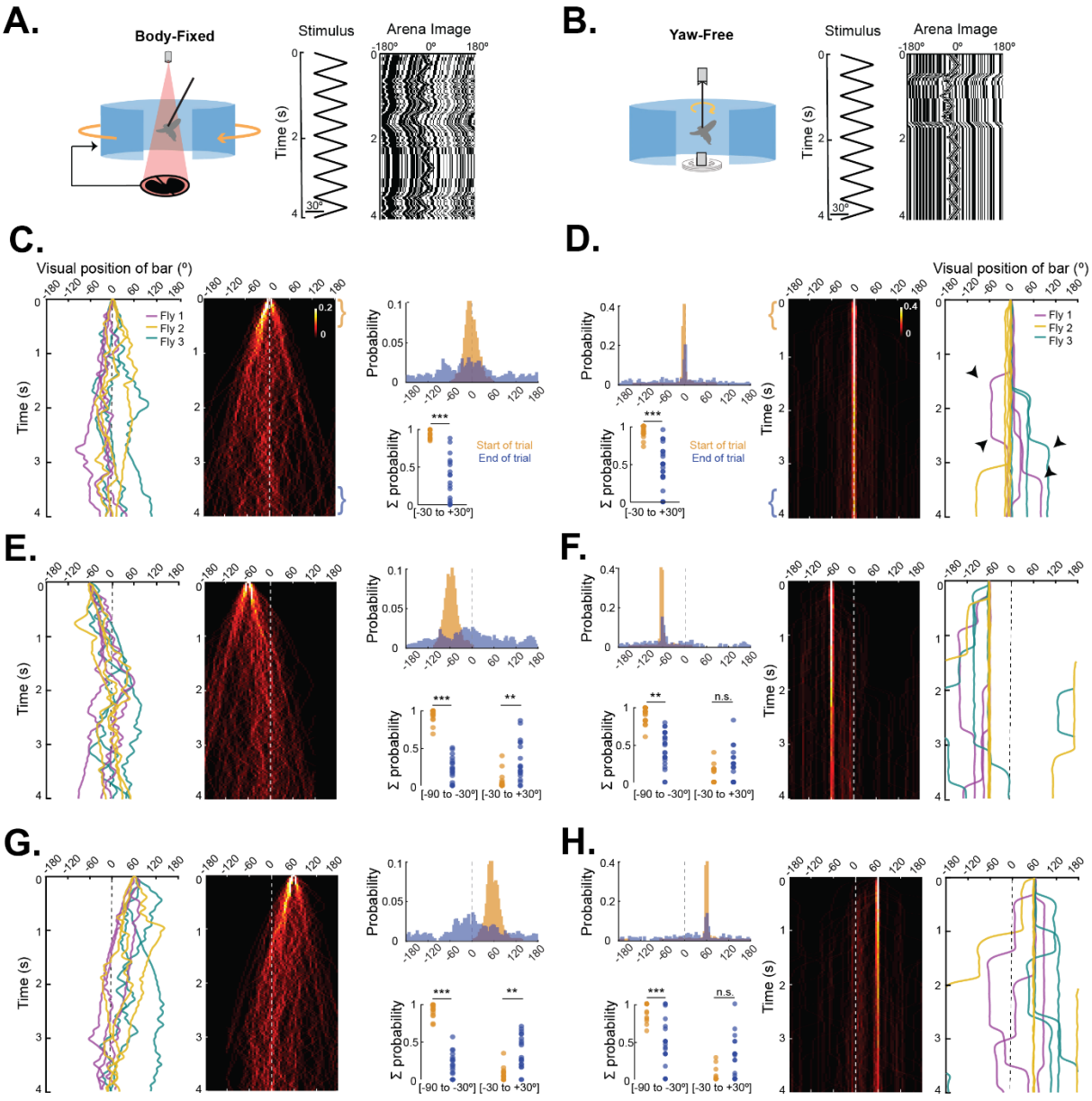

Figure 2. Active bar fixation is body-state dependent. Comparison of body-fixed artificial closed loop conditions in which steering effort of the stationary fly moves the bar (left panels) and yaw-free closed loop experiments in which steering effort moves the fly (right panels). **A.** (left) Cartoon of body-fixed experimental paradigm. (middle) Constant velocity trajectory of a motion-defined bar. (right) Example space-time plot of bar and ground motion as seen from the fly's visual midline. **B.** Similar to A for a fly in a yaw-free paradigm. **C.** Body-fixed artificial closed

loop bar fixation for a bar starting on visual midline. (left) Example traces of bar position for 3 trials each (same color) from 3 flies (3 colors). (middle) Heatmap plots (N = 19, flies, n = 97 trials) of bar position. Colormap indicates the probability of the bar occupying each bin (1ms x 5°). (right, top) Normalized probability histograms are computed from the first (yellow bracket) and last (blue bracket) 0.5 s of each trial. Dotted line indicates visual midline. (right, bottom) The summed probability of flies placing the bar within 30° of the frontal (0°) or lateral (-60° or 60°) angular position bin at the start (yellow) and end (blue) of the trial. Each dot is an individual fly sum. * = $p < 0.05$; ** = $p < 0.01$; *** = $p < 0.001$. **D.** (right) Yaw-free example traces of bar position relative to visual midline in 3 trials (same color) from 3 individual flies (3 colors), presented with a bar oscillating on midline. Saccades are indicated by black arrowheads. (middle) Heatmap plots (N = 24, n = 106 trials) for bar starting on midline (bins 10 ms x 5°). (left, top) Normalized probability histograms at the start and end of trials. **E.** Same as C for a bar starting 60° to the left of midline (N = 19, flies, n = 71 trials). The probability of flies placing the bar in the 0° bin increases from the start to the end of the trial (Kruskal-Wallis test). **F.** Same as D with a bar starting 60° to the left of the fly (N = 24, n = 99 trials) **G.** Same as C for a bar starting 60° to the right of midline (N = 19, flies, n = 104 trials). **H.** Same as D with a bar starting 60° to the right of the fly (N = 24, n = 80 trials). Note that the probability of flies placing the bar in the 0° bin at the end of the trial is not significantly higher than at the start. See also Fig. S1.

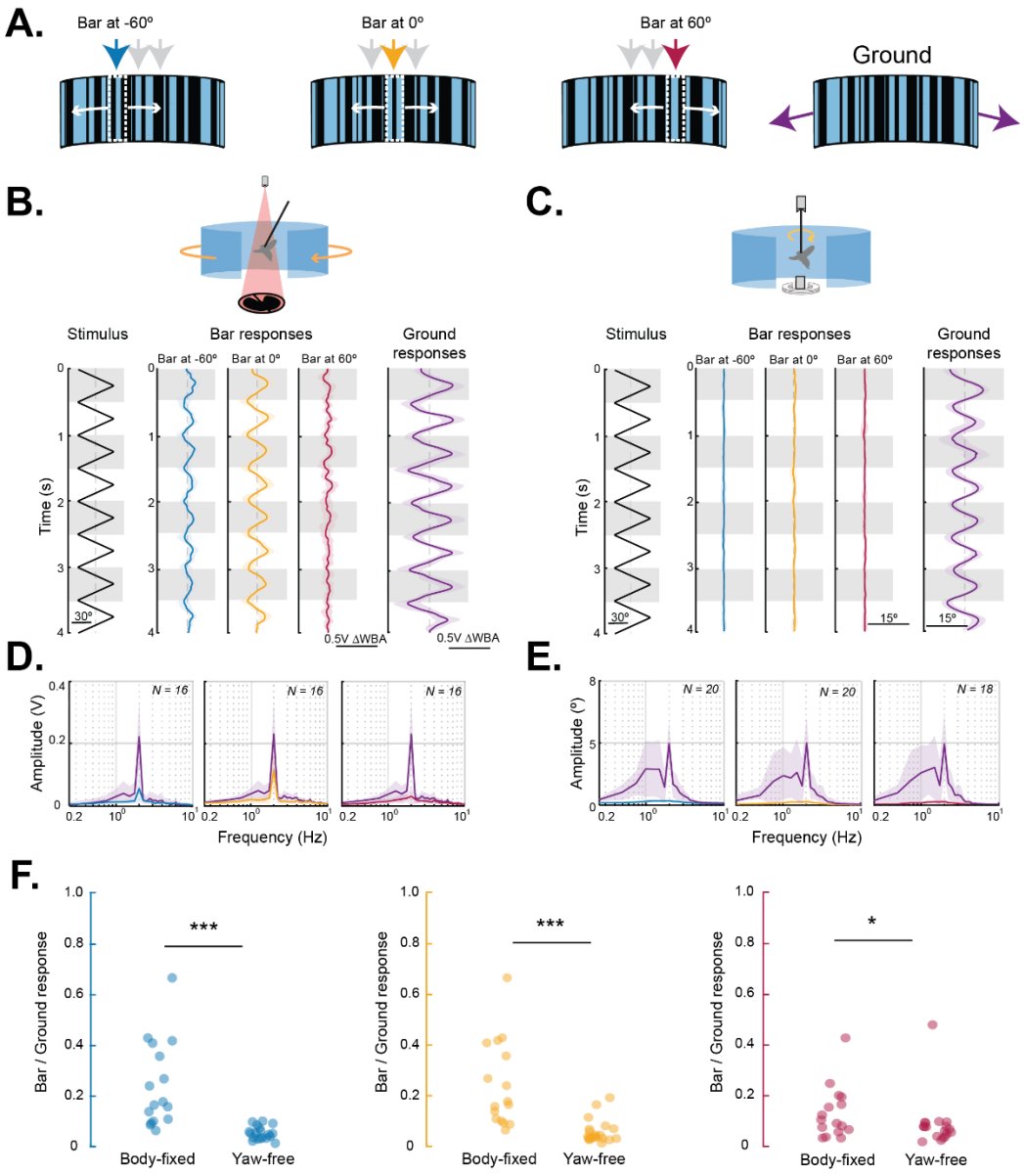

Figure 3. Smooth bar tracking dynamics are body-state dependent. A. Depictions of motion-defined bars oscillating about different azimuthal positions (blue = 60° left of midline; yellow = midline; red = 60° right of midline) and randomly textured large-field ground stimulus (purple). **B.** Open-loop responses of body-fixed flies (N = 16) to bars at three azimuthal positions as indicated. Data were high-pass filtered in order to remove slow DC steering offsets. Note that bar-elicited steering responses are ~60% the amplitude of ground-elicited responses.

Shaded envelopes around solid traces represent standard deviation of mean population responses. Gray bands highlight alternate stimulus cycles. The zero ΔWBA position is indicated by a dotted gray line. **C.** Closed-loop responses of yaw-free flies (N = 20) to the same stimuli as B. Saccades are eliminated from these traces to isolate inter-saccadic bouts in which the bar is in a near-constant position relative to the fly's body axis. **D.** Body-fixed (FFTs) of steering responses in B, color coded for bar position. **E.** Same as D but for yaw-free conditions. **F.** Ratio of bar responses to ground responses, compared between body state conditions, color coded for bar position. Each circle represents an individual fly. Unpaired two-sample t-tests were performed with * = $p < 0.05$; ** = $p < 0.01$; *** = $p < 0.001$. See also Fig S2.

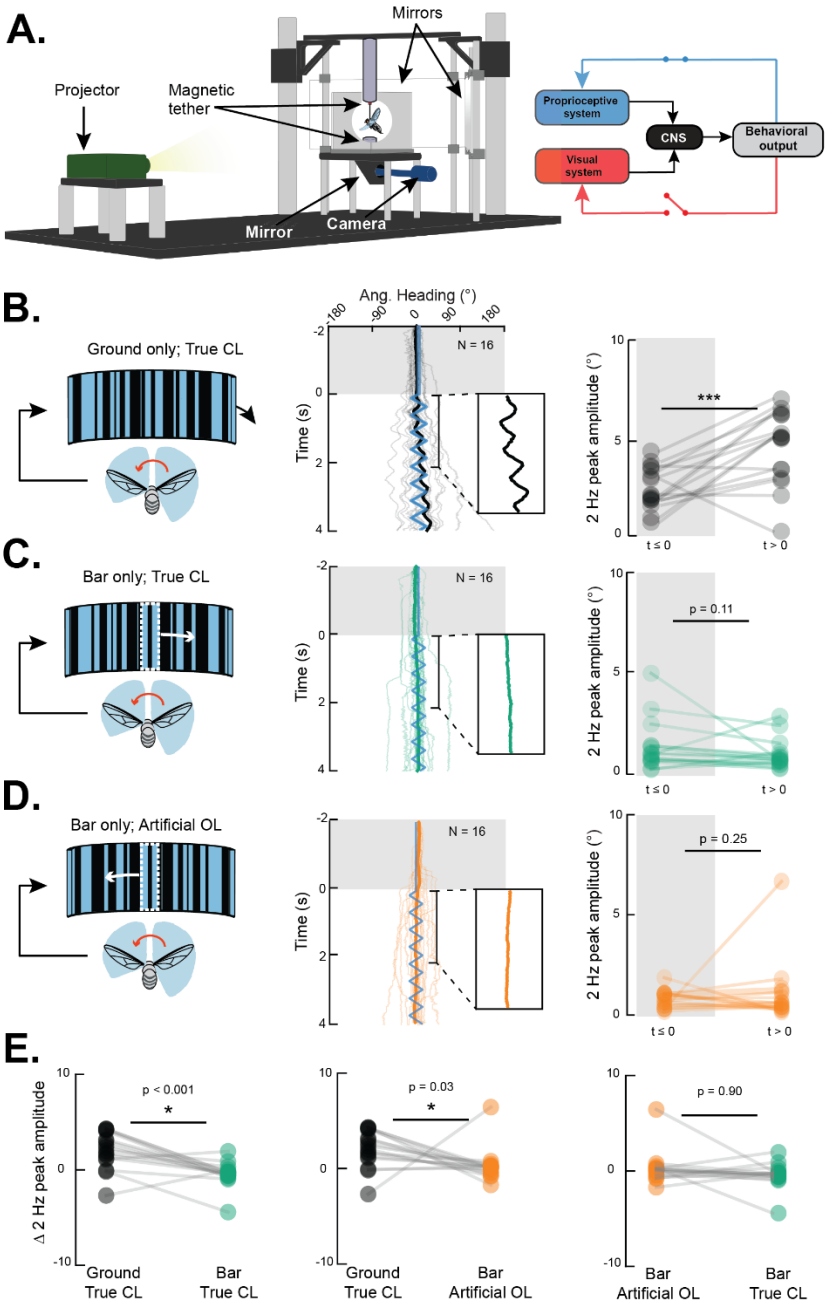

Figure 4. Manipulating visual feedback dynamics does not influence smooth object tracking dynamics. A. Setup for a modified magnetic tether arena in which computer controlled visual stimuli are projected onto a cube surrounding the fly on all sides. Live video tracking allows for “visual clamp” conditions that maintain an image at a fixed position relative to the fly’s major body axis. Thus, proprioceptive feedback is intact, but visual feedback is perturbed. **B.**

(left) In true closed loop yaw-free conditions, a leftward steering effort produced by the fly (red arrow) will generate rightward image motion relative to the body axis (black arrow). (middle) Like Fig. 3, constant velocity ground oscillation (blue trace) elicits smooth optomotor movements of the body. Each trial starts with a stationary phase (gray shaded box). (right) Paired dot plot of FFT magnitude for 2-second periods before and after stimulus motion onset. Each dot represents an individual fly's mean response. Paired Student's t-tests were performed. **C.** (left) Responses to movement of a 30° bar, in true visual and proprioceptive closed loop conditions. Middle and right panels are the same as in B. **D.** (left) Under visual clamp conditions, leftward steering effort produced by the fly results in a matched leftward displacement of the bar such that the position of the bar remains constant. Middle and right panels are the same as in B. Insets in B,C,D (center) zoom in on the population mean. **E.** Comparison of responses before and after motion onset across all three experimental conditions. Each circle represents an individual fly. See also Fig. S3.

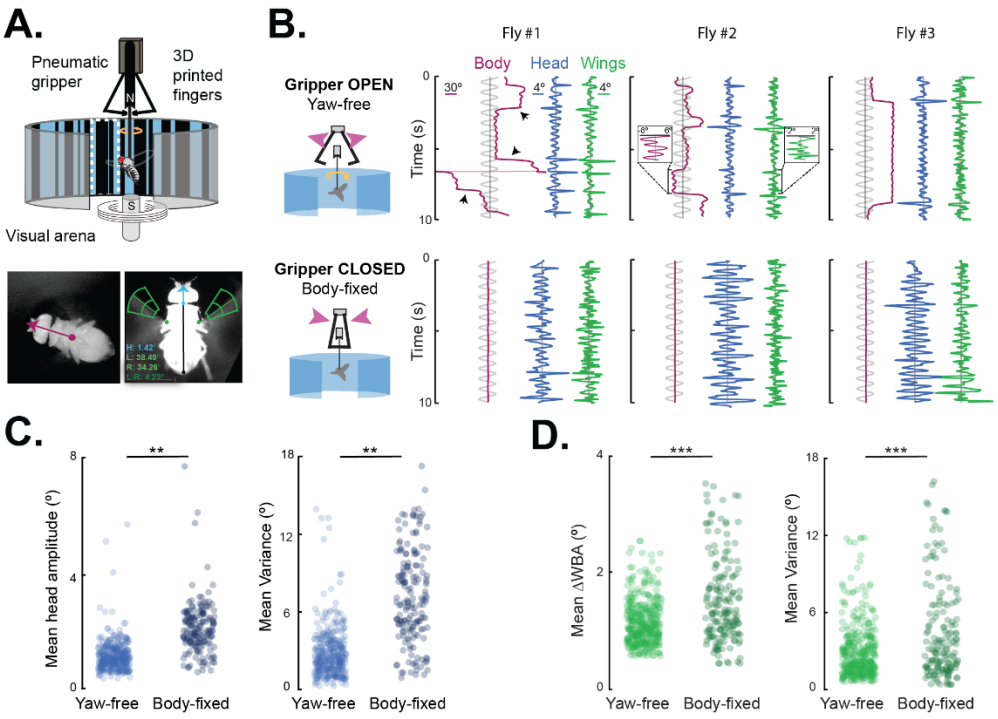

Figure 5. Body-fixing increases amplitude and variance of wing and head movements. A. An actuated gripper modifies the magnetic tether to rapidly switch between body states. Video registers the fly's heading (magenta vector). Head and wing steering kinematics are extracted (blue, green frames). **B.** (top row) Example traces of one yaw-free trial across 3 individuals. The stimulus is a 10 s sinusoidal ground oscillation indicated in light gray. Black arrowheads indicate body saccades, observed in wing and head traces. (bottom row) Upon closing the gripper on the same animals, the body angle is fixed in place. **C.** Mean head dynamics amplitude (left) and variance (right) for 374 yaw-free trials and 175 body-fixed trials in N = 34 flies. Each dot represents a single trial. Unpaired student's t-tests were performed with * = $p < 0.05$; ** = $p < 0.01$; *** = $p < 0.001$. **D.** Mean amplitude of Left minus Right wing beat amplitude (left) and variance (right) for 383 yaw-free trials and 171 body-fixed trials in N =35 flies. Response amplitude represents the averaged absolute value throughout the trial. Variance was similarly computed across the length of each trial. Each dot represents one trial.

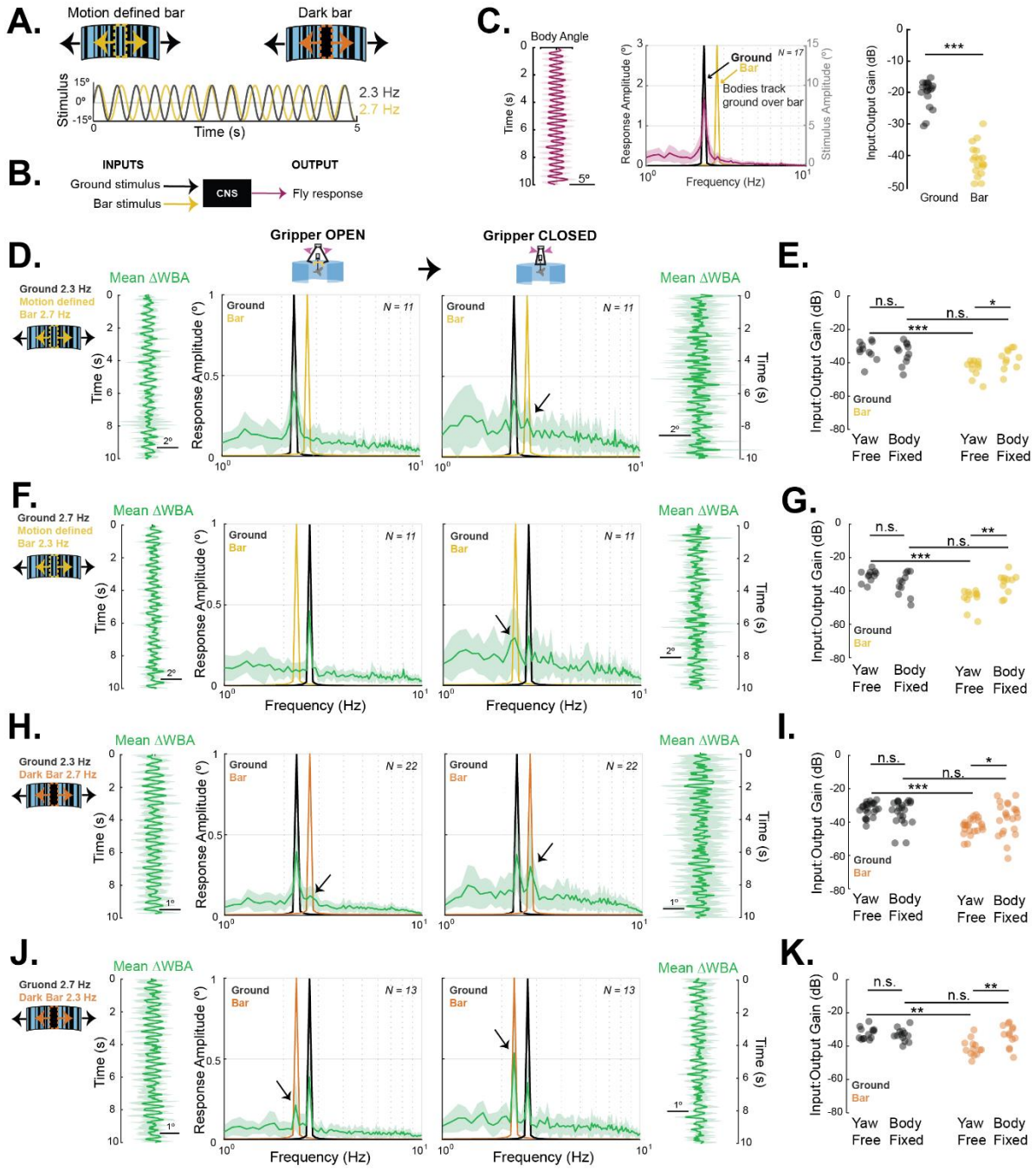

Figure 6. Body-fixing increases the wing steering bar response gain. A. (top) Motion-defined bar or dark bar stimuli are oscillated within an oscillating ground. (bottom) Partial stimulus traces for ground oscillating at 2.3 Hz (black) and bar oscillating at 2.7 Hz (yellow), with 15°amplitude. Note that stimuli move in and out of phase. **B.** Systems identification framework

where the two sinusoidal stimuli are inputs to the central nervous system (CNS) and the fly's steering response is the sole output. **C.** (left) Body movement response for N = 18 flies to compound bar/ground stimuli. Magenta line represents mean body angular position, shaded envelope represents standard deviation. (middle) FFT plots of the body response (left y-axis, black) overlaid with FFT amplitude of ground and bar stimulus inputs (right y-axis, gray). (right) Gain of body responses to the ground (black) and bar (yellow). Gain in decibels is negative as the amplitude of the response output is smaller than the input. Each point represents an individual fly's mean response. Nonparametric Wilcoxon Rank-sum tests were performed. **D.** Population (N=11) wing steering responses in the yaw-free, open gripper condition (left) and body-fixed, gripper closed condition (right). Time domain mean response +/- SD flank FFT plots throughout (green). **E.** Mean response gain, as in C, for ground (black) and bar (yellow) were compared across body states and stimulus types. **F.** Same as D but with motion-defined bar and ground oscillation frequencies swapped. **G.** Same as E but with motion-defined bar and ground oscillation frequencies swapped. **H-K.** Same as D-G but using a 30° solid dark bar stimulus. See also Fig. S4.

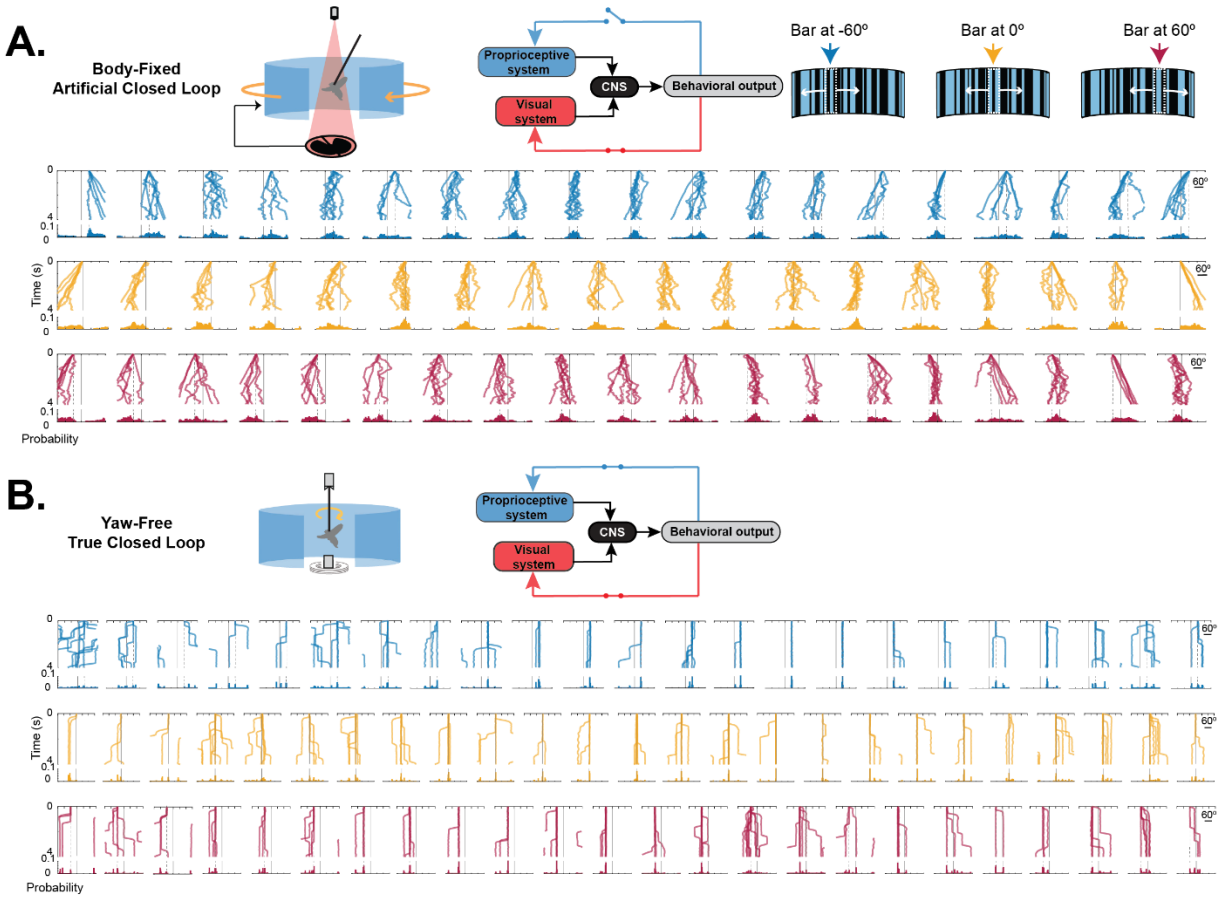

Figure S1. Individual trials, related to Figure 2. A. Body-fixed condition with visual feedback loop artificially closed. Colors represent the azimuthal start location for a motion-defined bar as indicated by cartoons. Each panel shows data from one fly. Top panels show individual responses, with at least 2 trials per fly. Bottom panels show corresponding normalized fixation histograms for those trials. Vertical gray solid lines represent visual midline, vertical dotted lines represent bar starting position. Flies are sorted in order of strongest steering effort away from the bar on the far left to strongest steering efforts toward the bar on the far right. Thus flies that most strongly orient towards the bar are in the middle panels. **B.** Same as A but for yaw-free condition with visual feedback loop artificially closed. Note that while in some trials, flies saccade towards the motion-defined bar, the majority of flies in most trials maintain their original heading relative to the bar.

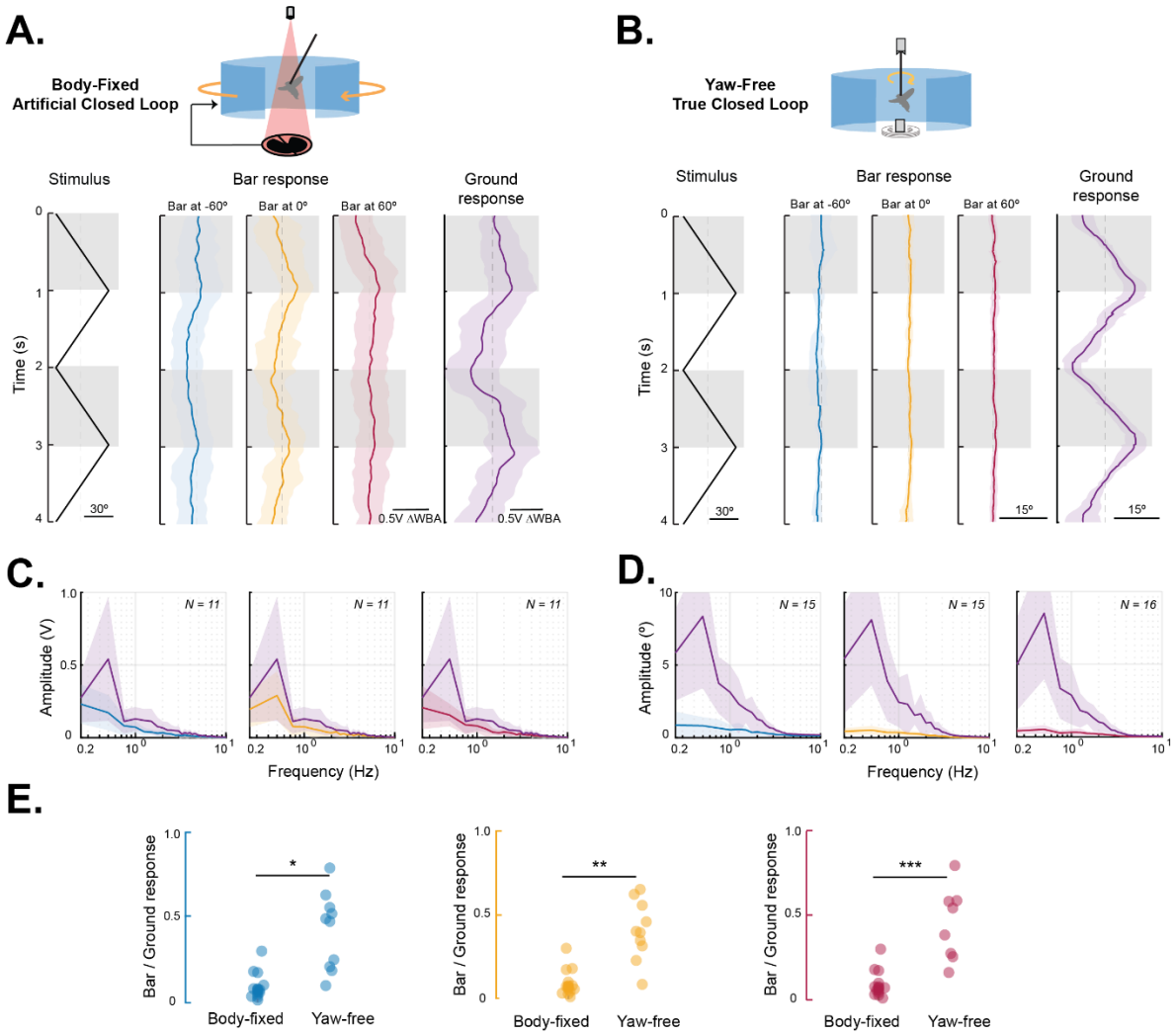

Figure S2. Reduced stimulus velocity does not affect body-state dependence of smooth tracking dynamics, related to Figure 3. A-E. The experiment performed in Fig. 3 was repeated with a motion-defined bar oscillating at 30˚/s (0.5 Hz compared to 2 Hz in Fig. 3). Raw data traces were low-pass filtered with a cutoff frequency of 6 Hz before FFT analysis. Unpaired student's t-tests were performed with * = $p < 0.05$; ** = $p < 0.01$; *** = $p < 0.001$..

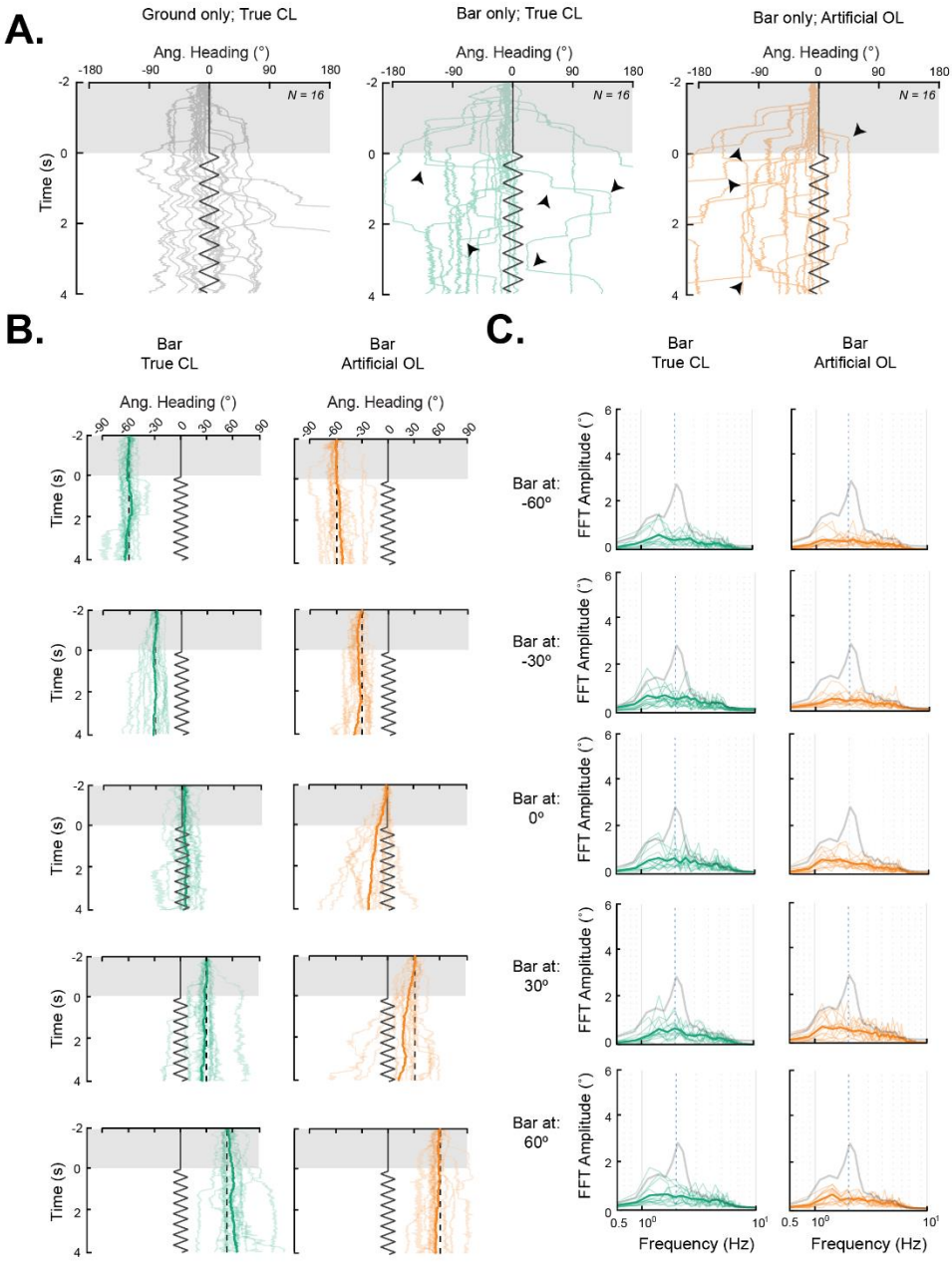

Figure S3. Flies in visual open loop do not smoothly track a motion-defined bar, regardless of initial position, related to Figure 4. A. Raw traces are shown. Yaw-free flies in visual closed loop with the ground moving on a 2 Hz triangle wave trajectory (solid black line) and no bar motion show smooth tracking dynamics (left panel, gray traces) while flies in either visual open- or closed-loop show considerably less smooth dynamics and more saccadic behavior (middle panel, green traces and right panel, orange traces). Saccades are highlighted

with black arrowheads. Stimulus onset occurs at t = 0. **B.** (left) In normal visual closed-loop, flies tend to saccade towards and away from the bar. (right). In artificial visual open loop, flies display similar saccadic behavior regardless of the starting position of the bar. Individual flies are indicated in light color and mean trajectory in darker color. Dotted black line indicates the starting position of the bar. **C.** FFTs of body angle in response to visual closed loop (left, green) and visual open-loop (right, orange). The mean population strength of the ground response is plotted in gray for reference. Note the absence of a peak at 2 Hz, the oscillation frequency of the bar indicated by a dotted blue line.

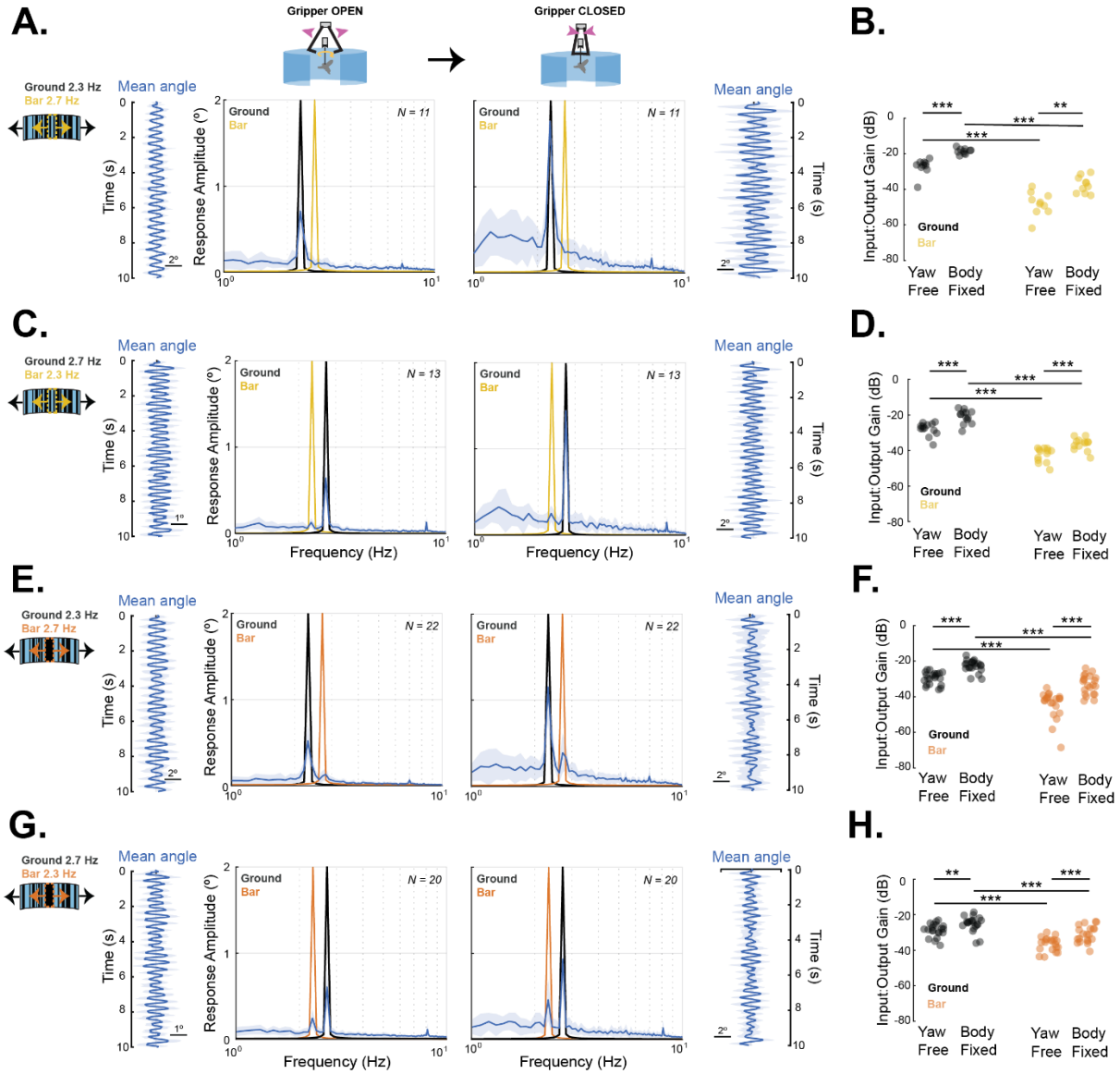

Figure S4. Head steering responses to compound bar and ground stimuli, related to Figures 5&6. A-H. Similar to Fig. 6, the mean time series of head responses flank FFTs for ground and bar stimuli under yaw-free and body-fixed (gripper closed) conditions for within-subjects trials.

REFERENCES

1. Reichardt, W., and Wenking, H. (1969). Optical detection and fixation of objects by fixed flying flies. Naturwissenschaften, 424.

2. Poggio, T., and Reichardt, W. (1973). A theory of the pattern induced flight orientation of the fly Musca domestica. Kybernetik, 185–203.

3. Reichardt, W., Poggio, T., and Hausen, K. (1983). Figure-ground discrimination by relative movement in the visual system of the fly. Biol. Cybern. *46*, 1–30.

4. Reiser, M.B., and Dickinson, M.H. (2010). Drosophila fly straight by fixating objects in the face of expanding optic flow. J. Exp. Biol. *213*, 1771–1781.

5. Fox, J.L., Aptekar, J.W., Zolotova, N.M., Shoemaker, P.A., and Frye, M.A. (2014). Figure-ground discrimination behavior in Drosophila. I. Spatial organization of wing-steering responses. J. Exp. Biol. *217*, 558–569.

6. Götz, K.G. (1987). Course-Control, Metabolism and Wing Interference During Ultralong Tethered Flight in Drosophila Melanogaster. J. Exp. Biol. *128*, 35–46.

7. Reichardt, W., and Poggio, T. (1976). Visual control of orientation behaviour in the fly: Part I. A quantitative analysis. Q. Rev. Biophys. *9*, 311–375.

8. Bausenwein, B., Wolf, R., and Heisenberg, M. (1986). Genetic dissection of optomotor behavior in Drosophila melanogaster. Studies on wild-type and the mutant optomotor-blindH31. J. Neurogenet. *3*, 87–109.

9. Theobald, J.C., Duistermars, B.J., Ringach, D.L., and Frye, M.A. (2008). Flies see second-order motion. Curr. Biol. *18*, R464–R465.

10. Aptekar, J.W., Shoemaker, P.A., and Frye, M.A. (2012). Figure tracking by flies is supported by parallel visual streams. Curr. Biol. *22*, 482–487.

11. Theobald, J.C., Shoemaker, P.A., Ringach, D.L., and Frye, M.A. (2010). Theta motion processing in fruit flies. Front. Behav. Neurosci. *4*. 10.3389/fnbeh.2010.00035.

12. Fenk, L.M., Poehlmann, A., and Straw, A.D. (2014). Asymmetric Processing of Visual Motion for Simultaneous Object and Background Responses. Current Biology *24*, 2913–2919. 10.1016/j.cub.2014.10.042.

13. Reiser, M.B., and Dickinson, M.H. (2008). A modular display system for insect behavioral neuroscience. J. Neurosci. Methods *167*, 127–139.

14. Bender, J.A., and Dickinson, M.H. (2006). Visual stimulation of saccades in magnetically tethered Drosophila. J. Exp. Biol. *209*, 3170–3182.

15. Bender, J.A., and Dickinson, M.H. (2006). A comparison of visual and haltere-mediated feedback in the control of body saccades in Drosophila melanogaster. J. Exp. Biol. *209*, 4597–4606.

16. Duistermars, B.J., and Frye, M. (2008). A magnetic tether system to investigate visual and olfactory mediated flight control in Drosophila. J. Vis. Exp. 10.3791/1063.

17. Mongeau, J.-M., and Frye, M.A. (2017). Drosophila Spatiotemporally Integrates Visual Signals to Control Saccades. Curr. Biol. *27*, 2901–2914.e2.

18. Keleş, M.F., Mongeau, J.-M., and Frye, M.A. (2019). Object features and T4/T5 motion detectors modulate the dynamics of bar tracking by Drosophila. J. Exp. Biol. *222*. 10.1242/jeb.190017.

19. Cellini, B., and Mongeau, J.-M. (2022). Nested mechanosensory feedback actively damps visually guided head movements in Drosophila. Elife *11*. 10.7554/eLife.80880.

20. Elzinga, M.J., Dickson, W.B., and Dickinson, M.H. (2012). The influence of sensory delay on the yaw dynamics of a flapping insect. J. R. Soc. Interface *9*, 1685–1696.

21. Bartussek, J., and Lehmann, F.-O. (2016). Proprioceptive feedback determines visuomotor gain in Drosophila. R. Soc. open sci. 10.1098/rsos.150562.

22. Mongeau, J.-M., and Frye, M.A. (2017). Drosophila Spatiotemporally Integrates Visual Signals to Control Saccades. Curr. Biol. *27*, 2901–2914.e2.

23. Mongeau, J.-M., Cheng, K.Y., Aptekar, J., and Frye, M.A. (2019). Visuomotor strategies for object approach and aversion in Drosophila melanogaster. J. Exp. Biol. *222*. 10.1242/jeb.193730.

24. Fox, J.L., and Frye, M.A. (2014). Figure-ground discrimination behavior in Drosophila. II. Visual influences on head movement behavior. J. Exp. Biol. *217*, 570–579.

25. Cellini, B., and Mongeau, J.-M. (2020). Active vision shapes and coordinates flight motor responses in flies. Proc. Natl. Acad. Sci. U. S. A. *117*, 23085–23095.

26. Duistermars, B.J., Reiser, M.B., Zhu, Y., and Frye, M.A. (2007). Dynamic properties of large-field and small-field optomotor flight responses in Drosophila. J. Comp. Physiol. A *193*, 787–799.

27. Cellini, B., Salem, W., and Mongeau, J.-M. (2022). Complementary feedback control enables effective gaze stabilization in animals. Proc. Natl. Acad. Sci. U. S. A. *119*, e2121660119.

28. Hardcastle, B.J., and Krapp, H.G. (2016). Evolution of Biological Image Stabilization. Curr. Biol. *26*, R1010–R1021.

29. Blondeau, J., and Heisenberg, M. (1982). The three-dimensional optomotor torque system of Drosophila melanogaster. J. Comp. Physiol. *145*, 321–329.

30. Bahl, A., Ammer, G., Schilling, T., and Borst, A. (2013). Object tracking in motion-blind flies. Nat. Neurosci. *16*, 730–738.

31. Busch, C., Borst, A., and Mauss, A.S. (2018). Bi-directional Control of Walking Behavior by Horizontal Optic Flow Sensors. Curr. Biol. *28*, 4037–4045.e5.

32. Egelhaaf, M., and Reichardt, W. (1987). Dynamic response properties of movement detectors: Theoretical analysis and electrophysiological investigation in the visual system of the fly. Biol. Cybern. *56*, 69–87.

33. Virsik, R.P., and Reichardt, W. (1976). Detection and Tracking of Moving Objects by the Fly Musca domestica. Biol. Cybern. *23*, 83–98.

34. Fujiwara, T., Brotas, M., and Chiappe, M.E. (2022). Walking strides direct rapid and flexible recruitment of visual circuits for course control in Drosophila. Neuron *110*, 2124–2138.e8.

35. Egelhaaf, M. (1987). Dynamic properties of two control systems underlying visually guided turning in house-flies. Journal of Comparative Physiology A *161*, 777–783.

36. Hesselberg, T., and Lehmann, F.-O. (2007). Turning behaviour depends on frictional damping in the fruit fly Drosophila. J. Exp. Biol. *210*, 4319–4334.

37. Mureli, S., and Fox, J.L. (2015). Haltere mechanosensory influence on tethered flight behavior in Drosophila. J. Exp. Biol. *218*, 2528–2537.

38. Sherman, A., and Dickinson, M.H. (2004). Summation of visual and mechanosensory feedback in Drosophila flight control. J. Exp. Biol. *207*, 133–142.

39. Straw, A.D., Tómasson, E., and Dickinson, M.H. (2011). Active and passive antennal movements during visually guided steering in flying Drosophila. Journal of.

40. Cellini, B., and Mongeau, J.-M. (2020). Hybrid visual control in fly flight: insights into gaze shift via saccades. Curr Opin Insect Sci *42*, 23–31.

41. Taylor, G.K., and Krapp, H.G. (2007). Sensory Systems and Flight Stability: What do Insects Measure and Why? In Advances in Insect Physiology, J. Casas and S. J. Simpson, eds. (Academic Press), pp. 231–316.

42. Sane, S.P., Dieudonné, A., Willis, M.A., and Daniel, T.L. (2007). Antennal mechanosensors mediate flight control in moths. Science *315*, 863–866.

43. Pringle, J.W.S. (1948). The gyroscopic mechanism of the halteres of Diptera. Philos. Trans. R. Soc. Lond. B Biol. Sci. *233*, 347–384.

44. Fayyazuddin, A., and Dickinson, M.H. (1996). Haltere afferents provide direct, electrotonic input to a steering motor neuron in the blowfly, Calliphora. Journal of Neuroscience *16*, 5225–5232.

45. Fayyazuddin, A., and Dickinson, M.H. (1999). Convergent mechanosensory input structures the firing phase of a steering motor neuron in the blowfly, Calliphora. J. Neurophysiol. *82*, 1916–1926.

46. Chan, W.P., Prete, F., and Dickinson, M.H. (1998). Visual input to the efferent control system of a fly's" gyroscope." Science *280*, 289–292.

47. Dickerson, B.H., De Souza, A.M., Huda, A., and Dickinson Correspondence, M.H. (2019). Flies Regulate Wing Motion via Active Control of a Dual-Function Gyroscope. Curr. Biol. *29*, 3517–3524.e3.

48. Frye, M.A., Tarsitano, M., and Dickinson, M.H. (2003). Odor localization requires visual feedback during free flight in Drosophila melanogaster. J. Exp. Biol. *206*, 843–855.

49. Maimon, G., Straw, A.D., and Dickinson, M.H. (2008). A simple vision-based algorithm for decision making in flying Drosophila. Curr. Biol. *18*, 464–470.

50. van Breugel, F., and Dickinson, M.H. (2012). The visual control of landing and obstacle avoidance in the fruit fly Drosophila melanogaster. J. Exp. Biol. *215*, 1783–1798.

51. Linneweber, G.A., Andriatsilavo, M., Dutta, S.B., Bengochea, M., Hellbruegge, L., Liu, G., Ejsmont, R.K., Straw, A.D., Wernet, M., Hiesinger, P.R., et al. (2020). A neurodevelopmental origin of behavioral individuality in the *Drosophila* visual system. Science *367*, 1112–1119.

52. Park, E.J., and Wasserman, S.M. (2018). Diversity of visuomotor reflexes in two Drosophila species. Curr. Biol. *28*, R865–R866.

53. Cheng, K.Y., and Frye, M.A. (2021). Odour boosts visual object approach in flies. Biol. Lett. *17*, 20200770.

54. Wolf, R., and Heisenberg, M. (1990). Visual control of straight flight in Drosophila melanogaster. J. Comp. Physiol. A *167*, 269–283.

55. Roth, E., Sponberg, S., and Cowan, N.J. (2014). A comparative approach to closed-loop computation. Curr. Opin. Neurobiol. *25*, 54–62.

56. Reichardt, W. (1962). Nervous integration in the facet eye. Biophys. J. *2*, 121–143.

57. Tammero, L.F., Frye, M.A., and Dickinson, M.H. (2004). Spatial organization of visuomotor reflexes in Drosophila. J. Exp. Biol. *207*, 113–122.

58. Cabrera, S., and Theobald, J.C. (2013). Flying fruit flies correct for visual sideslip depending on relative speed of forward optic flow. Front. Behav. Neurosci. *7*, 76.

59. Currea, J.P., Smith, J.L., and Theobald, J.C. (2018). Small fruit flies sacrifice temporal acuity to maintain contrast sensitivity. Vision Res. *149*, 1–8.

60. Roth, E., Zhuang, K., Stamper, S.A., Fortune, E.S., and Cowan, N.J. (2011). Stimulus predictability mediates a switch in locomotor smooth pursuit performance for Eigenmannia virescens. J. Exp. Biol. *214*, 1170–1180.

Chapter 3

The role of haltere-mediated proprioceptive feedback in modulating visual object tracking in *D. melanogaster*

INTRODUCTION

Owing to the high-performance requirements for flight control in insects, the visual control of flight and target fixation in flies has enjoyed a rich history of research and discovery by engineers and neurobiologists. Like virtually every seeing system on the planet, flies shift their direction of gaze in order to minimize image blur and maintain visual acuity. During fly flight, optomotor reflexes steer the body and head to balance optic flow across the two eyes. Stabilizing optomotor reflexes are interrupted by voluntary gaze shifts to pursue salient visual targets [1].

The canonical control models for balancing “wide-field” (occupying the full visual field) panoramic optic flow and pursuing “small-field” (narrow region of visual field) targets, or objects, are both based on directional motion vision [2]. The strength of continuous optomotor steering responses is proportional to stimulus velocity and operates at near unity gain [3–5]. Steering responses in the direction of the velocity of motion are so powerful under open loop feedback conditions [6,7] that when the animal is put under artificial closed loop feedback conditions in which steering rate is electronically coupled to object velocity, a tethered fly will actively steer to “fixate” the object on visual midline for up to 36 hours [8]. Midline centering or “fixation” is a highly robust visual reflex in flies, persisting even for objects that are camouflaged against the visual surroundings [7,9,10], or for objects made of flicker, counter-directional motion, or other higher order cues [11].

Frontal object fixation is typically demonstrated using a flight simulator in which the animal is “body-fixed”, or rigidly tethered in place, and for which wing torque signals are electronically coupled to yaw image velocity, generating “virtual reality closed-loop” feedback conditions. To study the effects of body movement feedback on visual object fixation, we have recently carried out a study in which the animal is “yaw-free”, or able to produce naturalistic turning maneuvers in the yaw plane, using a magnetic tether apparatus. We discovered that smooth dynamic responses to object motion are gated by body state such that compromising proprioceptive feedback via

body-fixing results in artificially high gain optomotor responses to object motion [12]. The corollary to this finding is that in the presence of appropriate body state feedback, as is the case in yaw-free flight preparations, eliminates the robust velocity-driven small-field smooth object responses characterized in body-fixed preparations. This result indicates that a neural signal related to yaw body dynamics must strongly modulate visuo-motor processing for object orientation. Such interactions are at present not included in any conceptual or quantitative model of active object vision.

Proprioception is the sense of body position and movement. In flies, numerous mechanosensory organs encode body dynamics during flight, including the wings, antennae, and most notably the gyroscopic haltere organs [1,13–16]. The halteres are modified from hindwings into small fluid-filled dumbbells that consist of a stalk, housing fields of campaniform sensilla, and a bulb, which beats 180° out of phase with the wings but serves no aerodynamic role (Figure 1A). The halteres are deeply integrated in complex feedforward and feedback circuits with local wing motor centers through direct electrical synapses and with the central brain through less understood circuits whose wiring diagram involves both efferent and afferent pathways (Figure 1B). The cross-product of the linear velocity of the beating halteres and the angular velocity of the fly's body produces a Coriolis force that acts upon minute campaniform sensilla strain gauges that precisely encode this force [17]. Thus, the haltere sensory organs, like aeronautic gyroscopes, are exquisitely sensitive to angular rotation rates, and elicit rapid compensatory course corrections in flight [16,18,19].

Because vision and mechanosensation operate on divergent timescales, rapid proprioceptive reflexes have been modeled within an 'inner loop' of flight stabilization reflexes operating at high frequency yaw rate, whereas slower visuomotor processing of object motion has traditionally been modeled by an 'outer loop' pathway that is tuned to low frequency yaw motion [1,14]. The underlying biology supports this split control architecture; mechanosensory neurons from the gyroscopic halteres form direct electrical synapses with flight muscle motoneurons, whereas

visual signals are conveyed along poly-synaptic signaling pathways from the retina through the brain, into the ventral motor centers [20,21].

Although the frequency fractionation of mechano-motor (mechanically induced flight steering reflexes) and optomotor stabilization (visually induced reflexes) implies separate control circuits, the two systems have been shown to interact. Mechanical rotation about any axis reduces the gain of responses to visual rotation in body-fixed flies, and therefore feedback from the gyroscopic haltere sensory organs seems to act like a “switch” to attenuate the gain of optomotor responses [16]. It is thought that this interaction occurs at the synapse between wide-field motion detecting neurons and descending pre-motor commands.

Why would rapid mechanosensory feedback *attenuate* optomotor equilibrium dynamics? High gain optomotor control preserves visual sensitivity by reducing blur, but any high gain system is susceptible to instabilities such as oscillatory ringing [22]. Accordingly, a body-fixed fly under virtual closed-loop control shows conspicuous ringing oscillations when the coupling gain is high [23]. For robust, stable and rapid object tracking, *active damping* is required for stability under large tracking gain [24]. Indeed, work with a dynamically scaled robotic platform demonstrated that rapid mechano-motor reflexes can act on the time scale of a single wing stroke to actively damp yaw rate, thereby imparting the high gain visuomotor control system with robustness and stability [25]. In a well-tuned system such as this, perturbing compensatory active damping, as would occur by rigidly tethering a fly and eliminating proper proprioceptive signals, would be expected to extend the duration of yaw dynamics beyond those seen under naturalistic free flight conditions [25]. Intuitively, this means that a yaw torque command to fixate a visual target, executed without the mechanosensory feedback to dampen body rotation, could be expected to extend the duration of the steering maneuver. Under virtual reality closed-loop conditions, extended yaw would result in correspondingly extended image slip, and another delayed optomotor stabilization command. The sequence would repeat itself resulting in ‘ringing’. This visual phenomenon is observable by any lab that uses these VR devices when the coupling gain is set too high. Thus, underdamped

steering responses due to increased proprioceptive delays could, paradoxically, *enhance* the strength of frontal object fixation. This phenomenon has been demonstrated experimentally: ablating sensory signals from the haltere strain sensors causes *increased* frontal object fixation by body-fixed flies [26], yet the field still has no satisfying explanation for why.

Disrupting natural mechanosensory feedback dynamics by rigidly fixing the body seems to qualitatively alter visual object responses during flight. This finding is unexpected and, to date, there has been no experimental or theoretical evidence to suggest how this interaction between the visual and proprioceptive systems impacts object vision. Thus, the goal of the studies described in this chapter is to discover the functional cellular circuits that implement the proprioceptive control of active target vision. We hypothesize a mechanism regulated through a visuo-proprioceptive feedback loop that is composed of (i) feedforward neurons descending from the brain to innervate haltere proprioceptive sensors and (ii) feedback haltere sensory neurons ascending into the brain to actively damp visual processes. Discovering how proprioceptive mechanosensory signals interact with visual processing at a mechanistic level will transform our understanding of the neural underpinnings of active target vision and deeply impact our theoretical models of object tracking and flight control algorithms.

PRELIMINARY RESULTS AND METHODS

Silencing of a haltere-targeting descending neuron increases bar fixation

We first conducted an experiment aiming to perturb the haltere sensorimotor circuit by targeting a recently classified descending neuron, DNp17. This bilateral neuron is primarily postsynaptic in the Inferior Posterior Slope (IPS), a visual premotor area, and selectively innervates the haltere motor center located between the meso- and meta-thoracic neuropils in the VNC (Figure 1C) [27]. We silenced 6-8 pairs of DNp17 using the readily available Janelia split Gal 4 driver line SS02553 and the temperature-sensitive silencing reagent, UAS-Shibire(ts).

This inducible effector impairs the function of the fly ortholog of dynamin at high-temperatures (restrictive condition, above 30 ℃) prohibiting synaptic vesicle release and effectively silencing the neuron, and allows normal synaptic release and neural transmission at the lower permissive temperatures below 30 ℃ [28]. To assess object tracking behavior, we performed all experiments in the yaw-free magnetic tether paradigm, which allows unrestricted movement and turning within the yaw plane of motion, enabling closed loop feedback in both the visual and proprioceptive modality (Figure 1D). As in previous studies, we presented a visual object consisting of a 30° wide vertical motion-defined bar, oscillating at 2 Hz on a broadband, stationary patterned ground (Figure 1E). Bars were presented at all locations around the arena, and object orientation behavior towards objects appearing 60° to the left or the right of the fly was quantified as previously described [12].

We found that the probability of flies fixating the oscillating bar on visual midline increased significantly when DNp17 was silenced (Figure 1E-H). While small shifts in the probability distribution were observed for all treatment groups, including promotorless “empty” split Gal4 genetic controls, between the start and the end of a 4s trial (yellow and blue distributions), only within the experimental group (DNp17-Gal4 > UAS-Shibire(ts) at 35 ℃) did flies significantly re-orient towards the bar. This result was independent of the initial left or right bar placement and also resulted in visible increase in oscillatory smooth tracking dynamics within 1s of stimulus onset in some individuals (Figure 1F, white arrows; quantification not shown).

This is remarkable! An intuitive interpretation is that silencing these bilateral pairs of descending neurons breaks the visuo-mechanosensory feedback loop in a manner that recapitulates the effect of body-fixing a fly. These data support our hypothesis that mechanosensory signaling is part of a control circuit for active target vision. These preliminary findings suggest that intact signaling between central brain regions and the haltere motor center are necessary to maintain the appropriately damped low gain object-directed responses we

have previously observed in yaw-free paradigms. There are, however, considerable limitations associated with the SS02553 driver line. In addition to DNp17, this line also targets VNC interneurons in the leg neuropils, lower tectulum and, importantly, the accessory mesothoracic neuropil (AMNp) which receives sensory afferents from the wing and notum (Figure 1B). Thus, this experiment alone cannot connect the object orientation behavioral phenotype we observed to haltere circuit function.

Intersectional split Gal4 genetic screen yielded haltere-specific reagents

To confirm that the underdamped object responses we observed are due to haltere-related function, more cell-specific drivers that selectively label DNp17 are necessary. To this end, we performed a split Gal4 screen to generate driver lines that selectively target the haltere efferent DNp17 and haltere afferent neurons (hANs) (Figure 2A). Building upon the binary Gal4-UAS system, the split Gal-4 approach in Drosophila allows restriction of expression to very few cell types through the intersectional logic of combining two enhancers (hemi-drivers) that label largely non-overlapping cell groups - expression of a target effector is only achieved in the few cells belonging to both groups (Figure 2B) [29].

We selected 32 enhancer combinations for screening, with 6 combinations targeting the efferent DNp17 cell type and the other 26 combinations targeting primary sensory afferents that carry campaniform sensilla sensory signals to the VNC through the haltere nerve (HN) (Table 1). Hand-selected hemi-driver lines were balanced and crossed to each other to establish stable populations of the genotype w1118; x-AD/Cyo; y- DBD/TM6B; +. These new split Gal4 reagents were then crossed to the reporter line w+; DL+; UAS-Kir2.1::eGFP; +. Whole brains were dissected, immunostained using anti-Brp (NC82) and anti-GFP antibodies and imaged using confocal microscopy. Expression patterns in the brain and VNC of candidate hemi-driver

combinations were visualized in search of sparse labeling of target cells. The following characteristics were qualitatively assessed (Table 2):

1. Whether the candidate driver was a hit for the cells targeted.
2. The relative number of cells expressed in the driver.
3. Sparsity of labeling for the cells targeted.

17 hemi-driver combinations, 4 targeting DNp17 and 13 targeting hANs, were hits for the cells targeted and assigned individual shorthand IDs. An exemplar subset of these candidates are represented in Figure 4C-K. The DNp17 screen specifically targeted a known cell line and was successful in isolating the desired descending neurons with few to no off-target cells (Figure 2C-E). The hAN screen, on the other hand, did not target a specific cell population but rather broadly aimed to isolate primary sensory afferents in the haltere nerve that may receive input from any single or combination of campaniform sensilla fields on the haltere. Thus, the identity of the hAN neural populations isolated and their potential overlap in the various candidate drivers remains to be further characterized. The diversity of expression patterns isolated in the 13 hAN candidates provides ample opportunities for behavioral and functional neurophysiology assays. Some lines, such as hAN_2 and hAN_6, that target very few cells provide the advantage of a highly specific neural manipulation - however, a behavioral phenotype may be difficult to isolate if it is rescued by redundancies in the haltere circuit. Other lines with denser labeling, such as hAN_8 and hAN_10 label more cells, providing the advantage of more robust circuit-breaking perturbations at the cost of specificity as they label some off-target cells as well. In this case, appropriate controls can be used to eliminate such confounds and multiple lines can be used for cross-validation. Overall, this genetic screen yielded a number of unique reagents that provide an entry-point into targeted mechanistic

manipulations of the proprioceptive haltere feedback circuit proposed to actively damp visual responses.

EXPERIMENTAL PLAN

Using the preliminary findings and new neuronal labeling lines generated, this study will make use of an innovative experimental pipeline composed of electronic virtual reality flight simulators, the mathematical language of control theory and system identification, genetically targeted neuronal silencing proteins and optically activated ion channels, and live activity imaging. This pipeline allows us to “read” information from neural circuits from functional visual and mechanosensory systems, and “write” functional activity back into these same circuits. We therefore have the power to test hypotheses both at the level of behavioral function (algorithms) and neural activity (circuits).

Assessment of the role of haltere function on visual object pursuit using circuit-breaking behavioral assays

A first set of experiments will test the hypothesis that perturbations to haltere feedback “phenocopies” the effect of body-fixing flies with a rigid tether and results in frontal bar fixation. We will manipulate the *in vivo* function of haltere circuit neurons in flies that are free to steer in the yaw plane. Specifically, DNp17 and hAN candidate drivers will be constitutively silenced using neuronal inactivators including the inward current rectifying potassium channel Kir2.1 that maintains a hyperpolarized membrane potential, and tetanus toxin light chain TNT that deactivates synaptic vesicle fusion. The behavioral effects of silencing will be preliminarily quantified using the already described object orientation behavioral assay where bars can be oscillated at single frequencies (Figure 3A) - moreover, in this simple assay, the stimulus properties can easily be expanded to more complex motion trajectories spanning ecologically relevant frequency ranges as demonstrated in Chapter 4. This provides an opportunity to use

control theory modeling to generate specific hypotheses that address exactly how silencing circuit components might be modulating the visuomotor control loop.

Once we identify a static (constitutively active) silencing phenotype from a specific Gal4 population, we will complement these results using inducible effectors, including thermally and optically activated ion channels to dynamically perturb the same neurons during our behavioral assay. As a particularly valuable tool, precise temporal and spatial stimulation can be achieved using channelrhodopsin optogenetic tools including GtACR (hyperpolarizing) and CsChrimson (depolarizing) [30,31], in a newly modified version of the magnetic tether paradigm in which optogenetic stimulation light is focused directly onto the fly's thorax using a dichroic filter, without interrupting the tracking video image (Figure 3B). This precision focusing apparatus will allow the stimulation of densely labeled hAN candidates in the ventral nerve cord, without exciting off-target expression in the brain. This apparatus will also minimize the deleterious effects of stimulating the visual system, which has limited the interpretation of results from other work that used csChrimson [32].

The complement of loss-of-function via static silencing effectors and gain-of-function via dynamic activators gives us high experimental power to resolve and cross-validate potentially subtle effects of manipulating neuronal function *in vivo*. Neuronal manipulations may manifest in a band-specific manner in the frequency domain, for example by selectively impacting low frequency visuo-motor object motion responses and not high-frequency responses. We anticipate that optogenetic activation acts in a similar manner as neuronal silencing - as a perturbation. In other words, we do not hold *a priori* expectations that neuronal activation will be the logical inverse of neuronal silencing. Importantly, any genetic perturbation that results in enhanced closed-loop frontal bar fixation by yaw-free flies would support our overall hypothesis that the visuo-mechanosensory control loop is crucial for active object vision and our conceptual model that proprioceptive mechanosensory signaling is important for damping or attenuating or stabilizing high gain visual reflexes.

Assessment of the haltere feedback on visual system using in vivo calcium imaging

A second set of studies using the new split-Gal4 screen shall additionally explore the functional neurophysiological link between haltere centers and the visual system directly using two-photon excitation microscopy. We will use the generated candidate driver lines to image calcium activity *in vivo* in flies presented with visual stimuli (Figure 3C). Such experiments can be performed both in quiescent preparations using protocols already published in the Frye lab [33], as well as in “flying fly” preparations where the animal’s wings and thorax are unrestricted, thereby more closely reflecting a flight behavioral state where the body is experiencing a limited amount of body motion feedback.

Using this approach, we will specifically test two hypotheses. First we will test whether descending neurons to the haltere motor centers carry visual signals. To do this, we will present both large-field and small-field visual stimuli *in vivo*, while recording calcium dynamics in sparsely labeled DNp17 cell populations in both quiescent and flying states. We expect to find that DNp17 activity is modulated by visual input, perhaps in a permissive manner whereby any motion vision input will act as a switch to generate tonic haltere output that signals a “flying” body state and gain-modulates visual circuits. In this setup, the motion kinematics of the haltere can also be readily monitored to quantify vision-driven steering dynamics in the halteres.

Secondly, we will test whether ascending neurons to the optic lobe influence the activity of motion-detecting neurons. Here, hANs will be optogenetically stimulated while imaging from visual system neurons to test the influence of mechanosensory activity on visual motion processing. Due to their anatomical location as output visual integrators and their well documented gain-modulation, LPTCs are good candidate visual neurons in which haltere body-state sensory afferent input may be represented. Thus, within the same fly, we will optogenetically drive hANs while recording calcium activity in LPTCs. As we do not know the campaniform fields, and therefore naturalistic patterns of activation, providing the input to the various hAN lines we

generated, this experiment may require some tweaking of both optogenetic stimulus dynamics and exact lines used. In this setup, the halteres can also be mechanically oscillated while recording from LPTCs if the lines available prove to be too sparse to drive a visual response.

FIGURES AND TABLES

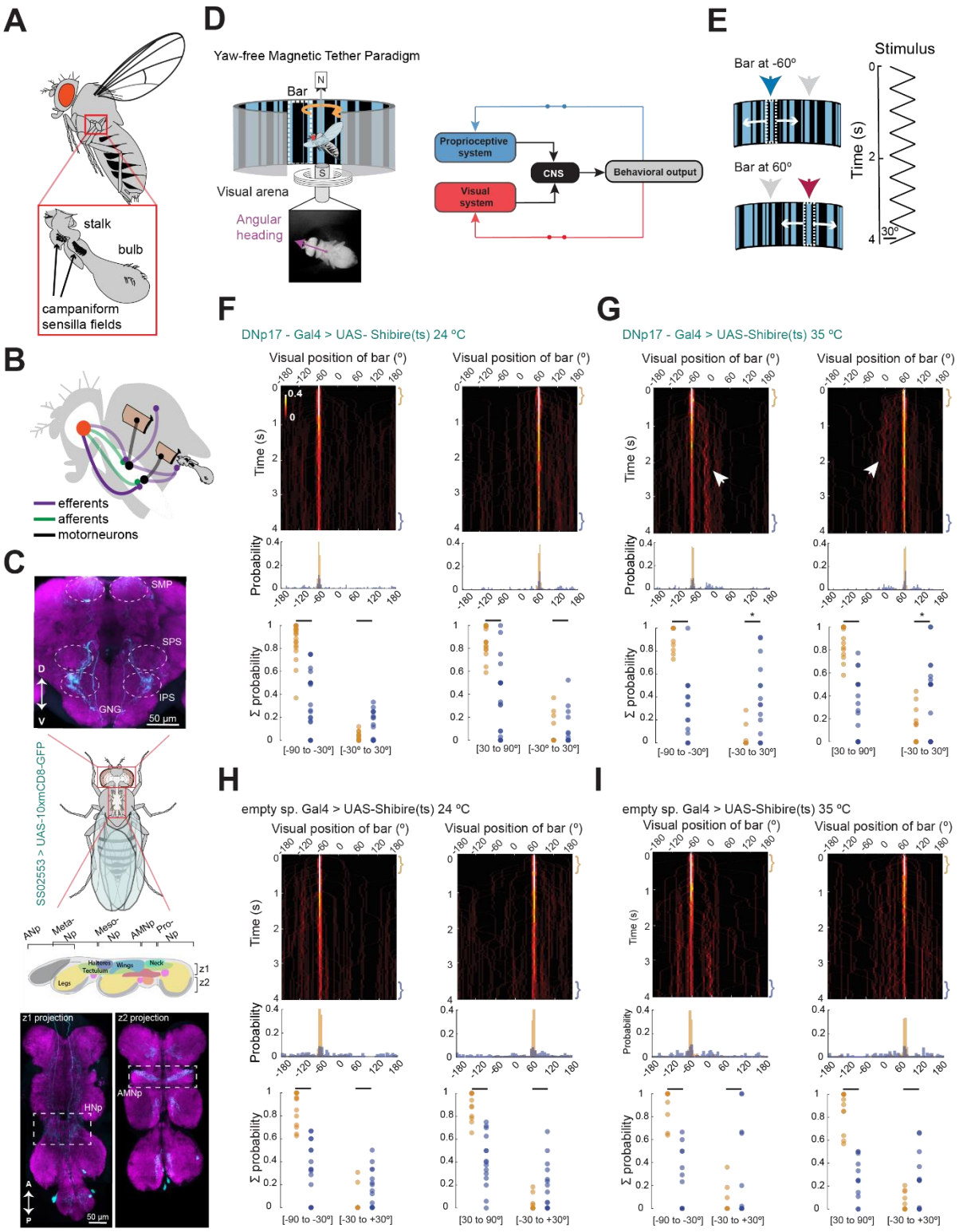

Figure 1. Preliminary silencing perturbation of haltere descending neuron increases frontal bar fixation. Please refer to Table 1 for list of anatomical abbreviations. **A.** Schematic of *D. melanogaster* with proprioceptive haltere gross morphology indicated. **B.** Schematic of circuit connections between brain and wing, neck and haltere motor centers. Bold purple connection represents descending efferent pathways, which include but are not limited to DNp17 cell population. **C.** Confocal microscopy (40x magnification) images of SS02553 Gal4 line driving expression of UAS-GFP. Cyan depicts GFP staining and magenta depicts NC82 neuropil staining used for anatomical reference. Top: Standard deviation Z-projection of central brain expression shows DNp17 innervation in the IPS (dotted white area) as well as 2 bilateral off-target cells in the SMP. The SPS is also indicated for anatomical reference. Middle: *D. melanogaster* schematic indicating position of the nervous system and a lateral video of the VNC with major neuropils indicated. Adapted from [34]. Bottom: Standard deviation Z-projection of VNC expression. The z1 projection covers the 70µm dorsal volume while the z2 projection covers the 60µm ventral volume as indicated in the top schematic. The haltere neuropil (HNp) and accessory mesothoracic neuropil (AMNp) are indicated in white dotted rectangles. **D.** Left: In a magnetic tether paradigm, the fly's body is glued to a magnetic pin suspended between magnetic North and South poles. The fly's instantaneous angular heading in the 360º arena is recorded with a high-speed camera below the setup. The fly's body is free to rotate in the yaw plane and orient toward visual objects. Right: In this condition, both the proprioceptive and visual feedback channels are naturalistically closed. **E.** Left: "Motion-defined" visual object stimuli presented to flies in a yaw-free magnetic paradigm. Right: Triangle wave motion trajectory of the visual object over a 4s trial duration. **F.** Bar fixation for a bar starting at -60° (left) and 60° (right) for N = 25 flies for the mutant DNp17 genotype at the permissive temperature of 24°C. Top row: Black/red heatmap shows probability of bar position for all trials. Colormap indicates the probability of the bar occupying each bin (1ms x 5°). Middle row: Normalized probability histograms are computed from the first (yellow bracket) and last (blue

bracket) 0.5 s of each trial. Bottom row: The summed probability of flies placing the bar within 30° of the angular position bin at the start (yellow) and end (blue) of the trial. Each dot is an individual fly sum. Nonparametric Kruskal- Wallis tests were ran with *$p < 0.05$. **G.** Same as F, but for N = 20 mutant DNp17 flies at the restrictive (silencing) temperature of 35°C. Note the smooth 2 Hz dynamics in trials where the fly orients towards the bar (white arrowheads). **H-I.** Same as F-G but for promoterless split Gal 4 genetic controls with N = 17 flies at the permissive temperature and N = 14 flies at the restrictive temperature.

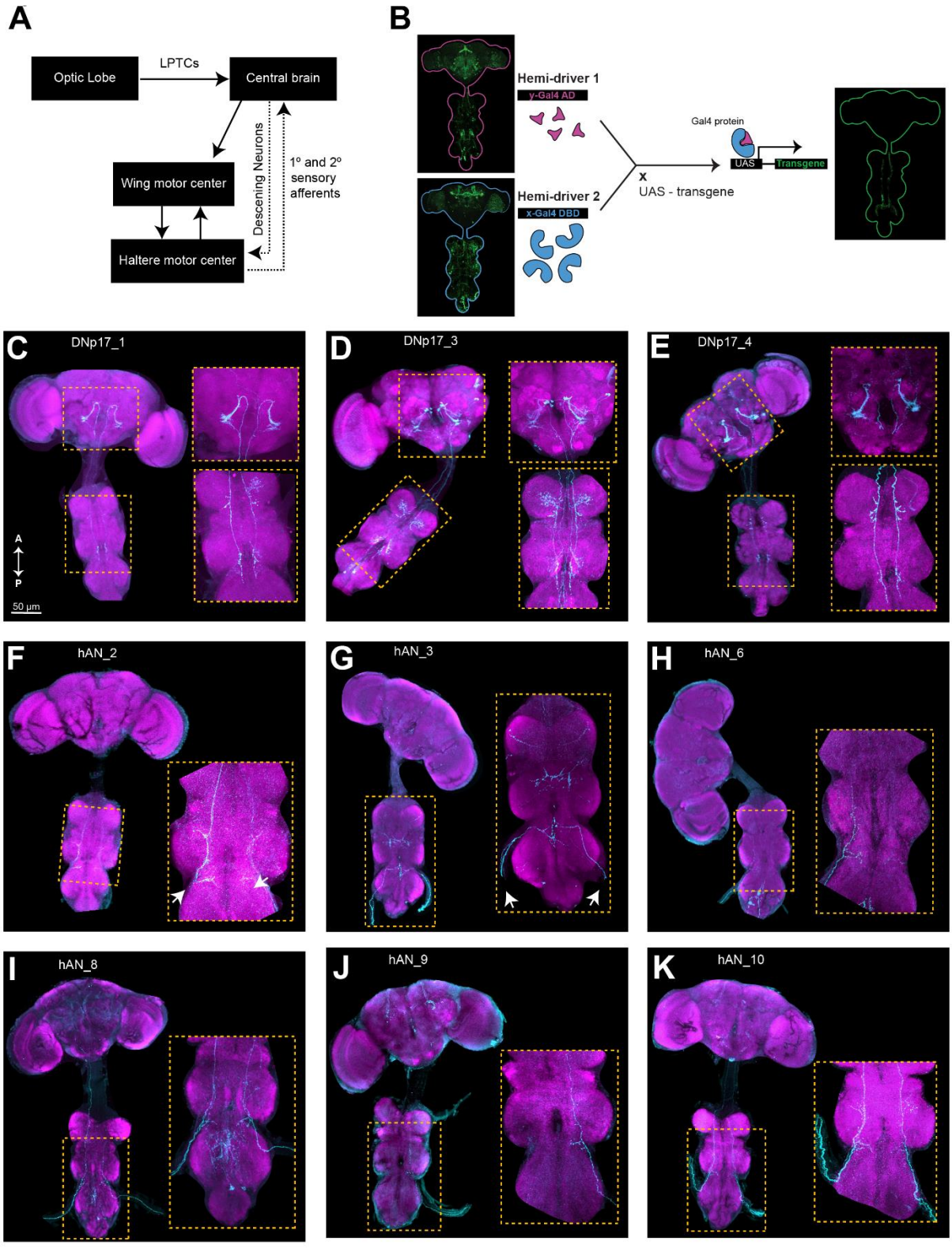
A
Optic Lobe
LPTCs
Central brain
Wing motor center
Haltere motor center
Descening Neurons
1º and 2º sensory afferents
B
Hemi-driver 1
y-Gal4 AD
Hemi-driver 2
x-Gal4 DBD
x
UAS - transgene
Gal4 protein
UAS
Transgene
C
DNp17_1
A
P
50 µm
D
DNp17_3
E
DNp17_4
F
hAN_2
G
hAN_3
H
hAN_6
I
hAN_8
J
hAN_9
K
hAN_10

Figure 2. Strategy for generating novel haltere circuit reagents. A. Schematic of major connections between neuropils involved in visuomotor control. Note the feedforward and feedback dotted arrows between the haltere motor center and central brain. **B.** Cartoon of intersectional split Gal4 approach for isolating sparsely labeled lines. Each hemi-driver is under the control of a different enhancer and has its own individual expression pattern (pink and blue). The two units of a functional Gal4 protein consist of an activating domain (AD) and a DNA-binding domain (DBD) that must coincide to reconstitute the functional protein necessary for the transcription of the transgene of choice. **C-E**. Exemplar expression pattern of select DNp17 candidates isolated. Confocal Z-projections were captured at 10x. Cyan depicts GFP staining and magenta depicts NC82 neuropil staining used for anatomical reference. Yellow dotted insets depict 40x Z-projections of varying depths and may be used to more accurately characterize arborization patterns in the central brain and VNC. **F-K.** Same as in C, but for haltere ascending neuron (hAN) candidates. White arrows indicate the insertion of the campaniform sensory neurons through the haltere nerve tract. Note the varying density of staining indicating the number of cells targeted, as well as the limited but varying off-target cell populations present in different drivers.

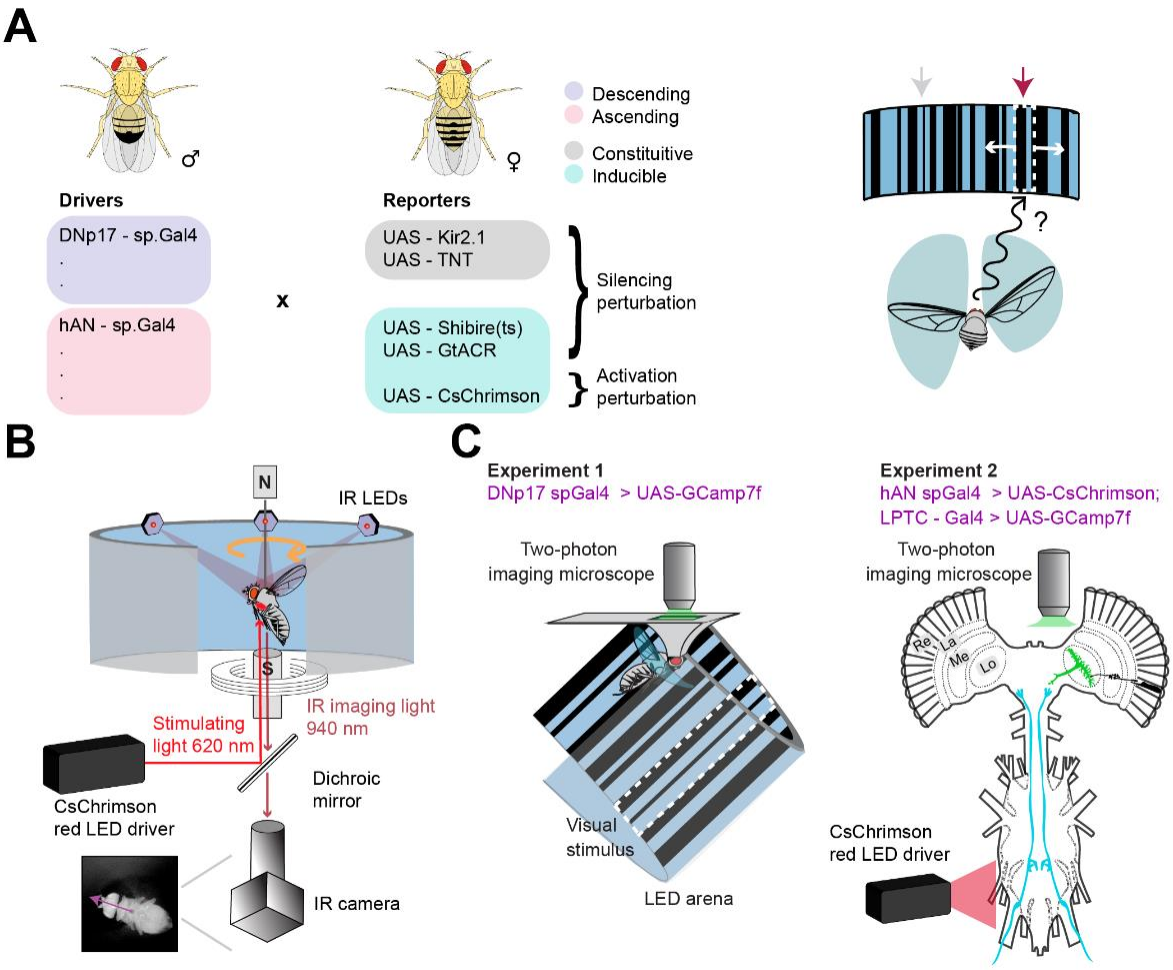

Figure 3. Future directions comprise behavioral and live functional imaging experiments.

A. Left: Novel driver lines generated for ascending (pink) and descending (purple) haltere circuit components will be crossed to a variety of readily available reporters under the control of the UAS promoter. Right: Yaw-free object orientation responses will be quantified in the already established behavioral pipeline using a motion-defined oscillating bar at different locations off visual midline. **B.** Adapted magnetic tether paradigm for simultaneous imaging of fly behavioral responses and optogenetic activation using a dichroic mirror to split the IR-wavelength light used to illuminate the fly and the red-shifted light used to stimulate the channelrhodopsin CsChrimson. Precise spatial precision in this setup allows focused mm-scale activation of VNC cell populations (red dot on fly thorax) while minimizing scattering. **C.** Live calcium imaging using a two-photon microscope will quantify functional neurophysiology of haltere circuit

components. Fly genotypes for the two experiments described are indicated in purple. In experiment 2, exemplar large-field LPTC cells imaged are indicated in green while haltere ascending neurons optogenetically stimulated are indicated in cyan.

Abbreviation	Full Name
Re	Retina
La	Lamina
Me	Medulla
Lo	Lobula
Lop	Lobula Plate
SMP	Superior Medial Protocerebrum
SPS	Superior Posterior Slope
IPS	Inferior Posterior Slope
GNG	Gnathal Ganglion
Pro-Np	Prothoracic Neuropil
AMNp	Accessory Mesothoracic Neuropil
Meso-Np	Mesothoracic Neuropil
Meta-Np	Metathoracic Neuropil
ANp	Abdominal Neuropil
HNp	Haltere Neuropil
HN	Haltere Nerve

Table 1: Anatomical brain region terminology

Target Cell Type	Hemi-driver 1 (AD)	Hemi-driver 2 (DBD)	Hit	# target cells	Brain expression	VNC expression	Shorthand ID
DNp17	R67E08	R47B04	yes	few	clean	clean	DNp17_1
DNp17	R67E08	VT013121	no	n/a	n/a	n/a	n/a
DNp17	R67E08	VT019902	yes	few	clean	clean	DNp17_2
DNp17	VT025789	R47B04	yes	many	dirty - bilateral neuron in anterior brain, OL lamina	dirty - leg neuropils	DNp17_3
DNp17	VT025789	VT013121	no	n/a	n/a	n/a	n/a
DNp17	VT025789	VT019902	yes	many	dirty - retina & lamina	clean	DNp17_4
hAN	VT059775	R16G01	yes	few	dirty - medulla	clean	hAN_1
hAN	VT059775	R42B05	no	n/a	n/a	n/a	n/a
hAN	VT059775	R45H03	yes	few	clean	clean	hAN_2
hAN	VT059775	R60B12	no	n/a	n/a	n/a	n/a
hAN	VT059775	R71C02	no	n/a	n/a	n/a	n/a
hAN	VT059775	R76B01	no	n/a	n/a	n/a	n/a
hAN	VT059775	VT008194	no	n/a	n/a	n/a	n/a
hAN	VT059775	VT023863	yes	medium	dirty - lobula	dirty - tectulum/wing motor center	hAN_3
hAN	VT059775	VT026179	yes	many	dirty - SMP & EB	clean	hAN_4
hAN	VT059775	VT026661	yes	very few	clean	clean	hAN_5
hAN	VT059775	VT026753	yes	very few	clean	mostly clean - couple of Abdominal Segment (AS) neurons	nAN_6
hAN	VT059775	VT040919	no	n/a	n/a	n/a	n/a
hAN	VT059775	VT048331	yes	very few	unclear	clean	hAN_7
hAN	R53E11	R16G01	yes	few	clean	mostly clean - couple of Abdominal Segment (AS) neurons	hAN_8
hAN	R53E11	R42B05	yes	very few	dirty - mushroom body	clean	hAN_9

hAN	R53E11	R45H03	yes	few	dirty - mushroom body	clean	hAN_10
hAN	R53E11	R60B12	no	n/a	n/a	n/a	n/a
hAN	R53E11	R71C02	yes	few	dirty - bilateral neuron, OL lamina	mostly clean - couple of Abdominal Segment (AS) neurons	hAN_11
hAN	R53E11	R74G01	no	n/a	n/a	n/a	n/a
hAN	R53E11	R76B01	no	n/a	n/a	n/a	n/a
hAN	R53E11	VT006460	no	n/a	n/a	n/a	n/a
hAN	R53E11	VT008194	no	n/a	n/a	n/a	n/a
hAN	R53E11	VT026179	no	n/a	n/a	n/a	n/a
hAN	R53E11	VT026753	yes	very few	clean	clean	hAN_12
hAN	R53E11	VT040919	no	n/a	n/a	n/a	n/a
hAN	R53E11	VT048331	yes	very few	clean	mostly clean - leg interneurons	hAN_13

Table 2: Haltere candidate split Gal4 lines screened and their qualitative characterization.

REFERENCES

1. Cellini, B., and Mongeau, J.-M. (2020). Hybrid visual control in fly flight: insights into gaze shift via saccades. Curr Opin Insect Sci *42*, 23–31.

2. Reichardt, W., and Poggio, T. (1976). Visual control of orientation behaviour in the fly. Part I. A quantitative analysis. Q. Rev. Biophys. *9*, 311–75, 428–38.

3. Duistermars, B.J., Reiser, M.B., Zhu, Y., and Frye, M.A. (2007). Dynamic properties of large-field and small-field optomotor flight responses in Drosophila. J. Comp. Physiol. A Neuroethol. Sens. Neural Behav. Physiol. *193*, 787–799.

4. Mronz, M., and Lehmann, F.-O. (2008). The free-flight response of Drosophila to motion of the visual environment. J. Exp. Biol. *211*, 2026–2045.

5. Mongeau, J.-M., and Frye, M.A. (2017). Drosophila Spatiotemporally Integrates Visual Signals to Control Saccades. Curr. Biol. *27*, 2901–2914.e2.

6. Theobald, J.C., Shoemaker, P.A., Ringach, D.L., and Frye, M.A. (2010). Theta motion processing in fruit flies. Front. Behav. Neurosci. *4*. 10.3389/fnbeh.2010.00035.

7. Fox, J.L., Aptekar, J.W., Zolotova, N.M., Shoemaker, P.A., and Frye, M.A. (2014). Figure-ground discrimination behavior in Drosophila. I. Spatial organization of wing-steering responses. Journal of Experimental Biology *217*, 558–569. 10.1242/jeb.097220.

8. Götz, K.G. (1987). Course-Control, Metabolism and Wing Interference During Ultralong Tethered Flight in Drosophila Melanogaster. J. Exp. Biol. *128*, 35–46.

9. Reichardt, W., and Wenking, H. (1969). Optical detection and fixation of objects by fixed flying flies. Die Naturwissenschaften *56*, 424–424. 10.1007/bf00593644.

10. Kimmerle, B., and Egelhaaf, M. (2000). Performance of fly visual interneurons during object fixation. J. Neurosci. *20*, 6256–6266.

11. Theobald, J.C., Duistermars, B.J., Ringach, D.L., and Frye, M.A. (2008). Flies see second-order motion. Curr. Biol. *18*, R464–5.

12. Rimniceanu, M., Currea, J.P., and Frye, M.A. (2023). Proprioception gates visual object fixation in flying flies. Curr. Biol. *33*, 1459–1471.e3.

13. Straw, A.D., Tómasson, E., and Dickinson, M.H. (2011). Active and passive antennal movements during visually guided steering in flying Drosophila. Journal of.

14. Taylor, G.K., and Krapp, H.G. (2007). Sensory Systems and Flight Stability: What do Insects Measure and Why? In Advances in Insect Physiology, J. Casas and S. J. Simpson, eds. (Academic Press), pp. 231–316.

15. Sane, S.P., Dieudonné, A., Willis, M.A., and Daniel, T.L. (2007). Antennal mechanosensors mediate flight control in moths. Science *315*, 863–866.

16. Sherman, A., and Dickinson, M.H. (2004). Summation of visual and mechanosensory feedback in Drosophila flight control. J. Exp. Biol. *207*, 133–142.

17. Bender, J.A., and Frye, M.A. (2009). Invertebrate solutions for sensing gravity. Curr. Biol. *19*, R186–90.

18. Bender, J.A., and Dickinson, M.H. (2006). A comparison of visual and haltere-mediated feedback in the control of body saccades in Drosophila melanogaster. J. Exp. Biol. *209*, 4597–4606.

19. Dickinson, M.H. (1999). Haltere-mediated equilibrium reflexes of the fruit fly, Drosophila melanogaster. Philos. Trans. R. Soc. Lond. B Biol. Sci. *354*, 903–916.

20. Dickerson, B.H., de Souza, A.M., Huda, A., and Dickinson, M.H. (2019). Flies Regulate Wing Motion via Active Control of a Dual-Function Gyroscope. Curr. Biol. *29*, 3517–3524.e3.

21. Schnell, B., Ros, I.G., and Dickinson, M.H. (2017). A Descending Neuron Correlated with the Rapid Steering Maneuvers of Flying Drosophila. Curr. Biol. *27*, 1200–1205.

22. Åström, K.J., and Murray, R.M. (2010). Feedback Systems: An Introduction for Scientists and Engineers (Princeton University Press).

23. Fenk, L.M., Poehlmann, A., and Straw, A.D. (2014). Asymmetric processing of visual motion for simultaneous object and background responses. Curr. Biol. *24*, 2913–2919.

24. Land, M.F. (1992). Visual tracking and pursuit: Humans and arthropods compared. J. Insect Physiol. *38*, 939–951.

25. Elzinga, M.J., Dickson, W.B., and Dickinson, M.H. (2012). The influence of sensory delay on the yaw dynamics of a flapping insect. J. R. Soc. Interface *9*, 1685–1696.

26. Bartussek, J., and Lehmann, F.-O. (2016). Proprioceptive feedback determines visuomotor gain in Drosophila. R Soc Open Sci *3*, 150562.

27. Namiki, S., Dickinson, M.H., Wong, A.M., Korff, W., and Card, G.M. (2018). The functional organization of descending sensory-motor pathways in Drosophila. Elife *7*. 10.7554/eLife.34272.

28. Kitamoto, T. (2001). Conditional modification of behavior in Drosophila by targeted expression of a temperature-sensitive shibire allele in defined neurons. J. Neurobiol. *47*, 81–92.

29. Luan, H., Diao, F., Scott, R.L., and White, B.H. (2020). The Drosophila Split Gal4 System for Neural Circuit Mapping. Front. Neural Circuits *14*, 603397.

30. Mauss, A.S., Busch, C., and Borst, A. (2017). Optogenetic Neuronal Silencing in Drosophila during Visual Processing. Sci. Rep. *7*, 13823.

31. Simpson, J.H., and Looger, L.L. (2018). Functional Imaging and Optogenetics in Drosophila. Genetics *208*, 1291–1309.

32. Cheng, K.Y., Colbath, R.A., and Frye, M.A. (2019). Olfactory and Neuromodulatory Signals Reverse Visual Object Avoidance to Approach in Drosophila. Curr. Biol. *29*, 2058–2065.e2.

33. Keleş, M.F., Hardcastle, B.J., Städele, C., Xiao, Q., and Frye, M.A. (2020). Inhibitory interactions and columnar inputs to an object motion detector in Drosophila. Cell Rep.

34. Venkatasubramanian, L., and Mann, R.S. (2019). The development and assembly of the Drosophila adult ventral nerve cord. Curr. Opin. Neurobiol. *56*, 135–143.

Chapter 4

Cosmopolitan and cactophilic *Drosophila* species implement divergent visual tracking strategies

SUMMARY

Eye movements to maintain stable gaze, while tracking visual features, is challenging yet commonplace across animal taxa. During flight, the fruit eating fly *Drosophila melanogaster* maintains course using optomotor control, making smooth steering adjustments to fixate the image of broadband background foliage on the retina and changing course to investigate individual objects such as plant stalks by executing body saccades. Cactophilic species of the Mojavensis clade live in deserts in which “background” and “objects” are one and the same - comprising resources such as cacti. We tested whether *D. mojavensis baja* and *D. mojavensis mojavensis* have adapted their flight control strategies for a visually sparse landscape. We used a magnetic tether that allows free movement in the yaw axis. In response to a narrow bar moving across a stationary background, *D. melanogaster* fixates the background, then spatiotemporally integrates bar position error to generate threshold-triggered tracking saccades. By contrast, the desert species steer to smoothly fixate the bar, centering it on visual midline, while seemingly disregarding slip of the background. Like their cosmopolitan relatives, desert flies also execute bar saccades, and do so more frequently, but theirs are triggered when bar velocity is too high to fixate. Thus, *D.melanogaster* leverages the optical disparities between nearby objects and distant foliage for a hybrid control strategy: “ground-fixate, object-saccade”. Cactophilic flies use a fused control strategy operating on any available visual cue: “fixate-and-saccade”, which would be adaptive in a visually sparse environment where foliage is both to be approached and used to fly straight.

INTRODUCTION

The visual landscapes that locomoting animals encounter often consist of spatially complex and dynamical features. Coherent motion of the panorama subtending a large portion

of the total visual field, so-called “large-field” motion, is generated by self-movement against distant visual clutter, and engages ubiquitous optomotor responses to reduce retinal slip and maintain stable gaze. Fixated gaze allows easy discrimination of the relative movement dynamics of nearby “small-field” features or objects that subtend a narrow region of the visual field, representing navigational goals. For example, a fly cruising through a forest might fixate the panoramic image of distant background foliage to maintain a stable course, while the movement disparity generated by the translation of a nearby tree trunk evokes a steering maneuver. But what if the visual environment is sparse, consisting of a single tree on an open horizon? Would this feature drive both optomotor gaze fixation and object navigation?

Differences between the retinal size and movement dynamics of large-field and small-field cues have provided a classical conceptual framework to analyze flight control strategies and visual processing circuits in flies [1]. More recently, the widely used model system *Drosophila melanogaster* has provided much of our emerging understanding of visual flight control [2,3] and the cellular mechanisms of motion vision and feature detection [4–6]*. D. melanogaster* originated in sub-Saharan Africa and radiated outward starting 10,000 years ago to colonize essentially all niches where climate conditions are favorable [7,8]. *D. melanogaster* is an ecological generalist that is part of the “cosmopolitan guild” of the sophophora subgenus of *Drosophila*, feeding and breeding on varied decomposing fruit matter, which contributes to their success in diverse environments [9,10].

As a human commensal, *D. melanogaster* is adapted to generic cluttered visual environments ranging from forests to cityscapes. Such ecologies present a complex figure-ground discrimination challenge as they are largely composed of vertically elongated features that both define the distant panoramic background and nearby objects. In the face of this sensory challenge, *D. melanogaster* has evolved a hybrid control strategy in which large-field motion engages smooth optomotor gaze fixation, which is interspersed with nystagmus or catch-up saccades [3], whereas nearby small-field objects trigger course changing body saccades

while optomotor responses are suppressed [11–13]. Smooth optomotor corrections rely upon directionally selective motion detecting neurons called T4 and T5 [14], whereas object tracking body saccades are mediated by T3 feature detectors [15,16]. Thus, during flight, *D. melanogaster* elegantly maps visual features to distinct visual control algorithms.

However, not all visual landscapes are densely cluttered. By contrast to cosmopolitan *D. melanogaster*, *D. mojavensis* evolved within visually sparse desert landscapes. Separated from *D. melanogaster* by approximately 30 million years, these members of the repleta subgroup first radiated in South America and specialized on fermenting cacti [17,18]. Today, four geographically separated subspecies comprise the *D. mojavensis* species. Within these, *D. moj. baja* and *D. moj. mojavensis* are hypothesized to have diverged approximately 250,000 years ago and specialize on agria cacti (*Stenocereus gummosus*) and barrel cacti (*Ferocactus cylindraceus*) respectively [17,19,20]. The host cacti of both subspecies are native to bright, barren desert environments where the fewer vertical features available comprise both large-field panoramic cues and small-field landscape features representing food and breeding sites. Presumably driven by their distinct visual habitats, *D. melanogaster* approach vertical bars or edges that likely represent landscape features while avoiding threatening small objects, whereas cactophilic *D. mojavensis* are attracted to objects of any size [21].

Motivated by their different visual ecologies, we tested the hypothesis that the control strategies for gaze stabilization and object tracking have diverged between cosmopolitan and cactophilic Drosophilids. We characterized flight steering responses to a camouflaged vertical bar that is observable only while it is moving during tethered yaw-free flight by *D. melanogaster*, *D. moj. baja* and *D. moj. moj*. Surprisingly, desert-adapted species readily center the bar on their visual midline, whereas bar centering responses in yaw-free *D. melanogaster* are absent. Bar-centering responses by desert flies are achieved with smooth fixation dynamics that typify large-field optomotor control. For objects that move along a continuous path, saccadic pursuit ensues in all three species, albeit with species-specific dynamics. In direct contrast to *D.*

melanogaster, and more akin to primate visual pursuit, desert flies heavily rely on both smooth fixation dynamics and catch-up saccades to track a moving object, triggering saccades when object velocity is high. These results support the hypothesis that a sparse visual landscape promotes the fused control of gaze stabilization and object pursuit. Our findings build upon previous work showing contextual modulation of object pursuit behavior and its underlying neural mechanisms [22], within a comparative visual ecological context.

RESULTS

Distinct from *D. melanogaster*, yaw-free *D. mojavensis* center a bar on visual midline

We compared the visual responses to a vertical object in the cosmopolitan generalist *D. melanogaster*, which occupy cluttered landscapes, and cactophilic specialists *D. mojavensis baja* and *D. mojavensis mojavensis,* which occupy visually sparse landscapes (Figure 1A). We presented a bar oscillating +/- 30° amplitude at constant velocity on a triangle waveform at randomly selected azimuthal locations relative to the fly's visual midline. The bar was presented on a stationary randomly patterned background. The randomly textured bar was therefore defined only by the relative motion between the bar and background rather than any static luminance cues that would provide position cues independent from object motion (e.g. a dark bar on a bright background). Our previous work found that in these visual conditions, transitioning from a rigidly tethered body-fixed state to a magnetically tethered yaw-free body state, strongly modulates object orientation responses in *D.melanogaster* [22]. Here, all experiments were conducted in a magnetic tether apparatus in which flies may orient freely on a frictionless pivot within the yaw plane, "yaw-free", thereby receiving naturalistic proprioceptive feedback (Figure 1B).

Regardless of the starting position on the fly's visual azimuth of an oscillating bar superposed on a stationary background, *D. melanogaster* did not orient towards the object

(Figure 1C, left). Plotting the population data onto a circular probability heat map showed a uniform likelihood of flies orienting at all angular positions relative to the bar throughout all trials (Figure 1C, right). For repeated trials from each individual fly, we computed an average resultant heading vector, the magnitude of which represents the strength of the average response. A vector magnitude of 1 is equivalent to the fly spending the entire trial at a constant angular heading. In this representation, *D. melanogaster* shows uniformly distributed population responses resulting from generally weak resultant vectors (~0.20) across all individuals (Figure 1C, right). By contrast, *D. moj. baja* shows a distinct bar orientation response within the first second of the onset of a trial (Figure 1D, left). Most individuals strongly orient towards the oscillating bar, yielding a high probability of the bar becoming centered on the visual midline (Figure 1D, right). *D. moj. moj* displayed similarly strong orientation responses, with all but one fly's resultant vector oriented within 30° of the position of the bar (Figure 1E).

Distinct from *D. melanogaster, D. mojavensis* smoothly track bar dynamics against a stationary background

A study we conducted previously in yaw-free flies showed that whereas *D. melanogaste*r responds to large-field displacements with smooth steering kinematics to stabilize the direction of gaze, they track visual objects with saccades. Rigidly tethered body-fixed flies steer smoothly to follow the dynamics of object motion, but when magnetically tethered, with naturalistic proprioceptive feedback, they do not smoothly track an object [22]. In surprising contrast to *D. melanogaster*, both *D. moj. baja* and *D. moj. moj.* oscillate with the bar and center it on their visual midline (Figure 1C,D,E).

We adopted the same approach we used previously to quantify smooth steering responses in the desert-dwelling *Drosophila* species; a motion defined bar was moved a fixed

velocity (120 °/s) and fixed oscillation frequency (2 Hz) positioned at either -60°, 0°, or 60° from the fly's longitudinal midline at the start of each trial (Figure 2A). Positioning the bar at defined egocentric positions was accomplished with real-time heading measurements (see STAR Methods). We also tested responses to the randomly textured large-field background moved on the same motion trajectory. Under these conditions, *D.melanogaster* does not produce smooth steering responses to the bar, only to the visual ground (Figure 2B). By contrast, and rather surprisingly, *D. moj. baja* smoothly steer to follow the bar trajectory (Figure 2C). *D. moj. moj.* showed even stronger average bar responses than *D. moj. baja* - in fact, these responses approached or exceeded the responses to the magnitude of ground responses (Figure 2D).

We quantified the strength of smooth steering responses by plotting the magnitude component of the Fast-Fourier Transform (FFT) for both bar and ground responses. As expected and previously demonstrated, whereas the ground response peaks at 2 Hz, the amplitude of the bar response at this frequency was near zero for *D. mel.* (Figure 2E top row). By contrast, the bar FFT amplitude for *D. moj. baja* was roughly half that of their ground response (Figure 2E, middle row). Peak bar response amplitude was even higher for *D. moj. moj.* (Figure 2E, bottom row). The ratio of bar-to-ground response amplitudes allows a comparison across species, at each of the three azimuthal stimulus positions. Both desert species, *D. moj. baja* and *D. moj moj,* track bar motion significantly more strongly than *D. melanogaster* regardless of whether the stimulus is on visual midline or offset to the right or left (Figure 2F; Kruskal-Wallis nonparametric test). Note that some individual *D. moj. moj.* show bar:ground ratios greater than 1. i.e. the bar, subtending 10% of the visual field, stimulated larger smooth steering responses than the ground, subtending 90% of the visual field. We observed a trend toward intra-species differences within the two desert drosophilids, with *D. moj. moj* displaying stronger bar-elicited steering dynamics than *D. moj. baja*, but these differences were not statistically significant.

Distinct from *D. melanogaster, D. mojavensis* implement a fixate-and-saccade bar tracking strategy

Small-field bar and wide-field optomotor responses have long been known to be differentially sensitive to velocity dynamics [23]. Thus, to probe object centering behavior, the experiments in Figures 1 and 2 were designed to keep image velocity constant, while changing direction twice per second. To explore more naturalistic dynamics, we next designed a complex motion stimulus that comprised nine frequencies spanning a 10-fold range between 0.3 Hz and 11.3 Hz (see STAR Methods). In addition to eliminating predictability confounds that can occur for constant frequency stimuli, a sum-of-sines (SoS) stimulus can probe the strength of smooth steering responses across a range of frequencies [24].

Figure 3 shows steering response to the SoS stimulus across the three *Drosophila* species. At the start of each trial, the bar was centered near the fly's visual midline. As found in prior work [12,22], *D. melanogaster* tend to fixate the stationary visual background, without smoothly tracking the bar, maintaining steady gaze while integrating the positional error of the bar to trigger stepwise tracking saccades (Figure 3A). We plotted the SoS stimulus trajectory against the measured mean response values at each time point, which for *D. melanogaster* indicates that steering responses were only weakly correlated to the SoS stimulus trajectory (Figure 3B); the correlation coefficient (r) was 0.54, the square of which yields the coefficient of determination ($r^2 = 0.29$), indicating that the average *D. melanogaster* response accounted for merely one third of variation within the SoS stimulus. Conversely, both desert species showed robust tracking of the SoS stimulus (Figure 3C,E), leading to similarly large r-values (0.93) and corresponding r^2 values that explain 86% of the variation within the SoS stimulus (Figure 3D,F).

In a separate series of experiments, we presented bar stimuli on a uniform, rather than a textured, background. For desert species, such a stimulus might more accurately represent the

natural visual conditions. We tested bar widths that subtended between 7.5 and 120 ° on the retina (Figure S1A). We found that even the narrowest 7.5 ° bars elicited strong steering in desert flies, predicting at least 58% of the variability in the flies' steering responses (Figure S1D-G). By comparison, achieving a similar response in *D. melanogaster* required a 120 ° bar (Figure S1C). The r^2 values were larger for both *D.moj.* flies. than for *D.mel*. for each bar width. To highlight this result, we color-grouped linear fits across all bar widths for each species, showing that the correlation between stimulus and response was higher for desert species than *D. melanogaster* (Figure 3L).

Our initial intention was to incorporate the SoS stimulus into a systems identification approach to quantify the frequency tuning of object tracking error across the different species. The assumptions of the analysis require linear relationships between the stimuli and the fly's responses. However, we discovered that desert flies produce many more body saccades than *D. melanogaster* (Figure 3J,K). Body saccades represent abrupt changes in flight heading that violate the assumption of stationarity, thereby precluding a linear systems analysis. For analysis of large-field behavior, the comparatively fewer saccades can be filtered out without compromising a systems identification approach [25,26]. Due to the high rate of saccades executed by desert flies during object tracking, we instead used the naturalistic SoS stimulus for an unconstrained time-domain analysis.

We computationally isolated bar-evoked saccades, and plotted trial-by-trial rasters (Figure 3G-I top row) as well as binned probability histograms (Figure 3G-I middle row). As expected, *D. melanogaster* executed saccades to track the bar (Figure 3G). We were surprised to find that in addition to increased smooth fixation by comparison to *D.melanogaster*, both desert fly species also performed bar tracking saccades, and did so at a significantly higher rate than *D. melanogaster* (Figure 3J,K). Across the three species, saccades were structured by the SoS dynamics, with "hot spots" in the saccade rasters coinciding with peaks in the velocity of the SoS stimulus after a short delay (Figure 3G-I middle row), suggesting that velocity, possibly

in addition to position, might be strong predictor of saccade triggering particularly in the *D. mojavensis* species (Figure 3G-I bottom row).

In this study, we tested frontal centering and smooth fixation strategies among species occupying different visual ecological niches. Developing a predictive model of object evoked saccades is beyond the scope of our efforts. However, upon noting the strong patterning of saccades, we performed a preliminary analysis to assess the proportion of variability in saccade execution that could be explained by the position and velocity of the SoS stimulus. We cross-correlated the stimulus position and velocity waveforms with saccade probability point for point in time. In all three species, the maximum correlation coefficient occurred at negative time lag to the SoS position trace: *D. mel.* (-120ms) *D. moj. baja* (-210ms) and *D. moj. moj.* (-150ms) (Figure S2). Thus, the saccades are triggered in advance of changes in bar position, making this variable a poor predictor of saccade probability, at least when considered on its own. By contrast, saccade probability lagged the stimulus velocity trace for *D. mel.* (270ms), *D. moj. baja* (270ms) and *D. moj. moj.* (330ms). We found that bar velocity is a stronger predictor of saccades for *D. moj. baja* (41%) and *D. moj. moj.* (38%) than for *D. melanogaster* (14%) (Figure S2, and Figure 3G-I middle and bottom row). Further modeling efforts that might combine these variables are needed to describe the different strategies for saccadic object vision deployed by these fly species.

Although the average steering responses are smooth and highly correlated with the bar motion trajectory, the high saccade rates by desert flies make individual trials ‘jitter’ around the SoS bar trajectory (Figure 3A,C,E right panel). Thus, one could argue that the strategy used by the desert species is qualitatively similar to *D. melanogaster* - fixating the stationary ground and firing lots of small saccades to track the bar - rather than a contrasting strategy of smoothly fixating the bar and firing catch-up saccades. Resolving this issue is challenging with an SoS stimulus because it changes direction at random intervals, triggering more saccades in some intervals than others and thereby making it difficult to assess how body angle changes between

saccades. In order to sample inter-saccade bouts consistently, we designed an experiment in which the bar revolved at a constant velocity, corresponding to the (70°/s) velocity of each component sine wave in the previous experiment, for 10 s trials, in both CW (+) and CCW (-) directions.

As previously demonstrated [12], this experiment elicited bar pursuit characteristics in which *D. melanogaster* fixated the stationary ground in between bar-directed saccades, maintaining near zero angular velocity during the inter-saccadic interval (ISI) (Figure 4A,D, Movie S1). By contrast, and as predicted by the sum-of-sines results (Figure 3), desert-dwelling *D. moj baja* fixate the revolving bar in between saccades, not the stationary background, thus tracking the bar during the ISI with smooth pursuit (Figure 4B,E, Movie S2). Similarly, *D. moj moj.* fixate the bar during the ISI (Figure 4C,F, Movie S3). The distribution of ISI velocity values for *D. melanogaster* was skewed toward zero (Figure 4G, green) whereas both *D. mojavensis* subspecies' velocity distributions shifted toward the bar velocity (Figure 4G, orange & magenta). We compared the difference in means of ISI velocity across species, and tested these differences with bootstrapped simulations, resampling with replacement from combined data sets, to find strong differences between species that are independent of stimulus direction (Figure 4H). In essence, we discovered that whereas *D. melanogaster* remains stationary, fixating the stationary ground in between saccades, *D. moj baja* and *D. moj. moj.* continue moving to fixate the bar with interspersed saccades - a fixate-and-saccade tracking strategy.

These species differences in bar tracking are particularly noteworthy given that all three species smoothly track the oscillation of a large-field ground (Figure 2B-D, Figure S3A-C, Movies S4-6), and between saccades show similar stimulus-matched optomotor fixation for a constant-velocity ground (Figure S3D-F). However, the structure of optomotor saccades differs across species. In particular, *D. moj. moj.* shows erratic saccadic behavior, with individuals seeming to overshoot the stimulus rather than fixating it (Figure S3C), with correspondingly high

ISI velocity (Figure S3G,H). Accordingly, *D. moj. moj.* large-field optomotor saccade dynamics are exaggerated in their amplitude, torque, and frequency compared to both *D. melanogaster* and *D. moj. baja* (Figure S3I-P). While a deep analysis of large-field optomotor behavior is beyond the scope of this study, it would seem that *D. moj. moj.* use underdamped optomotor control by comparison to *D. melanogaster* flies [27].

D. mojavensis execute stronger, smaller and more frequent bar tracking saccades than *D. melanogaster*

By contrast to the strong temporal patterning in response to the SoS stimulus (Figure 3G-I), the constant velocity bar produced evenly distributed tracking saccades by all three species (Figure 5A). As bar direction largely had no effect on saccade parameters within each species (Figure S4), we combined CW and CCW saccades together to measure saccade-triggered average kinematic parameters. Previous work has shown that saccades dynamics can be tuned to characteristics of the visual stimulus (e.g. large-field ground vs. small-field bars, low vs. high stimulus velocity) [12]. Do saccade dynamics also vary across species? To address this question, we first measured the average trajectory of body position, velocity, acceleration, and torque for the three species (Figure 5B-E). We found quantitative differences across species, even within *D. mojavensis* subspecies, for all kinematic variables that we tested (Figure 5F-I). Both desert species produced lower duration and more frequent saccades than *D. melanogaster* (Figure 5G,I). *D. moj. baja* produced the most frequent, smallest amplitude, shortest and slowest saccades. For the rest of the dynamics we quantified, we found differences both between *D. melanogaster* and each desert species, as well as between the desert species themselves. *D. moj. moj.* saccades were larger in amplitude than *D. moj. baja* but smaller than *D. melanogaster,* though the latter difference was subtle and not statistically significant (Figure 5C). In *D. moj. moj.*, these shorter and smaller saccades were achieved by increasing the

torque produced by the animal, which resulted in higher acceleration and peak velocity during the body turn, and producing the braking counter-torque earlier in the saccade profile than *D. moj. baja.* (Figure 5D,E). Overall these varying dynamics support the hypothesis that, in addition to engaging smooth pursuit for object motion, specialist desert species trigger bar-directed saccades more frequently and modulate them to be smaller, shorter, and executed with higher torque than *D. melanogaster*.

DISCUSSION

The present study aimed to investigate the behavioral strategy used by different Drosophila species to pursue ecologically relevant objects during tethered flight. We found that unlike *D. melanogaster*, flying *D. mojavensis* frontally center a textured object moving on a stationary textured ground when free to orient in the yaw plane. This is achieved using smooth dynamics that are sensitive to figure motion across the frontal third of the visual field. Like many species across taxa including cosmopolitan *D. melanogaster*, desert-adapted Mojavensis species also use saccades to track objects, particularly when the target velocity is high. These saccades are smaller, quicker and more frequent in desert flies as compared to *D. melanogaster*. Importantly and in stark contrast to *D. melanogaster*, we found that flight bouts in between saccades in desert fly species are dominated by high-gain smooth object tracking. Desert flies appear to suppress their large-field ground stabilization smooth optomotor reflex in favor of smoothly tracking small-field object motion, interspersed with catch-up saccades. Overall, we demonstrate that while *D. melanogaster* alternate between smoothly stabilizing ground motion using the classical optomotor reflex and tracking objects using saccades, *D. mojavensis* robustly pursue objects using both strategies combined. Our results support the hypothesis that the visual strategy that balances smooth optomotor pursuit and saccadic pursuit differs fundamentally across closely related species adapted for different visual landscapes.

Large-field optomotor responses in flies are flexible and differentially tuned in Drosophilids

Visual flight control in insects is achieved using two prominent visual behaviors: smooth gaze stabilization and saccades, the combination of which manifest as segments of straight flight interspersed with re-orientation body saccades. Straight flight is maintained by optomotor movements of the head and body that actively reduce retinal slip and keep gaze level, keeping the image of the panorama fixated on the retina to counteract perturbations. This reflex is a low level “inner-loop” control process [28] that utilizes not only movements tuned to match image velocity, but also fast catch-up or nystagmus saccades when the retinal slip velocity exceeds an error threshold [15,29,30]. Layered on top of this process, an “outer” control loop initiates body saccades that rapidly re-orient the animal either to refresh the visual scene in the case of spontaneous exploration [31], or to orient toward objects of ecological relevance [11].

Visual signals for inner-loop optomotor reflexes are provided by directionally selective motion detectors T4/T5, which are small-field columnar neurons that synaptically supply the large-field dendrites of lobula plate tangential cells (LPTCs). LPTCs, in turn, supply select premotor descending neurons to trim wing and head steering responses and maintain stable flight [32]. While high gain inner-loop control provides robust stability to maintain course control and stable visual gaze, these reflexes are highly modulated. As an animal initiates flight, looming circuits are differentially gated than when walking [33,34], and the amplitude of visual responses of the vertical system (VS) class of LPTCs doubles presumably to support the transition to high-velocity optic flow [35,36]. To voluntarily change course, outer-loop control of turns transiently hyperpolarizes the (horizontal system) HS class of LPTCs that maintain optomotor equilibrium [37,38]. Stabilization reflexes must also be sensitive to multisensory modulation cues. In response to an attractive odorant, the gain of optomotor responses increases [35,36] as do the visual responses of at least one LPTC class [39]. Within the

mechanosensory modality, proprioceptive feedback driven by active body movement has been shown to actively dampen optomotor responses [13,22]. Conversely, the onset of walking excites HS even in the absence of visual input [40,41].

Given the state dependent plasticity of optomotor control demonstrated both behaviorally and physiologically, it seems plausible that tuning the inner-loop optomotor control gain would be the simplest way to explain the switch from saccade-only bar tracking in *D.melanogaster* to smooth tracking observed in *D. mojavensis* (Figures 3, 4). If so, then the correlation between the fly's steering response and the smooth variation in our SoS bar stimulus ought to be consistently higher for *D. mojavensis* than for *D.melanogaster*, which was indeed the case for experiments that varied bar width (Figure 3L, S1). While more work is required in this area, our results expand the concept of flexible optomotor control to a comparative context and support a model in which closely related Drosophilid species have higher gain inner-loop optomotor responses tuned to smaller objects than *D. melanogaster*.

Small-field optomotor responses support bar centering and tracking in desert flies

The robust smooth optomotor steering responses to frontal bar oscillation that we observed in yaw-free *D.mojavensis* flies (Figure 2C,D,F) are similar to the responses to large-field ground motion. They are also similar to small-field responses observed in proprioception-compromised *D.melanogaster* for similar stimuli [22,42] whereby optomotor responses are thought to mediate frontal bar centering under virtual closed-loop feedback conditions in rigid tethered flight paradigms [43,44]. It therefore seems plausible that high gain optomotor responses to small-field bars likely underlies the robust centering responses we observed in yaw-free *D. mojavensis* species (Figure 1D,E). By contrast, active optomotor damping, presumably by proprioceptive mechanoreceptors that operate under yaw-free or free flight conditions, suppress these reflexes in *D. melanogaster* [22]. While the physiological mechanisms for active damping

mechanisms remain to be explored, our results suggest that visual responses are under-damped in species that have fewer optic flow cues available.

By comparison to inner-loop optomotor fixation control circuits, the mechanistic basis of saccadic outer loop object orientation is far less well understood. Small-field T3 columnar neurons have been recently shown to be omnidirectional feature detectors [45], which are robustly activated by the motion-defined bars that elicit object tracking, and must be functional for normal bar tracking saccades [16]. T3-analogous function remains to be explored in *D. mojavensis* species, but object pursuit in these flies is nonetheless strongly saccadic (Figure 3G-K).

In *D. melanogaster,* bar-evoked saccades have been shown to be triggered by at least two mechanisms depending on the stimulus characteristics. For continuous, constant velocity bar motion, *D. melanogaster* smoothly track the large-field background while spatiotemporally integrating the angular position error to saccade threshold as the bar moves away from visual midline [12]. For object displacements programmed by a white noise sequence for which positional error does not accumulate, object tracking saccades are triggered by slow onset non-directional higher-order motion signals [46]. Both of these experiments were performed under naturalistic visual conditions in which a moving object is presented against a similarly textured visual background. Bar tracking saccades were triggered when the animal was fixating the visual background, not the bar. In desert flies we find the opposite - they track bar velocity robustly (Figure 3D,F), and velocity is a robust predictor of saccades (Figures 3H,I, Figure S2). This suggests that the saccade triggering mechanism in *D. mojavensis* is inherently different from that which has been described in *D. melanogaster*. Canonical models for saccadic object pursuit in animals as diverse as primates and beetles incorporate both velocity and positional error components to trigger saccades [47–49]. While it is tempting to suggest that *D. melanogaster* is the outlier and desert species follow similar principles as other animals, a modeling effort is necessary to more fully explore the saccadic controller in *D. mojavensis,* and how it is predicated upon target velocity, position, or a combination of both variables.

Visual ecology likely drives distinct object-pursuit strategies

Animals across phyla tend to show some combination of smooth and saccadic visual object pursuit [47]. Within a single animal, the spatial composition of the visual background can modulate the balance of smooth and saccadic object pursuit. For example, in the praying mantis, a cluttered visual background influences the animal's target pursuit strategy; for a prey-like target superimposed upon a uniform grayscale background, their head/eye movements pursue the target smoothly, whereas the same target stimulus superimposed upon a natural cluttered background image causes a switch to saccadic target pursuit. The higher the contrast of the background, the longer the duration of stationary fixation bouts between saccades [50]. The interpretation is that the stationary visual background elicits bouts of gaze fixation *via* smooth optomotor control that is contrast sensitive, to be interspersed with saccadic re-orientations. Similarly, *D. melanogaster* on a magnetic tether smoothly pursue a bar only if it is presented against a visually uniform grayscale background, whereas pursuit is entirely saccadic against a naturally textured background [12,22], highlighting the interplay between the demands of gaze stabilization and object pursuit.

For cactophilic species of the Mojave desert, the visual landscape is inherently sparse, and much of the salient vegetation like cacti and yucca comprise food objects or refuges. Our findings suggest that this visual landscape containing salient objects elicits a more generalized flight mode in desert flies than in cosmopolitan species. This hypothesis is supported by studies showing that object responses differ across *Drosophilids* in other contexts as well. For example, tall vertical objects are attractive whereas short objects are aversive for *D. melanogaster* [51] while *D. moj. moj.* robustly approach objects of any vertical size [21]. Optical adaptations including higher spatial acuity in *D. mojavensis* flies may bias the visual system to better support detection of smaller objects [52]. It seems that in order to overcome the challenge of a sparse visual environment, the visual control strategy in *D. moj. baja* and *D. moj. moj* is geared towards

small-field stimuli, and essentially uses visual objects of any size both as a goal landmark to approach, and as a cue to visually stabilize. Which of these visual flight control strategies is the ancestral state and which is the derived state remains to be investigated.

A limitation of our study is that we did not test for potential regionalization of object responses in the dorso-ventral axis of the visual field where natural image projections vary considerably during flight. For example, hawkmoths show strong stabilizing optomotor reflexes in response to optic flow cues in the ventral (ground) and lateral visual field, driven by landscape foliage, but little to no optomotor responses in the empty dorsal sky. By contrast, contour following is driven by the image of the tree line in the dorsal field of view [53]. Because our visual display subtends only 60° across the fly's visual zenith, we have not examined dorsal-ventral specialization. With larger compound eyes composed of a larger number of more tightly packed ommatidia, *D. mojavensis* possesses a larger visual sensory volume than *D. melanogaster* [52]. As the horizon forms a prominent visual feature in desert landscapes, we might expect different functional adaptations across the elevational axis of the visual field, but this remains to be explored.

In conclusion, our results indicate that *D. melanogaster* uses a hybrid strategy of "ground-fixate and object-saccade", whereas *D. mojavensis* species use a fused "fixate-and-saccade" strategy for both ground-based gaze stabilization and orientation toward landscape features. We postulate that the distinct visual landscapes for these species (Figure 1A) support these divergent visual control strategies. If so, what are the neural mechanisms that drive these adaptations? The availability of whole genomes and recent development of genetic tools for several Drosophilids adapted to different ecologies presents a unique opportunity for comparative neuroethological studies, some already underway, that build on our deep understanding of *D. melanogaster* circuitry to explore generalized principles and the wealth of ecological specializations [54–56].

MATERIALS AND METHODS

Key Resources Table

REAGENT or RESOURCE	SOURCE	IDENTIFIER
Electronic equipment		
LED panel visual display system	IO Rodeo	[57]
Neutral density filters	Rosco	Cat# 59
BlackFly USB camera	FLIR	BFS-U3-04S2M-CS
Data Acquisition Hardware	National Instruments	NI USB-6212
Experimental models: Organisms/strains		
Drosophila melanogaster	Wild	Population Cage Flies (PCF)
Drosophila mojavensis mojavensis	Garrity Lab	https://www.drosophilaspecies.com/
Drosophila mojavensis baja	Garrity Lab	https://www.drosophilaspecies.com/
Software and algorithms		
MATLAB	MathWorks	http://www.mathworks.com/

Circular Statistics Toolbox	Philipp Berens	[58]
CircHeatMap	Joshua Welsh	https://github.com/joadwe/cirheatmap/releases/tag/v1.71

Experimental Model and Subject Details

A wild-type *Drosophila melanogaster* strain was maintained at 25°C under a 12 hr: 12 hr light:dark cycle with access to food and water *ad libitum*. *D. mojavensis mojavensis* and *D. mojavensis baja* originated from the Garrity Lab at Brandeis University and were subsequently reared in laboratory conditions for 100+ generations under the same temperature, circadian and nutrition conditions as *D. melanogaster*. All behavioral experiments were performed with randomly selected 3-6 day-old female flies within 4 hours of lights on and 4 hours of lights off.

Method Details

Animal preparation

We used a magnetic tether paradigm and prepared the animals for each experiment according to a protocol that has been previously described [22]. Briefly, we cold-anesthetized the flies by cooling them on a Peltier stage maintained at approximately 4°C. We glued stainless steel minutien pins (Fine Science Tools, SKU 26002-10) onto the thorax by applying UV-activated glue (Esslinger, SKU 12.201). The pin's length was approximately 1 cm to minimize the moment arm about which the fly can generate cross-field torques in pitch and roll. The pins were less than 1 percent of the fly's moment of inertia about the yaw axis. The pin was placed on the thorax projecting forward at an angle of approximately 30°, in order to closely mimic the fly body's angle of attack during low velocity free flight. Before running experiments, flies were allowed at least half an hour and no longer than 2 hours to recover upside-down in a custom-designed holder, inside a covered acrylic container where humidity and temperature could be

controlled in order to avoid rapid dehydration (~ 24°C, 50% humidity). After recovering from anesthesia, flies were given small pieces of Kimwipe as a proxy for a landing substrate to cling to and prevent flight and energy expenditure. It should be noted that *D. mojavensis* flies commonly released the Kimwipe and initiated flight whereas *D. melanogaster* more readily held on to the Kimwipe.

Magnetic tether experimental protocol

As previously described [59,60], the magnetic-tether arena is comprised of a cylindrical display that consists of an array of 96 × 16 blue light emitting diodes (470 nm emission peak) that wrap around the fly, subtending 360° horizontally and 60° vertically (Figure 1B). Each singular LED subtends 3.75° on the flies' retina. Flies were suspended between two magnets, allowing free rotation along the vertical (yaw) axis. We illuminated the fly from above with an array of six infrared LEDs (940 nm emission peak) and visualized the fly's body from below using an infrared-sensitive camera (BlackFly BFS-U3-04S2M-CS) fitted with a zoom lens (InfiniStix 1.0x/94mm, Edmund Optics) and an 850 nm long-pass filter (FGL850M, ThorLabs) to block light from the LED panels. We recorded the angular position of the fly within the arena at 100 frames/s. At the beginning of each experiment, we characterized flies' average optomotor behavior by presenting a large-field panorama rotating at 120°/s for 20 s in the CW and the CCW directions. Flies that did not complete this trial or displayed excessive wobble were discarded from the experiment. If a fly stopped flying during a trial, the experimenter blew a gentle puff of air to stimulate the fly to re-initiate flight. Only flies that flew continuously for at least 75% of the experimental trials were included in the analysis.

Visual stimuli

Experiments for figures 1 & 2 were designed to test responses to constant velocity stimuli, thus containing power across frequencies. Trials lasted 4 s with 2-4 s rests between trials. Bar trials used a 30° wide textured bar on a textured background panorama. Such motion-defined bars were used to elicit responses to object movement and minimize the influence of luminance contrast cues that might provoke static positional responses. In all cases, we presented objects on a spatially randomized static background scene to closely mimic spatially broadband panoramic visual landscapes. In each bar trial, bars were presented in one of 12 pseudorandomized evenly distributed azimuthal positions relative to the fly's heading. Bars were oscillated at 2 Hz on a triangle wave with 60° peak-to-peak amplitude moving at 120°/s. Ground trials where the whole panorama oscillated on the same motion trajectory were interleaved with bar trials as a positive control measurement of large-field optomotor performance. Flies that did not show significant optomotor responses were discarded from the dataset.

As discussed in the main text, for Figure 3, we designed a complex motion trajectory for the same 30° motion-defined bar object with the intention of using a frequency-domain analysis to quantify the strength of bar-elicited smooth responses across several oscillation frequencies. In addition to representing more naturalistic complex motion dynamics, this method would have allowed us to assess the frequency tuning of smooth responses observed in *D. mojavensis*. Following the approach adopted by Stockl et. al 2017 to explore flower-tracking performance across hawkmoth species, this motion trajectory was the sum of nine sine waves (0.3, 0.5, 0.7, 1.1, 1.9, 2.9, 4.6, 7.1, 11.3 Hz) selected to be non-overlapping prime multiples (Roth et al 2014, Stockl et al 2017). Trials were 10 s in duration and consisted of either bar motion on this trajectory or, like the previous experiment, broadband ground motion on this same trajectory. For bar trials, the angular position of the fly was extracted from the video feed at the start of

each trial and the stimulus was programmed to appear in the frontal field of view, +/- 60 ° from the longitudinal body axis.

Experiments for figures 4 and 5 were designed to explore how and whether saccades and inter-saccadic flight bouts differ across species. To do this, we revolved the same 30° motion-defined bar around the visual arena at a constant velocity of 70°/s, with the broadband background kept stationary. This motion trajectory was specifically chosen to elicit continuous object pursuit and assess its smooth and saccadic components separately, as previously described [12]. The bar again appeared on the fly's visual midline and revolved in randomly assigned CW and CCW directions for 10s trials, with 2-3 trials presented for each stimulus direction. These trials were again interleaved with trials where the broadband ground revolved on the same motion trajectories.

Quantification and Statistical Analysis

All heading angle extraction and statistical analyses were performed using MATLAB (MathWorks, Natick, MA, USA). All fly video data was recorded at 100 fps using a FLIR Blackfly camera (BFS-U3-04S2M-CS) and stimulus position data was recorded at 1000 fps using a National Instruments data acquisition board (NI USB-6212). Fly angular heading was extracted using custom-made algorithms that in part included training custom neural net classifiers using software provided by Dr. Ben Cellini (https://github.com/BenCellini/heading-detector-network). Post angular heading extraction, raw data was low-pass filtered using a 5th order Butterworth filter with a 20 Hz cutoff frequency. Clockwise (CW) was defined as the positive direction of motion throughout. Body saccades were extracted using peak-detection methods applied to body angular velocity as per [12], with adjustments in some detection parameters in order to accurately identify all saccades across species. Inter-saccadic flight bouts of at least 0.2 s duration were isolated and used for subsequent analyses.

For raw object orientation responses in Figure 1, we constructed circular probability heat maps to represent the overall likelihood of flies orienting towards a specific angular heading relative to the bar. For each trial performed by an individual fly, a circular mean resultant heading vector θ and resultant vector magnitude r were computed using a 50 ms scanning window [58]. r values represent the length of radii on a unit circle, and were therefore within the range of 0 to 1, with values closer to 1 representing less spread around the mean heading θ. We computed the normalized probability of both angular heading θ (bin width = 1°) and vector length r (bin width = 0.2) using the population dataset. We used the custom CircHeatmap function to represent the bivariate probability using a heat map (https://github.com/joadwe/cirheatmap).

For Figure 2, saccades were eliminated and inter-saccadic bouts were averaged within an individual fly to obtain a mean fly response. Fly means were averaged across the population for each dataset. Fast Fourier Transforms (FFTs) were performed for each individual fly and the amplitude of bar FFT for each fly was normalized to that fly's optomotor ground response. The magnitude ratios at the relevant peaks were compared across species using unpaired samples Student's t-test. Unless otherwise specified, each dot in a scatter plot represents an individual fly's mean response.

For Figure 3 & S1, when a linear systems identification approach has been previously applied in flying fly paradigm assessing performance of the gaze stabilization optomotor reflex, the key assumption of linearity was satisfied by the removal of the occasional nonlinearity represented by a sudden high-velocity change in angular heading i.e. a saccade [25,26]. However, in our study, we were surprised to find that in addition to smooth dynamics, the object-tracking responses in *D. mojavensis* were also strongly saccadic, patterned with the SoS stimulus dynamics (Figure 3). Thus, a linear systems identification analysis was inappropriate to characterize the frequency tuning of smooth object responses in desert flies and we opted for

an event-triggered time-domain analysis instead. Future studies might succeed with this method to characterize the frequency tuning of smooth object responses in desert flies by reducing the amplitude of object oscillation to trigger fewer saccades.

Here, we calculated the mean population response to the sum-of-sines stimulus and cross-correlated it with the stimulus trajectory to find the phase lag between the two signals. We then shifted the response by that lag and plotted the stimulus vs. response point-by-point. We tested the hypothesis that the fly's response is predicted by the stimulus trajectory by fitting a linear regression model to the data to determine the correlation coefficient (r), the coefficient of determination (r^2) and 95 % confidence intervals. We were thus able to estimate how much of the variability in the fly's object tracking response, including both smooth and saccadic components, was predicted by the stimulus dynamics across the three species. Removing the phase lag changes the intercept of the linear fit, but not the correlation coefficient. We constructed raster plots indicating the timing of each saccade within the 10 s trial across all trials, and obtained normalized saccade probability histograms, for CW and CCW saccades, binned into 200 ms time windows.

To determine the predictive power of stimulus position and velocity on saccade probability, we first interpolated the normalized saccade probability, grouping CW and CCW saccades together, to obtain a smooth trace (Figure S2). We then rectified the position trace and from this signal obtained a rectified stimulus velocity trace by differentiating using a 20 ms sliding window. We cross-correlated the saccade probability with both stimulus position and with stimulus velocity to determine the phase lags of each. As previously described, we used the lag-shifted stimulus velocity trace to determine the predictive power of bar angular velocity on saccade probability.

For statistical analysis of inter-saccadic bouts used to track a revolving bar, we first computed the mean velocity of each tracking bout and represented them in normalized probability histograms using 5°/s bins. We then used a bootstrapping technique to test the null hypothesis that inter-saccadic bouts across species all originate from the same dataset. We performed pairwise analyses by combining bout velocities for two species at a time, sampling with replacement 10,000 times and compared the distribution of bootstrap sampled difference in means to the observed difference in means. p-values indicate the proportion of bootstrapped difference in means that is greater than the observed difference in means between species. Thus, for p = 0.01 would indicate that one percent of the possible differences that these data sets could produce would be further apart (less similar) than the differences we observed, whereas ninety nine percent would be closer together (more similar).

Saccade measurement variables including amplitude, duration, peak velocity and inter-saccadic intervals (ISIs) were extracted using previously described methods [15]. For plotting saccade kinematics, we normalized traces to saccade onset. We obtained angular velocity and acceleration through linear derivation and computed angular torque using a previously established model where $\tau = I\ddot{\theta} + C\dot{\theta}$ [12]. Mean saccade metrics were calculated for all saccades performed by an individual fly throughout their experimental trials. Population means were calculated from these individual means. For revolving bar experiments, we used a bootstrapping analysis to show that CW and CCW saccade dynamics do not differ (Figure S4) and proceeded with the analysis on the combined directions dataset. We used non-parametric Kruskal-Wallis tests to compare dynamics across species with *$p < 0.05$; **$p < 0.01$; ***$p < 0.001$.

FIGURES

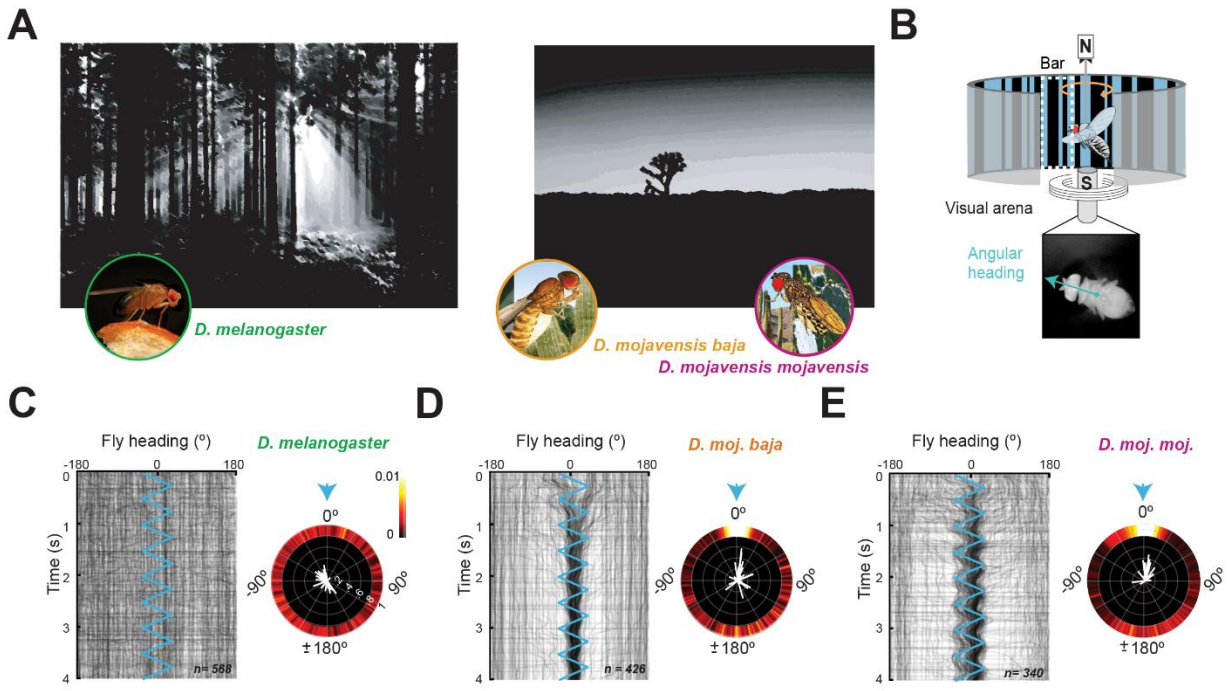

Figure 1. Object centering differs across Drosophila species. A. Left: Visual scene representing cluttered landscapes inhabited by cosmopolitan generalist *D. melanogaster* (green). Right: Visual scene representing sparse desert landscapes inhabited by cactophilic *D. moj. baja* (orange) and *D. moj. moj.* (magenta). Monochrome and Gaussian blur filters were applied to both images. **B.** Magnetic tether visual simulator allowing free movement within the yaw plane. A vertical bar of random ON-OFF pixels (white dashed rectangle) on a similar random textured background. Inset shows exemplar frame of fly in flight recorded from below and angular heading of the major body axis (cyan vector). **C.** Left: Fly azimuthal heading in the circular arena during short 4-second trials relative to the oscillating bar (0º). Gray traces represent individual trials. The stimulus trajectory is represented by the blue waveform. Right: Circular probability histograms of angular heading θ and resultant vector strength r for the population. Heatmap scalebar represents probability normalized by the number of trials in the data set so that total probability = 1. White lines are resultant vectors for each individual. n =

568 trials across N = 26 *D. melanogaster* flies. **D.** Same as C, but for n = 426 trials across N = 20 *D. moj. baja* flies. E. Same as C, but for n = 340 trials across N = 16 *D. moj. moj.* flies.

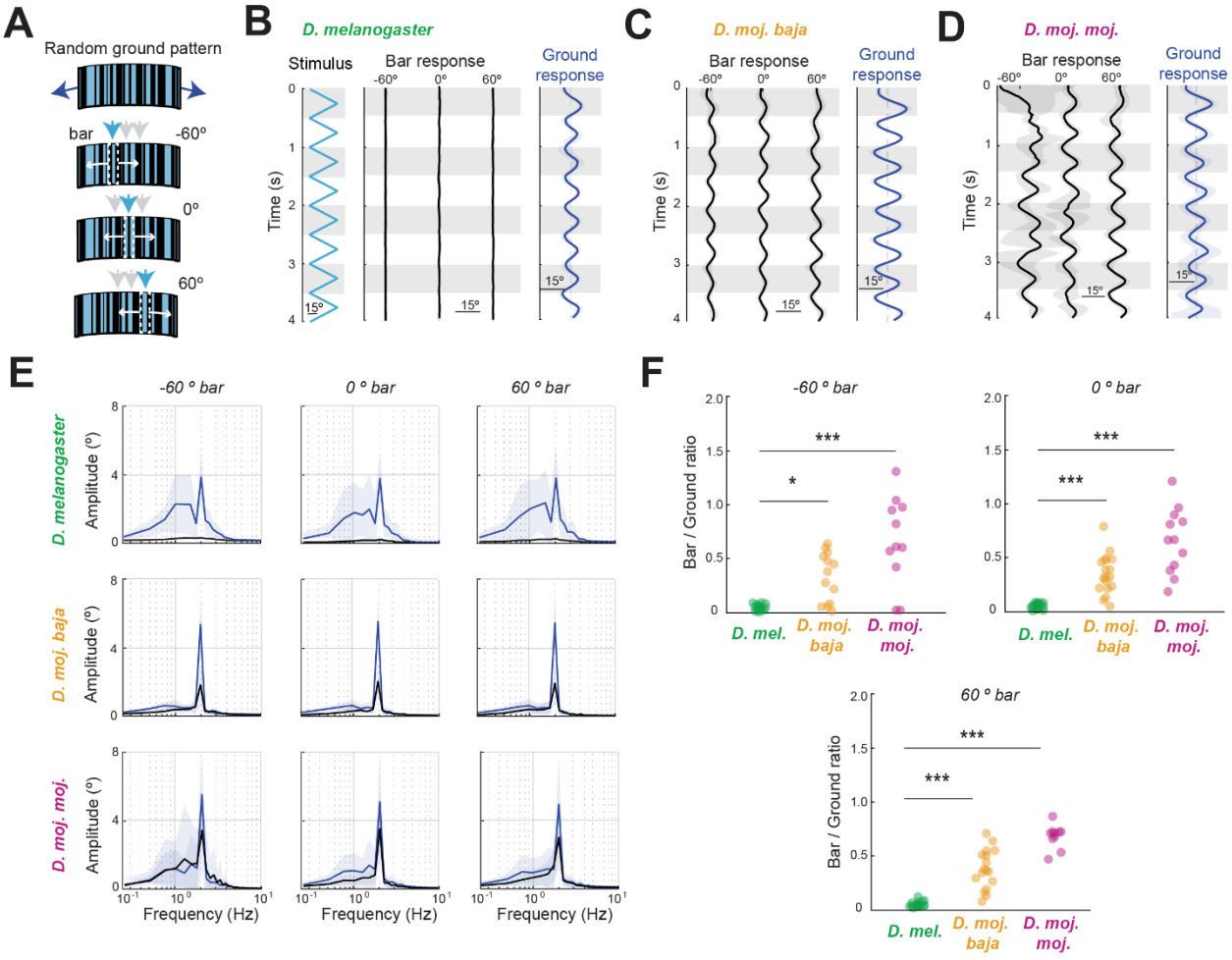

Figure 2. Smooth bar-tracking responses differ across Drosophila species, analogous to Figure 3 in [22]. A. Depictions of textured large-field ground stimulus and motion-defined bars oscillating about different azimuthal positions, as indicated by blue arrowheads. **B.** Yaw-free responses to oscillating bar (light blue) and ground (dark blue) stimuli in N = 20 *D. melanogaster*. Note the presence of optomotor ground stabilization smooth responses and absence of bar-elicited smooth dynamics. Shaded envelopes around the traces represent standard deviation of mean population responses. Black horizontal lines indicate scale bars. Gray bands highlight alternate stimulus cycles. Saccades are eliminated from these traces to

isolate inter-saccadic bouts in which the bar is in a constant position relative to the fly's body axis. **C.** Same as B, but for N = 20 *D. moj. baja*. **D.** Same as B, but for N = 16 *D. moj. moj.* **E.** FFT response magnitude to oscillating bar and ground stimuli in the frequency domain. Rows are species-specific and columns are bar-location specific, with the left-most row representing responses to a bar -60° from visual midline. **F.** Ratio of bar responses to ground responses, compared between species. Circles represent individual flies. Unpaired two-sample t tests were performed with *$p < 0.05$; **$p < 0.01$; ***$p < 0.001$.

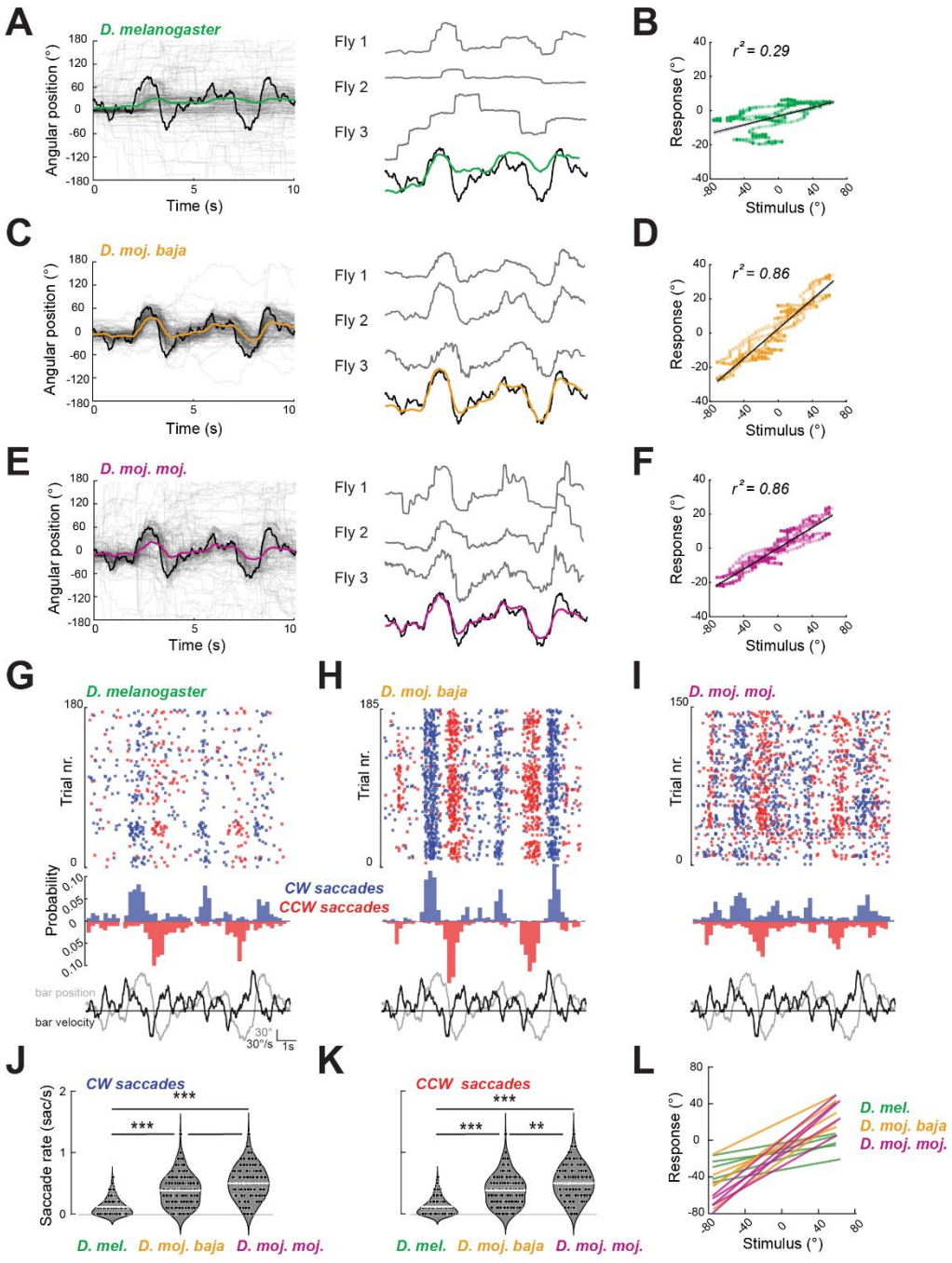

Figure 3. Desert fly species show stronger smooth & saccadic responses to complex motion dynamics. Fly species are color-coded throughout with green for *D. melanogaster*, orange for *D. moj. baja* and red for *D. moj. moj*. **A.** Left: Raw steering responses (gray) to a motion-defined bar on a sum-of-sines (SoS) motion trajectory (black) across n = 182 trials from N = 34 *D. melanogaster* flies. The frequencies comprising the SoS trajectory are as follows: 0.3,

0.5, 0.7, 1.1, 1.9, 2.9, 4.6, 7.1, 11.3 Hz. The colored trace represents the mean population response. Right: Exemplar trials from three different flies (top) and the mean population response overlaid with stimulus trace (bottom). Note: Mean traces are lag-shifted and normalized to their own maximum values for visualization purposes, which does not affect the correlation coefficients. **B.** Angular position of the stimulus vs. the mean fly response for *D. melanogaster,* with each dot representing one timepoint in the 10 s trial. The linear regression model fitted to the variables is plotted in black, with dotted gray lines depicting 95% confidence intervals. The coefficient of determination r^2 is indicated on each plot. **C.** Same as A, but for n = 186 trials from N = 38 *D. moj. baja* flies. **D.** Same as B, but for *D. moj. baja* flies. **E.** Same as A, but for n = 151 trials from N = 35 *D. moj. moj.* flies. **F.** Same as B, but for *D. moj. moj.* flies. **G.** Raster plots indicating timing for n = 557 saccades across *D. melanogaster* flies and trials (top). CW saccades are indicated in blue and CCW in red. Normalized saccade probability is plotted below, rectified to indicate saccade direction (middle). Onset-aligned angular position (black) and velocity (gray) are indicated (bottom). **H.** Same as G, but for the n = 1691 detected saccades in *D. moj. baja*. **I.** Same as G, but for the n = 1569 saccades detected in *D. moj. moj.* **J.** Quantified saccade rate across species for CW saccades. Each dot indicates the average saccade rate during one trial. White horizontal lines indicate the mean saccade rate. Nonparametric Kruskal-Wallis tests were performed with $*p < 0.05$; $**p < 0.01$; $***p < 0.001$. K. Same as J, but for CCW saccades. **L.** Regression as in B,D,F for bar width ranging 7.5-120 degrees. Within species, r^2 values are similar, thus are color-grouped.

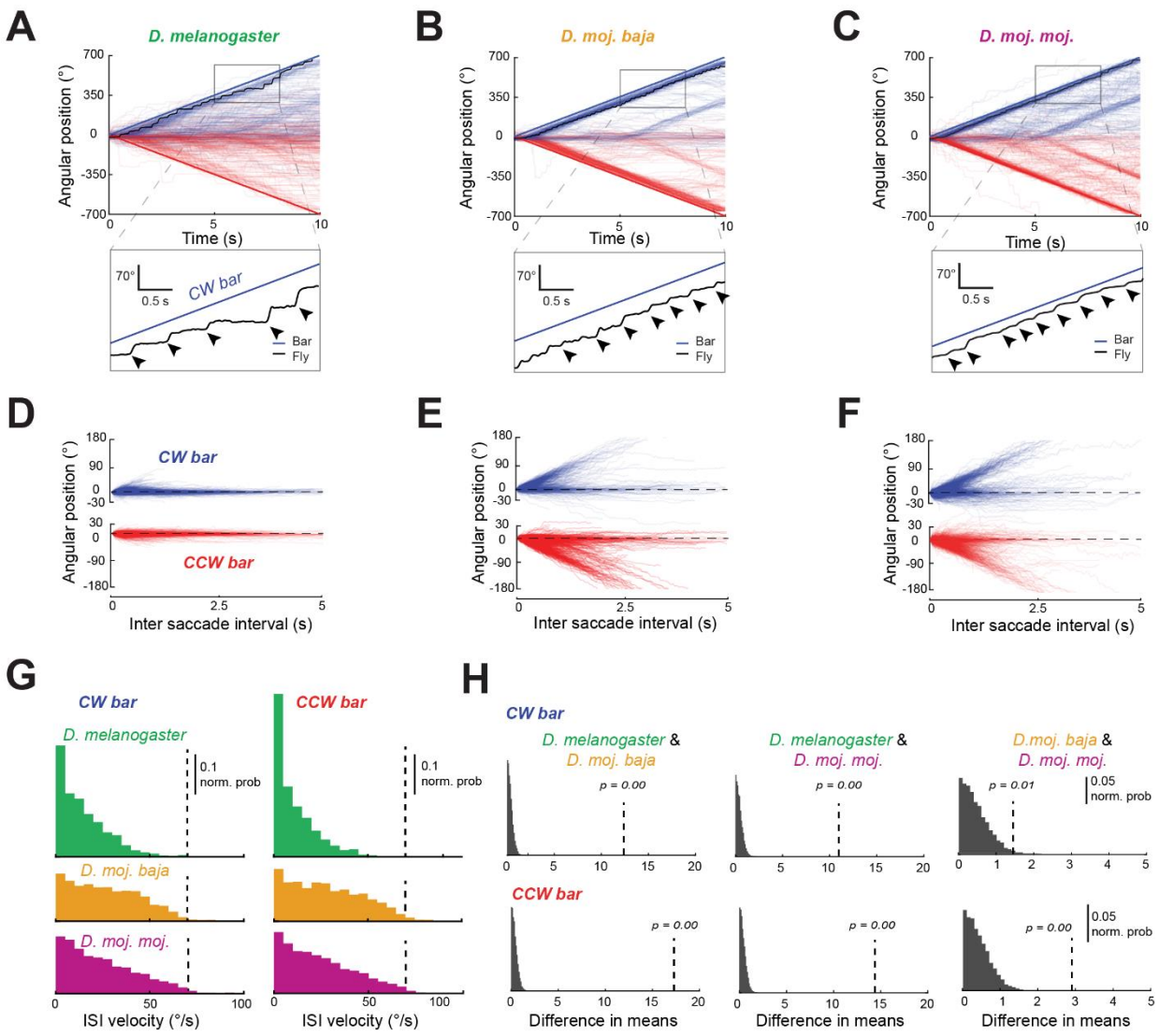

Figure 4. Steady state bar pursuit dynamics differ across Drosophila species. A. Individual unwrapped traces of revolving bar pursuit responses for n = 519 trials across N = 48 *D. melanogaster* flies, separated by bar direction (CW = blue and CCW = red). Bar trajectory is indicated with thick solid lines. An example trace is highlighted in black, with the gray inset magnified. Black arrowheads indicate saccades. **B.** Same as A, but for n = 425 trials across N = 45 *D. moj. baja* flies. **C.** Same as A, but for n = 461 trials across N = 48 *D. moj. moj.* flies. **D.** Inter-saccadic flight bouts, grouped by stimulus direction for *D. melanogaster*. **E.** Same as D, but for *D. moj. baja.* **F.** Same as D, but for *D. moj. moj*. **G.** Normalized probability histograms of

the mean angular velocity during inter-saccadic bouts represented in D - F, grouped by stimulus direction. The vertical dotted line indicates the constant velocity of the bar. **H.** Paired comparisons of inter-saccadic velocity across species. Data values were bootstrapped to compare the difference in means. Probability histograms depict the distribution of bootstrapped differences in means (bin size = 0.1) and the dotted vertical line indicates the observed difference in means. *p*-value is the proportion of sampled differences in means equal to or greater than the observed difference in means.

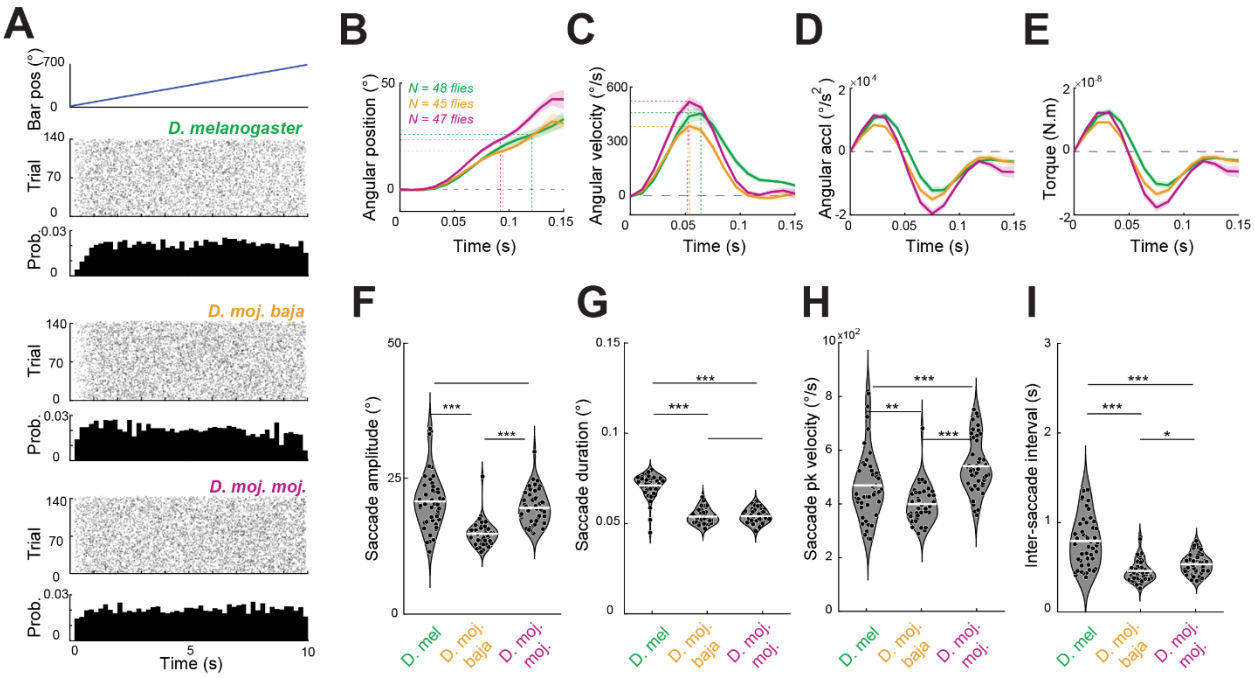

Figure 5. Object saccade dynamics differ across Drosophila species. A. Angular position of a motion-defined bar during a 10 s CW revolution trial (top). Raster plot of saccades triggered by revolving bar for N = 48 *D. melanogaster* flies with corresponding normalized probability histogram (bin size = 200 ms). Below are corresponding raster plots and probability histograms for *D. moj. baja* (N = 45 flies) and *D. moj. moj.* (N = 47 flies). **B.** Change in body angle during a saccade, normalized to body angle position at saccade onset and color-coded for fly species. Shaded color envelope indicates 95% confidence intervals. Dotted x-intercepts indicate the time

end point of the saccade and y-intercepts the corresponding angular position at the end of the saccade (details for saccade identification in Methods). **C.** Same as B for angular velocity. The peak velocities and the time points at which they occurred are indicated using dotted lines. **D.** Same as B for saccade acceleration. **E.** Same as B for saccade torque. **F.** Comparison of saccade amplitude across species. Dots signify trial means from individual flies, white horizontal bars indicate population means. Nonparametric Kruskal-Wallis test *$p < 0.05$; **$p < 0.01$; ***$p < 0.001$. **G.** Same as F for saccade duration. **H.** Same as F for saccade peak velocity. **I.** Same as F for inter-saccadic interval (ISI), which is inversely proportional to saccade frequency.

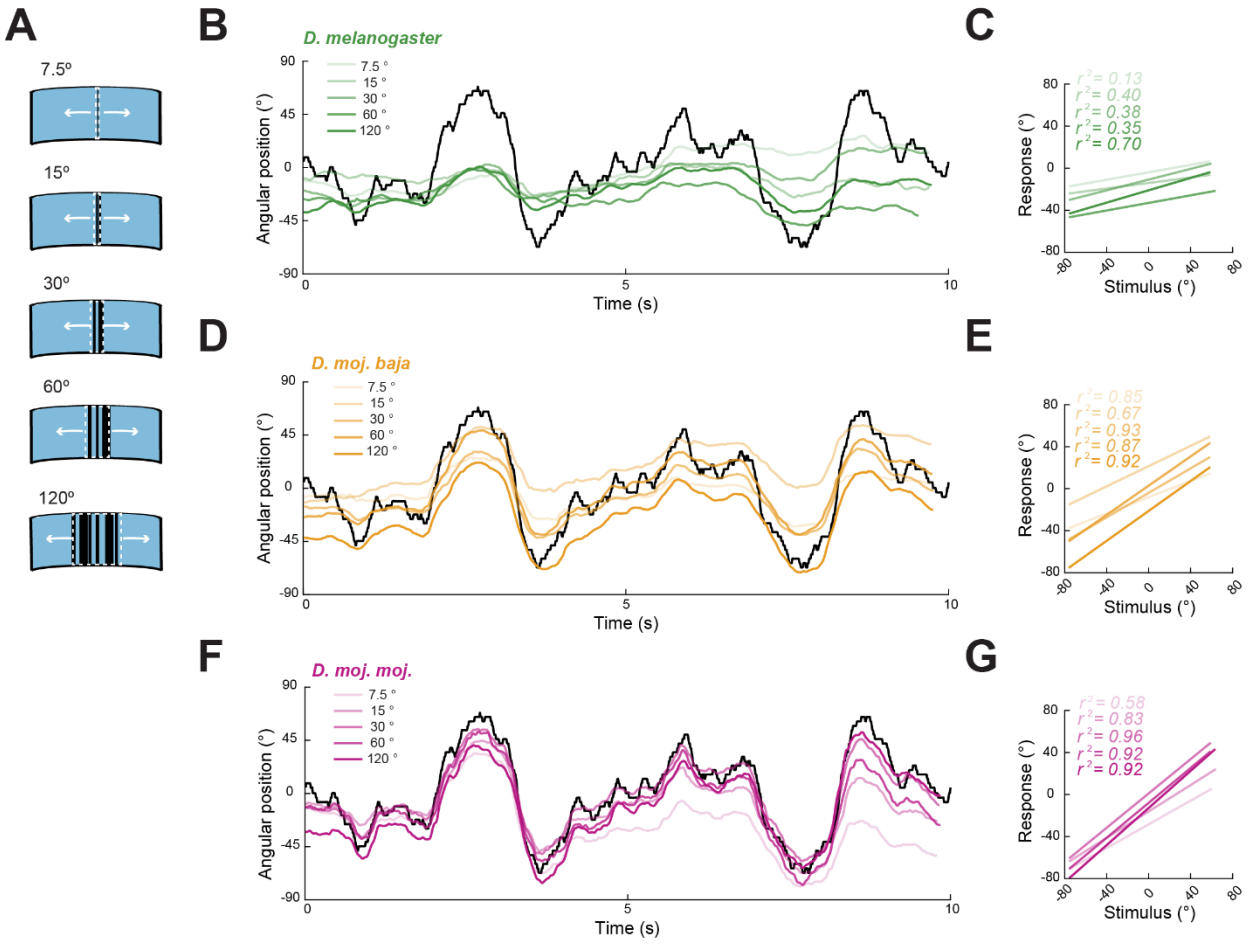

Figure S1. A wide range of bar widths elicit similarly strong tracking responses in desert flies, all larger than in a cosmopolitan fly, related to Figure 3. A. Depictions of bars of varying width on the uniform background cylindrical visual display. The dotted white rectangle is for visualization only. **B.** Mean tracking response for N = 20 *D. melanogaster*, at each bar width indicated with color depth. The SoS stimulus trajectory is indicated in black. **C.** Linear regression of bar stimulus plotted point-by-point with mean fly response, color-coded for bar widths as in B. r^2 coefficient of determination reflects how much of the variability in fly angular position can be explained by the bar angular position. **D.** Same as B, but for N = 22 *D. moj. baja* flies. **E.** Same as C, but for *D. moj. baja* data in panel D. **F.** Same as B, but for N = 22 *D. moj. moj.* **G.** Same as E, but for *D. moj. moj*. data in panel F.

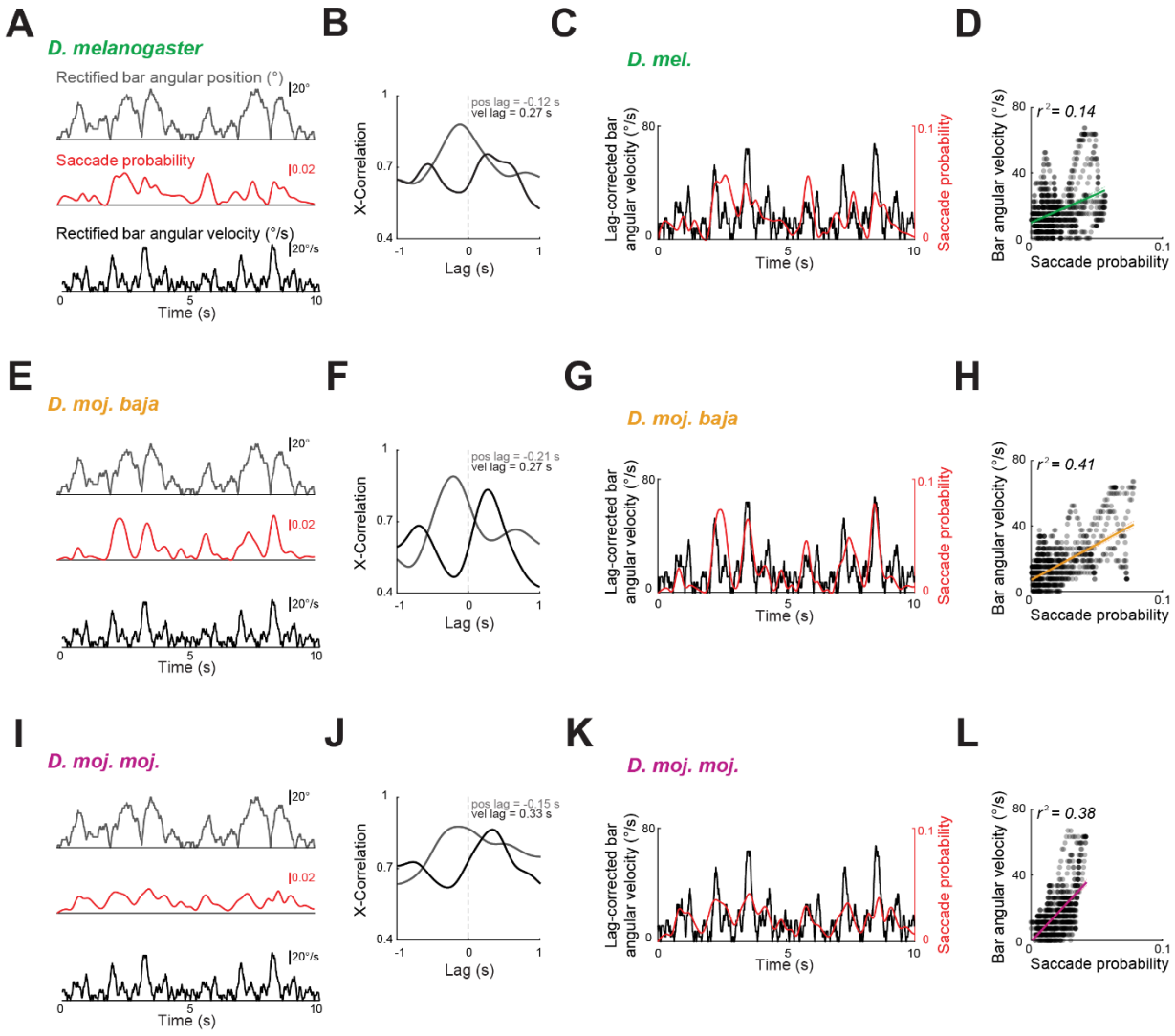

Figure S2. Bar angular velocity predicts saccade probability best in cactophilic flies, related to Figure 3. **A.** Rectified angular position traces (grey), normalized saccade probability (red) and rectified bar velocity (black) across the population of N = 34 *D. melanogaster* flies. Saccade probability was calculated using 200 ms bins and interpolated between bins. **B.** Cross-correlations of saccade probability with bar angular position (grey) and bar angular velocity (black). Adjusting the saccade probability bin size slightly changes the magnitude of the lags found but not their sign (not shown). **C.** Rectified bar angular velocity was shifted by its the lag at peak correlation and plotted with saccade probability to highlight the relationship between the two variables. **D.** Linear regression of bar angular velocity with mean saccade probability point-

by-point. Regression line is plotted in solid green and 95% confidence intervals in dotted light green. Black dots represent individual sampled time points with at 100 Hz sample rate. r^2 coefficient of determination is indicated above the plots. **E-H.** Similar to A-D, but for *D. moj. baja.* **I-L.** Similar to A-D, but for *D. moj. moj.*

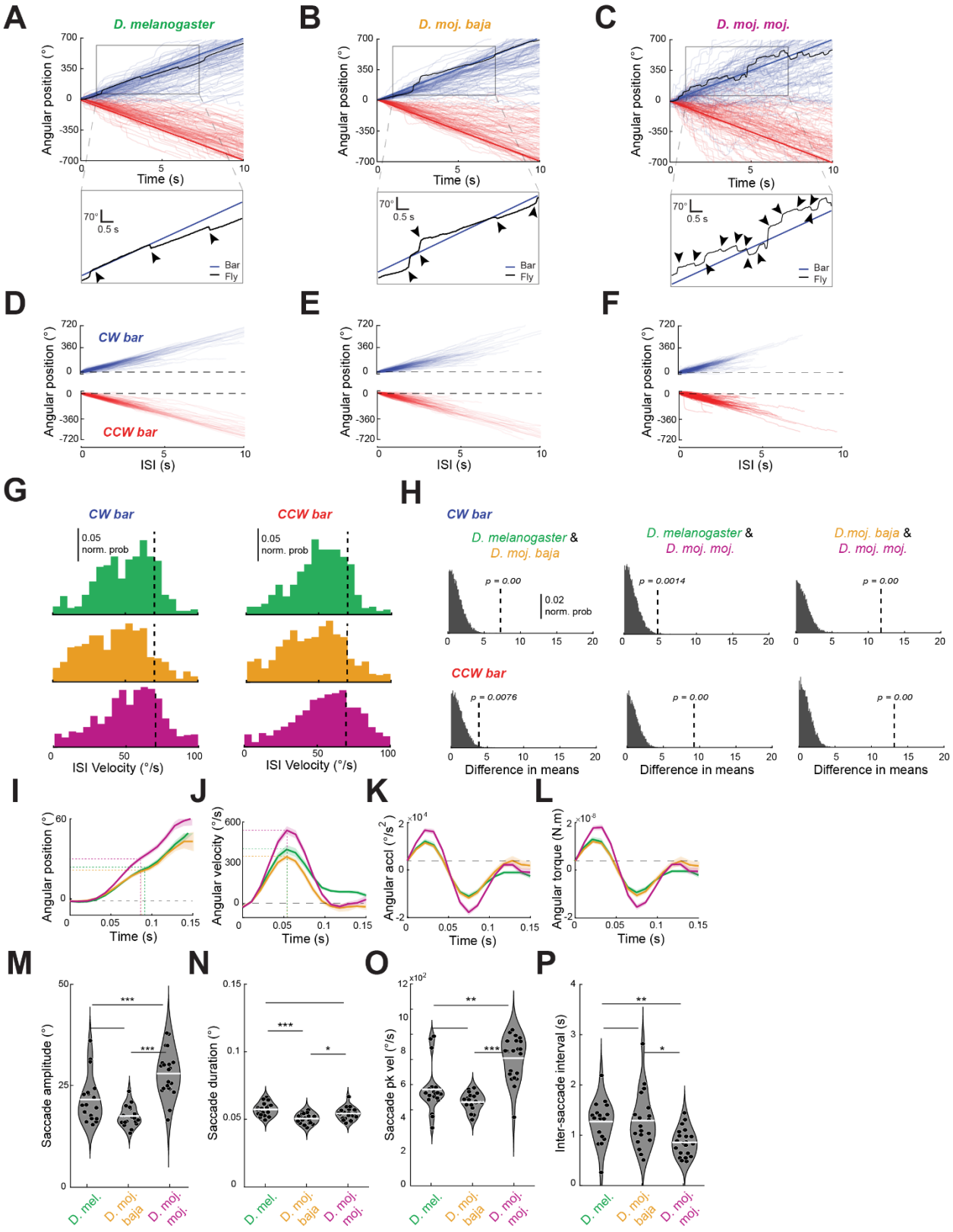
A
D. melanogaster
B
D. moj. baja
C
D. moj. moj.
Angular position (°)
Time (s)
70°
0.5 s
Bar
Fly
D
CW bar
CCW bar
ISI (s)
E
F
G
CW bar
CCW bar
0.05
norm. prob
ISI Velocity (°/s)
H
CW bar
D. melanogaster &
D. moj. baja
D. melanogaster &
D. moj. moj.
D.moj. baja &
D. moj. moj.
p = 0.00
p = 0.0014
0.02
norm. prob
CCW bar
p = 0.0076
Difference in means
I
Angular position (°)
J
Angular velocity (°/s)
K
Angular accl (°/s²)
L
Angular torque (N.m)
M
Saccade amplitude (°)
N
Saccade duration (°)
O
Saccade pk vel (°/s)
P
Inter-saccade interval (s)
D. mel.
D. moj. baja
D. moj. moj.

Figure S3. Optomotor gaze stabilization comprises smooth pursuit and saccades across cosmopolitan and cactophilic desert fly species, related to Figure 4 & 5. A - H. Analogous to Figure 4 A - H but for a revolving widefield ground stimulus. Populations comprise n = 193 trials across N = 19 *D. melanogaster* flies, n = 175 trials across N = 19 *D. moj. baja* flies and n = 207 trials across N = 21 *D. moj. moj* flies. **I - P.** Analogous to Figure 5 B - I but for a revolving widefield ground stimulus.

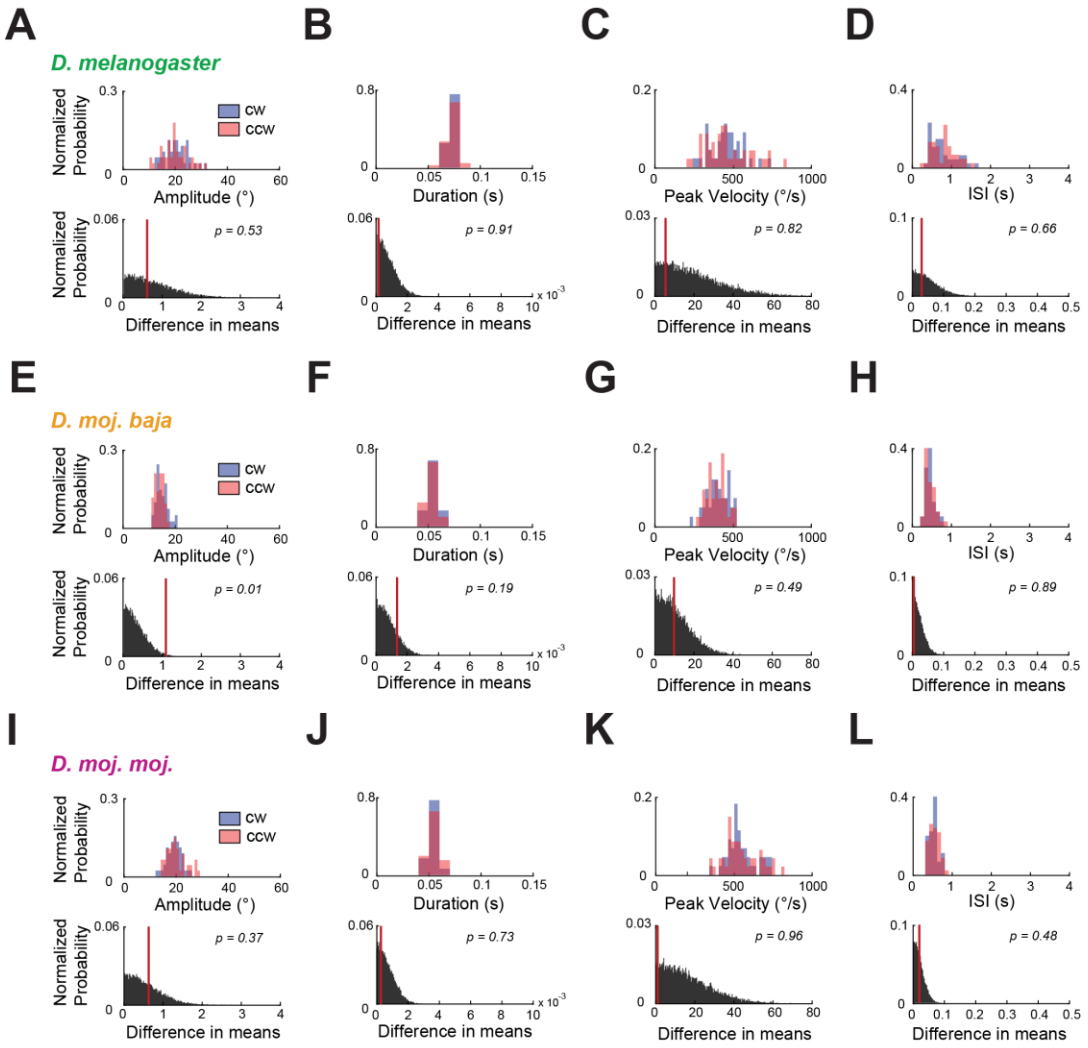

Figure S4. The kinematic variables for clockwise (CW, blue) and counter-clockwise (CCW, red) saccades are similar within species. Related to Figure 4. A. Normalized probability histograms of saccade amplitude within *D. melanogaster* for CW and CCW distributions (top). Normalized probability histograms of difference in means between bootstrapped saccade amplitude distributions randomly selected with replacement from the combined direction distribution (bottom). The red vertical line represents the observed experimental difference in means. *p*-value indicates the probability of encountering bootstrapped differences in means larger than the observed difference in means. **B-D.** Similar to A but for saccade duration, peak saccade velocity and inter-saccadic interval respectively, all

within *D. melanogaster* species. **E-H.** Similar to A-D but within *D. moj baja.* **I-L.** Similar to A-D but within *D. moj moj*.. All saccade dynamics distributions were generated from trial-averaged means across N = 42-48 individual flies.

REFERENCES

1. Egelhaaf, M. (1987). Dynamic properties of two control systems underlying visually guided turning in house-flies. Journal of Comparative Physiology A *161*, 777–783.

2. Götz, K.G. (1968). Flight control in Drosophila by visual perception of motion. Kybernetik *4*, 199–208.

3. Cellini, B., and Mongeau, J.-M. (2020). Hybrid visual control in fly flight: insights into gaze shift via saccades. Curr Opin Insect Sci *42*, 23–31.

4. Borst, A. (2014). Fly visual course control: behaviour, algorithms and circuits. Nat. Rev. Neurosci. *15*, 590–599.

5. Currier, T.A., Pang, M.M., and Clandinin, T.R. (2023). Visual processing in the fly, from photoreceptors to behavior. Genetics *224*. 10.1093/genetics/iyad064.

6. Shinomiya, K., Nern, A., Meinertzhagen, I.A., Plaza, S.M., and Reiser, M.B. (2022). Neuronal circuits integrating visual motion information in Drosophila melanogaster. Preprint, 10.1016/j.cub.2022.06.061 10.1016/j.cub.2022.06.061.

7. Lachaise, D., Cariou, M.-L., David, J.R., Lemeunier, F., Tsacas, L., and Ashburner, M. (1988). Historical Biogeography of the Drosophila melanogaster Species Subgroup. In Evolutionary Biology, M. K. Hecht, B. Wallace, and G. T. Prance, eds. (Springer US), pp. 159–225.

8. David, J.R., and Capy, P. (1988). Genetic variation of Drosophila melanogaster natural populations. Trends Genet. *4*, 106–111.

9. Atkinson, W., and Shorrocks, B. (1977). Breeding site specificity in the domestic species of Drosophila. Oecologia *29*, 223–232.

10. Markow, T.A. (2015). The secret lives of Drosophila flies. Elife *4*. 10.7554/eLife.06793.

11. van Breugel, F., and Dickinson, M.H. (2012). The visual control of landing and obstacle avoidance in the fruit fly Drosophila melanogaster. J. Exp. Biol. *215*, 1783–1798.

12. Mongeau, J.-M., and Frye, M.A. (2017). Drosophila Spatiotemporally Integrates Visual Signals to Control Saccades. Curr. Biol. *27*, 2901–2914.e2.

13. Mongeau, J.-M., Cheng, K.Y., Aptekar, J., and Frye, M.A. (2019). Visuomotor strategies for object approach and aversion in Drosophila melanogaster. J. Exp. Biol. *222*. 10.1242/jeb.193730.

14. Busch, C., Borst, A., and Mauss, A.S. (2018). Bi-directional Control of Walking Behavior by Horizontal Optic Flow Sensors. Curr. Biol. *28*, 4037–4045.e5.

15. Mongeau, J.-M., and Frye, M.A. (2017). Drosophila Spatiotemporally Integrates Visual Signals to Control Saccades. Curr. Biol. *27*, 2901–2914.e2.

16. Frighetto, G., and Frye, M.A. (2023). Columnar neurons support saccadic bar tracking in Drosophila. Elife *12*. 10.7554/eLife.83656.

17. Smith, G., Lohse, K., Etges, W.J., and Ritchie, M.G. (2012). Model-based comparisons of phylogeographic scenarios resolve the intraspecific divergence of cactophilic Drosophila mojavensis. Mol. Ecol. *21*, 3293–3307.

18. Throckmorton, L.H. (1975). The Phylogeny, Ecology & Geography of Drosophila. In Handbook of Genetics, R. C. King, ed., pp. 421–469.

19. Date, P., Crowley-Gall, A., Diefendorf, A.F., and Rollmann, S.M. (2017). Population differences in host plant preference and the importance of yeast and plant substrate to volatile composition. Ecol. Evol. *7*, 3815–3825.

20. Heed, W.B. (1982). Ecological genetics and evolution: The cactus-yeast-drosophila model system B. J. &. Wt, ed. (New York, NY: Academic Press.[Google Scholar]).

21. Park, E.J., and Wasserman, S.M. (2018). Diversity of visuomotor reflexes in two Drosophila species. Curr. Biol. *28*, R865–R866.

22. Rimniceanu, M., Currea, J.P., and Frye, M.A. (2023). Proprioception gates visual object fixation in flying flies. Curr. Biol. *33*, 1459–1471.e3.

23. Duistermars, B.J., Reiser, M.B., Zhu, Y., and Frye, M.A. (2007). Dynamic properties of large-field and small-field optomotor flight responses in Drosophila. J. Comp. Physiol. A Neuroethol. Sens. Neural Behav. Physiol. *193*, 787–799.

24. Roth, E., Zhuang, K., Stamper, S.A., Fortune, E.S., and Cowan, N.J. (2011). Stimulus predictability mediates a switch in locomotor smooth pursuit performance for Eigenmannia virescens. J. Exp. Biol. *214*, 1170–1180.

25. Cellini, B., and Mongeau, J.-M. (2020). Active vision shapes and coordinates flight motor responses in flies. Proc. Natl. Acad. Sci. U. S. A. *117*, 23085–23095.

26. Cellini, B., Salem, W., and Mongeau, J.-M. (2022). Complementary feedback control enables effective gaze stabilization in animals. Proc. Natl. Acad. Sci. U. S. A. *119*, e2121660119.

27. Cellini, B., and Mongeau, J.-M. (2022). Nested mechanosensory feedback actively damps visually guided head movements in Drosophila. Elife *11*. 10.7554/eLife.80880.

28. Hardcastle, B.J., and Krapp, H.G. (2016). Evolution of Biological Image Stabilization. Curr. Biol. *26*, R1010–R1021.

29. Davis, B.A., and Mongeau, J.-M. (2023). The influence of saccades on yaw gaze stabilization in fly flight. PLoS Comput. Biol. *19*, e1011746.

30. Cellini, B., Salem, W., and Mongeau, J.-M. (2021). Mechanisms of punctuated vision in fly flight. Curr. Biol. *31*, 4009–4024.e3.

31. Ros, I.G., Omoto, J.J., and Dickinson, M.H. (2024). Descending control and regulation of spontaneous flight turns in Drosophila. Curr. Biol. *34*, 531–540.e5.

32. Palmer, E.H., Omoto, J.J., and Dickinson, M.H. (2022). The role of a population of descending neurons in the optomotor response in flying Drosophila. bioRxiv, 2022.12.05.519224. 10.1101/2022.12.05.519224.

33. Ache, J.M., Namiki, S., Lee, A., Branson, K., and Card, G.M. (2019). State-dependent decoupling of sensory and motor circuits underlies behavioral flexibility in Drosophila. Nat. Neurosci. *22*, 1132–1139.

34. Ache, J.M., Polsky, J., Alghailani, S., Parekh, R., Breads, P., Peek, M.Y., Bock, D.D., von Reyn, C.R., and Card, G.M. (2019). Neural Basis for Looming Size and Velocity Encoding in the Drosophila Giant Fiber Escape Pathway. Curr. Biol. *29*, 1073–1081.e4.

35. Chow, D., and Frye, M. (2008). Context-dependent olfactory enhancement of optomotor flight control in D.melanogaster. J. Exp. Biol. 10.1242/jeb.018879.

36. Chow, D.M., Theobald, J.C., and Frye, M.A. (2011). An olfactory circuit increases the fidelity of visual behavior. J. Neurosci. *31*, 15035–15047.

37. Kim, A.J., Fitzgerald, J.K., and Maimon, G. (2015). Cellular evidence for efference copy in Drosophila visuomotor processing. Nat. Neurosci. *18*, 1247–1255.

38. Fenk, L.M., Kim, A.J., and Maimon, G. (2021). Suppression of motion vision during course-changing, but not course-stabilizing, navigational turns. Curr. Biol. *31*, 4608–4619.e3.

39. Wasserman, S.M., Aptekar, J.W., Larsen, C., and Correspondence, M.A.F. (2015). Olfactory Neuromodulation of Motion Vision Circuitry in Drosophila. Curr. Biol. *25*, 467–472.

40. Fujiwara, T., Cruz, T.L., Bohnslav, J.P., and Chiappe, M.E. (2017). A faithful internal representation of walking movements in the Drosophila visual system. Nat. Neurosci. *20*, 72–81.

41. Fujiwara, T., Brotas, M., and Chiappe, M.E. (2022). Walking strides direct rapid and flexible recruitment of visual circuits for course control in Drosophila. Neuron *110*, 2124–2138.e8.

42. Theobald, J.C., Shoemaker, P.A., Ringach, D.L., and Frye, M.A. (2010). Theta motion processing in fruit flies. Front. Behav. Neurosci. *4*. 10.3389/fnbeh.2010.00035.

43. Fenk, L.M., Poehlmann, A., and Straw, A.D. (2014). Asymmetric Processing of Visual Motion for Simultaneous Object and Background Responses. Preprint, 10.1016/j.cub.2014.10.042 10.1016/j.cub.2014.10.042.

44. Fox, J.L., Aptekar, J.W., Zolotova, N.M., Shoemaker, P.A., and Frye, M.A. (2014). Figure-ground discrimination behavior in Drosophila. I. Spatial organization of wing-steering responses. J. Exp. Biol. *217*, 558–569.

45. Keleş, M.F., Hardcastle, B.J., Städele, C., Xiao, Q., and Frye, M.A. (2020). Inhibitory interactions and columnar inputs to an object motion detector in Drosophila. Cell Rep.

46. Aptekar, J.W., Shoemaker, P.A., and Frye, M.A. (2012). Figure tracking by flies is supported by parallel visual streams. Curr. Biol. *22*, 482–487.

47. Land, M.F. (1992). Visual tracking and pursuit: Humans and arthropods compared. J. Insect Physiol. *38*, 939–951.

48. Lisberger, S.G., Morris, E.J., and Tychsen, L. (1987). Visual motion processing and sensory-motor integration for smooth pursuit eye movements. Annu. Rev. Neurosci. *10*, 97–129.

49. Talley, J., Pusdekar, S., Feltenberger, A., Ketner, N., Evers, J., Liu, M., Gosh, A., Palmer, S.E., Wardill, T.J., and Gonzalez-Bellido, P.T. (2023). Predictive saccades and decision making in the beetle-predating saffron robber fly. Curr. Biol. *33*, 2912–2924.e5.

50. Rossel, S. (1980). Foveal fixation and tracking in the praying mantis. J. Comp. Physiol. *139*, 307–331.

51. Maimon, G., Straw, A.D., and Dickinson, M.H. (2008). A simple vision-based algorithm for decision making in flying Drosophila. Curr. Biol. *18*, 464–470.

52. Currea, J.P., Frazer, R., Wasserman, S.M., and Theobald, J. (2022). Acuity and summation strategies differ in vinegar and desert fruit flies. iScience *25*, 103637.

53. Bigge, R., Pfefferle, M., Pfeiffer, K., and Stöckl, A. (2021). Natural image statistics in the dorsal and ventral visual field match a switch in flight behaviour of a hawkmoth. Curr. Biol. *31*, R280–R281.

54. Stern, D.L. (2022). Transgenic tools for targeted chromosome rearrangements allow construction of balancer chromosomes in non-melanogaster Drosophila species. G3 *12*. 10.1093/g3journal/jkac030.

55. Drosophila 12 Genomes Consortium, Clark, A.G., Eisen, M.B., Smith, D.R., Bergman, C.M., Oliver, B., Markow, T.A., Kaufman, T.C., Kellis, M., Gelbart, W., et al. (2007). Evolution of genes and genomes on the Drosophila phylogeny. Nature *450*, 203–218.

56. Coleman, R.T., Morantte, I., Koreman, G.T., Cheng, M.L., Ding, Y., and Ruta, V. (2023). A modular circuit architecture coordinates the diversification of courtship strategies in Drosophila. bioRxiv. 10.1101/2023.09.16.558080.

57. Reiser, M.B., and Dickinson, M.H. (2008). A modular display system for insect behavioral neuroscience. J. Neurosci. Methods *167*, 127–139.

58. Berens, P. (2009). CircStat: A MATLAB Toolbox for Circular Statistics. J. Stat. Softw. *31*, 1–21.

59. Bender, J.A., and Dickinson, M.H. (2006). Visual stimulation of saccades in magnetically tethered Drosophila. J. Exp. Biol. *209*, 3170–3182.

60. Duistermars, B.J., and Frye, M. (2008). A magnetic tether system to investigate visual and olfactory mediated flight control in Drosophila. J. Vis. Exp. 10.3791/1063.